A STUDY ON FAULT LOCATION ON TRANSMISSION LINE UTILIZING TWO-END SYNCHRONIZED AND UNSYNCHRONIZED MEASUREMENT

DARO DIN

A THESIS SUBMITTED IN PARTIAL FULFILLMENT
OF THE REQUIREMENT FOR THE DEGREE OF
MASTER OF ENGINEERING IN COMPUTING IN ENGINEERING SYSTEMS
INTERNATIONAL COLLEGE
KING MONGKUT'S INSTITUTE OF TECHNOLOGY LADKRABANG
ACADEMIC YEAR 2015
KMITL-2015-IC-M-11-02

Thesis Certification

International College

King Mongkut's Institute of Technology Ladkrabang

Thesis Title	**A STUDY ON FAULT LOCATION ON TRANSMISSION LINE UTILIZING TWO-END SYNCHRONIZED AND UNSYNCHRONIZED MEASUREMENT**
Student	**MR. DARO DIN**
Student ID.	57610020
Degree	Master of Engineering
Program	Computing in Engineering Systems (International Program)
Thesis Advisor	Asst.Prof.Dr.Peerawut Yutthagowith
Thesis Reference Number	KMITL-2015-IC-M-11-02

EXAMINERS		SIGNATURES
Assoc.Prof.Dr.Supat	Kittiratsatcha	
Asst.Prof.Dr.Surin	Kittitornkun	
Asst.Prof.Dr.Peerawut	Yutthagowith	
Assoc.Prof.Dr.Norasage	Pattanadech	
Asst.Prof.Dr.Nutthaphong	Tanthanuch	

Date : July 11th , 2016 Time 13.00 – 15.00 pm.
Place : International College, 8th floor, 55th Anniversary Chalermprakiat Building

KING MONGKUT'S INSTITUTE OF TECHNOLOGY LADKRABANG

(Assoc.Prof.Dr.Supat Kittiratsatcha)
Dean of International College
July 25 , 2016

Thesis Title	A Study on Fault Location on Transmission Line Utilizing Two-End Synchronized and Unsynchronized Measurement
Student	Mr. Daro Din
Student ID.	57610020
Degree	Master of Engineering
Program	Computing in Engineering Systems
Year	2015
Thesis Advisor	Asst. Prof. Dr. Peerawut Yutthagowith

ABSTRACT

Modern power systems are expanding and growing to a large interconnected system and the increased deregulation of utility markets have helped dedicated fault location systems garner much attention. Short-circuit faults are the most common and severe threat to power transmission lines. An effective and accurate fault location estimation technique can greatly improve the operation of a power system and provide useful information for fault analysis. This thesis proposes two alternative simple fault location algorithms for two-end short and long transmission line based on synchronized and unsynchronized measurement, respectively. Firstly, none line parameter requirement for fault location algorithm based on two-end synchronized measurement is presented. It is unconventional from the other fault location algorithms since it does not involve the use of any line parameters. It just needs the synchronized two-end measurement of voltages and currents in phasor quantities and transforms it to sequence components. Hence, it can be used to accurately and efficiently determine the distance to fault for all fault types. Non-ideal synchronization is also investigated. As a result, data synchronization problem is raised in this algorithm which demands careful consideration. Fortunately, two-end unsynchronized data sampling for fault location algorithm on the long transmission line is proposed to eliminate this problem and fulfill the economic considerations. Synchronization operator and angle are determined non-iteratively and accurately by combining only positive- and negative-sequence components for all fault types. This is a new approach to determine and select the valid solution of synchronization operator and angle. These presented algorithms have been simulated and validated thoroughly with credible fault data modeling obtained from ATP-EMTP software. Through overall algorithm testing on various fault types and conditions with varying fault location, fault resistance, ground resistance, and phase shift angle, it can be proved that the algorithms efficiently and accurately determine the distance to fault over the entire transmission line. Additionally, the accuracy and robustness of fault location algorithms still maintain a high level even adding severe noise ratio 40dB.

ACKNOWLEDGEMENTS

I am deeply indebted to my mentor and research advisor, Asst. Prof. Dr. Peerawut Yutthagowith, Head of High Voltage Engineering Laboratory (HVEL), King Mongkut's Institute of Technology Ladkrabang (KMITL), Thailand, for an incomparably rewarding educational and personal experience. I have been indescribably enlightened and inspired by his patient teaching and vast technical expertise. His constant support, gentle guidance, and warm encouragement gave a positive impetus to the successful completion of my thesis. His inspiring ability to treat problems from a new perspective integrated with many hours of constructive discussions was the main factor of the progressive improvements in this thesis. Indeed, being an advisee to him will definitely fortify my competence to stay in the forefront of my research area.

In the meantime, this is an opportunity to thank the person who has shaped my academic personality prior to my arrival to KMITL. Special thanks go to my co-investigator from Institute of Technology of Cambodia, Mr. Chanthea Khun, for his supports and undoubtedly paved the way for my being a graduate student in KMITL.

I am very grateful to Assoc. Prof. Dr. Norasage Pattanadech for not only serving as my thesis committee and for his comments on my work but also for giving me an inspiration with his immense knowledge in his areas of expertise.

I wish to express my sincere appreciation to AUN/SEED-Net for continuously provide the financial support during the time I have been studying for my master degree. I also extend my gratefully thank KMITL for giving me the valuable opportunity to do research in a warm and peaceful environment.

My grateful acknowledgements go to all committees, professors, lecturers and supporting staffs in both International College and Department of Electrical Engineering, who always help and give me a guideline during the whole period of my master degree and also my thesis defense.

I feel very fortunate to meet with great friends during my graduate study. I would like to thank all my senior and junior lab-mates in HVEL, Laos friends, Cambodia friends, Thai friends, and also Myanmar friends, for their great friendship, help, support, and for all the fun times we spent together.

Finally, my deepest gratitude and love is reserved for my family, for their endless support and love, and for making me who I am. Their love embraces me everywhere despite the long geographic distance between us.

Daro Din

TABLE OF CONTENTS

TABLE OF CONTENTS (Cont.)

TABLE OF CONTENTS (Cont.)

LIST OF TABLES

LIST OF TABLES (Cont.)

LIST OF FIGURES

LIST OF FIGURES (Cont.)

LIST OF FIGURES (Cont.)

Figures Page

LIST OF ABBREVATIONS

A/D	Analog-Digital
ANNs	Artificial Neural Networks
ATP-EMTP	Alternate Transient Program – Electromagnetic Transient Program
AWGN	Additive White Gaussian Noise
CTs	Current Transformers
DFRs	Digital Fault Recorders
DL	Double Line
DLG	Double Line to Ground
FFT	Fast Fourier Transform
FL	Fault Locator
GPS	Global Positioning System
MOVs	Metal Oxide Varistors
PMUs	Phasor Measurement Units
SCADA	Supervisory Control and Data Acquisition
SLG	Single Line to Ground
SNR	Signal-to-Noise
VTs	Voltage Transformers
3LG	Balanced Three-phase

CHAPTER 1

INTRODUCTION

This chapter begins with the basic concept of fault location in order to implement in the network. Due to the large-scale and complexity of the transmission line in the power system, statement of the problems is also raised up in order to push the attention on the faced problems. Then, aims of fault location implementation and motivation are presented. Brief differences between fault locator and distance relay are provided in order to clear the misunderstanding. Scope and limitations are also set in this chapter for limiting the trend of proposed fault location algorithm and the specific purposes of this study. Finally, thesis organization is provided in the last section.

1.1 Basic Concept of Fault Location

A typical electrical power system consists of generators, transformers, transmission lines, and distribution lines. Failure on transmitting the electricity in the power system can occur unexpectedly due to faults on the overhead transmission line. Free marketing and deregulation have been introduced and imposed plenty of seriously restrictive requirements to utilities on providing a continuity and reliability of power supply as well as power transmitting. Contemporary power system provides the continuity of power supply, dependability, and reliability to ensure the high demand from the customers. Since restrictive requirements are really needed to implement on the network, power system protection with supplementary equipment functioned as fault location appeared to be the prime important [1-3].

Storms, lightning, heavy rain, short circuits caused by birds or external objects, and insulation breakdown are the certain phenomenon to create the fault on the transmission line. The permanent fault which is the serious failure due to the mechanical breakdown must be repaired or isolated before returning the line to retransmit. The restoration can be expedited unless the location of the fault is known or estimated with acceptable accuracy. Fault locator is enhanced to locate both permanent and temporary fault. This enables the deregulated environment and can compete with other utilities in term of increasing the availability of the power transmitting to customers.

In a modern country, the customers are sensitive to the outages. As a result, fast and effective fault location methods, high-quality customer service, and supply

restoration are necessary. Identifying the fault location on the transmission line results in minimizing of customer complain inversely increasing the reliability of the network. Therefore, fault location is emphasized as one of the first function to be integrated into modern substation control system.

Fault location function can be implemented into [3, 4]:

- Microprocessor-based protective relays
- Digital fault recorders (DFRs)
- Stand-alone fault locators
- Post-fault analysis programs

1.2 Statement of Problems

A common problem faced during the fault occurrence is the specific distance where it took place. As stated, the maintenance crews have to repair the damaged part caused by fault before the line is reenergized. This means they have to inspect along the entire line to find the damaged place. In the case of a long line and rough terrain where the crews are difficult to inspect the line, outage time will increase due to the lack of ability to speed up the service restoration. Moreover, troubles cannot always be found by human inspection without prior indication of where the fault took place. A part of temporary fault which is self-cleared results many difficulties for inspectors as the weak spot cannot be figured out. This is mainly due to the outage time which caused more inconvenient to customers, waste time and money for inspection, and low reliability in the system which cannot follow the requirements of the deregulation.

1.3 Thesis Motivations

1.3.1 Aims of Fault Location

Fault location disables many difficulties for fault inspection of the maintenance crews by providing highly accurate of the specific location of a fault on the transmission line. By reversing from the stated problem, aims of fault location can be fulfilled as:

- With the use of fault location, our power system will lead into one step of the modern substation control system.
- It saves time and cost of sending out repair crews to search for the faulted point in the bad weather or unfriendly terrains.
- It improves system reliability, and the reduction of customers complaints will be proved as the restrictive requirements of deregulation.

- The weak spot on the line will be pinpointed in the case of a temporary fault, so the plan of maintenance schedules can be fixed for avoiding future problem.

1.3.2 Objectives of Proposed Fault Location Algorithms

In this research, two different fault location algorithms have been proposed with utilizing two-end synchronized and unsynchronized measurement through lump parameter line and distributed parameter line models, respectively.

The aim of the first fault location algorithm is to deliver and validate the accuracy of proposed algorithm which determines the distance to fault on transmission line without any knowledge of line parameters by processing synchronized two-end measurement of voltages and currents in phasor quantities and transform it to sequence components. Since it uses only positive- and negative-sequence component, it can be used to accurately and efficiently determine all fault types, i.e. balanced three-phase fault and unbalanced fault.

Moreover, the purpose of another presented fault location algorithm which also provided in this study is to refine and validate the method for analytical synchronization corresponding to all fault types by taking into account the distributed parameter line model to ensure the high accuracy of the fault location estimation from unsynchronized two terminals on long ideally transposed transmission line. Only positive- and negative-sequence components were combined together to get the unknown synchronization operator and angle for all fault types. Then the fault distance can be calculated non-iteratively after the accomplishment of the synchronization from both terminals.

1.4 Differences between Fault Locator and Distance Relay

Fault locator and distance relay are not much difference because fault locator is the developed function from distance relay and can exactly pinpoint the fault location. However, there are some significant differences between these two devices. Then, we can classify these differences in the following features [4]:

- Accuracy of fault location
- Speed of determining the fault position
- Speed of transmitting data from remote site
- Used data window
- Digital filtering of input signals and complexity of calculations

Through these features, fault locator is used for accurately pinpointing the fault distance whereas distance relays just provide the indication of the general area in term of the protective zone.

Distance relays are performed in an online mode and fault clearing time is a very important consideration in the selection of protective relays and their settings which needed to be carefully determined. Fast clearing of faults has to be done in short time. On the other hand, the calculation of fault location is performed in an offline mode which can be made by human users to calculate in seconds or even minutes.

Supervisory control and data acquisition (SCADA) can be associated with fault location purpose while communication used by protective relays.

The fault interval lasts from fault incipience up to a fault clearing by a circuit breaker, and usually, this takes around three fundamental frequency cycles which are wider than required for fault location.

The operation of a distance relay may be significantly influenced by the combined effect of load and fault resistance which is known as the reactance effect [5, 6]. The distance relay may cause failed operation for a forward external fault, or may not operate for an internal fault if the fault resistance is too large.

1.5 Scope and Limitations

In case of proposed algorithm using two-end synchronized measurement which considered as phasor-based approach, the limitations are listed in order to set the trend of the developed algorithm as follows:

- The transmission line was assumed as a short length of transposed line (100km) with two terminals based on synchronized data sampling, so the shunt capacitance in the derivation of the algorithm can be neglected.
- Since this presented algorithm separately determines the balanced three-phase fault and balanced fault, the method of selection fault types is not considered. Usually, it is provided by protective relays of a line.
- The method of improving the quality of extraction of voltage and current phasors are not taken into account since Fast Fourier Transform (FFT) is sufficiently sensitive to the decaying of the DC components in the fault currents.
- To validate this algorithm, Alternate Transient Program – Electromagnetic Transient Program (ATP-EMTP) was used to simulate the various fault types with varying the fault resistances, and FFT function was applied to extract the voltage and current phasors by Matlab.
- The random error introduced by irritated noise during Analog-Digital Conversion (A/D) and non-ideal synchronization are considered as the affected factors to the accuracy of the developed algorithm. Thus, these

factors were taken into account to clarify the effectiveness and accuracy of the fault location algorithm.

In case of proposed algorithm using two-end unsynchronized measurement which considered as impedance-based algorithm, the limitations are listed in order to set the trend of the developed algorithm as follows:

- The long transmission line (300km) modeled with distributed parameter line model with the use of correction factors for representing series and shunt parameters is strictly taken into account to ensure the high accuracy of the proposed algorithm.
- The presented algorithm is implemented for fault location on fully transposed line, so technique based on the fundamental frequency of voltages and currents appeared to be sufficient to fulfill the aim of fault locating.
- Positive- and negative-sequence component are assumed to be presented in all fault types in order to reduce to manipulation of the determination of the synchronization operator. Details of this assumption will provide explicitly in Chapter 3.
- To validate this algorithm, ATP-EMTP was used to simulate the various fault specifications i.e. fault types, fault resistance, and ground resistance have been considered over the entire line length, and FFT function was applied to extract the voltage and current phasors by Matlab.
- Second order analog anti-aliasing with 500Hz of the cutoff frequency which corresponds to 10^{th} harmonic was designed and applied by built-in function in Matlab to filter the secondary signals of the current transformers (CTs) and voltage transformers (VTs).
- Random error which introduced by irritated noise during A/D conversion and phase shift angle (pre-fault power flow direction) are further investigated since these are the affected factors on the proposed algorithm.

1.6 Thesis Organization

The rest of the thesis is organized as follows. In Chapter 2, theoretical backgrounds which are the basic point to enrich the knowledge on transmission line models, fault types, and methods of transforming the signals in time to frequency domain are introduced. Also, a detailed literature is presented in which various fault locating schemes based on transmission line characteristics are reviewed in order to grasp all the information related to the developed algorithm. Lastly, factors affected on the accuracy of the fault locating are briefly provided.

In Chapter 3, system modeling of the faulted point and problem formulation are classified separately in term of using lump parameter line model and distributed parameter model. Detailed algorithm derivations of these two different models with using synchronized and unsynchronized measurement from two terminals, respectively, are presented explicitly. In addition, a method for the determination and selection of synchronization operator in all fault types is extended to overcome the method using unsynchronized measurement.

In turn, Chapter 4 illustrates the performance evaluation and simulation results of the proposed algorithms by presenting detailed analysis on considered affected factors and finally, Chapter 5 concludes the thesis and suggests recommendations for future work.

CHAPTER 2

THEORETICAL BACKGROUNDS AND LITTERATURE REVIEWS

This chapter introduced the theoretical backgrounds i.e. fault types, transmission line models, and time-frequency domain transformation of the signals which are the basic point to enrich the knowledge involved with the developed fault location algorithm. Also, detailed literature reviews are presented on how various fault locating schemes have been developed. At the end of this chapter, fault location error and factors affected on the accuracy of the fault locating are briefly provided.

2.1 Fault Types

A fault is defined as the flow of a large current which could cause damages on equipment. If the current is very large, it might interrupt the power in the network. In addition, voltages below its minimum level could sometimes cause failure to equipment.

The main characteristic of faults is related to fault impedance involved which can obviously be considered as fault resistance. Commonly, fault resistances contain small value and in general, do not exceed 0.5 Ω for inter-phase fault. However, its value might higher during ground faults as tower footing resistance which may be as high as 10 Ω [7].

There are two types of faults which can occur on transmission line i.e. balanced fault and unbalanced fault also known as symmetrical and asymmetrical fault, respectively. The majority of fault occurred on the transmission line are unbalanced faults. Moreover, faults can be classified as shunt faults and series faults [8]. Series faults are those types of faults which occur in impedance of the line and does not involve neutral or ground, nor does it contacts any interconnection between the phases. The voltage and frequency in this type of fault increase whereas the current decreases in the faulted phases. For instance, the opening one or two lines by circuit breakers. Reversely, shunt faults are the unbalance between phases or between ground and phases whose current increase while voltage and frequency decrease in the faulted phases. This research is considered on the shunt faults which depicted in Figure 2.1.

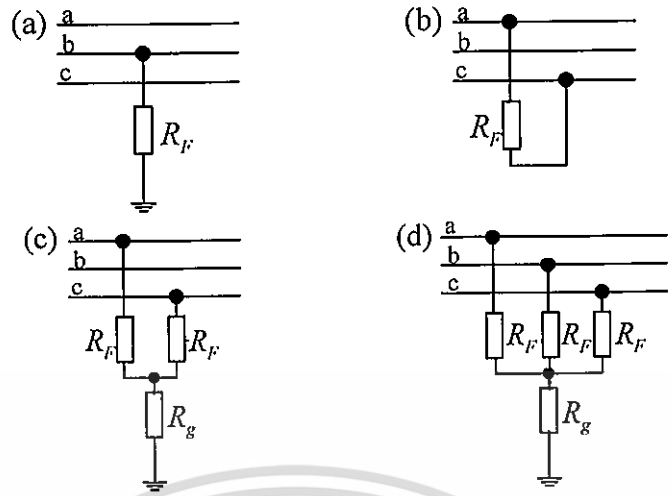

Figure 2.1 Typical shunt faults: (a) single line to ground, (b) double line, (c) double line to ground, and (d) three-phase to ground

2.2 Transmission Line Models

Models of overhead transmission lines are considered in restrictive relation to a certain application. Through different applications, the line models are taken into account in relation to the following criteria:

- Representing a faulted line in the fault location algorithm
- Simulating faults for generating the fault data which is modified in evaluation of the fault location algorithm [9, 10]

The representation of a faulted line in fault location algorithm is addressed in this section. The assumption of the line model is very important to start up the derivation of the fault location algorithm. In general, there are two types of line models:

- Lumped parameter line models
- Distributed parameter line models

2.2.1 Lumped Parameter Line Models

Lumped parameter line models are lines represented by lumped impedance elements. The impedance parameters are calculated using a single frequency, usually the fundamental power frequency. In the simplest lumped parameter model of an overhead line, only the series resistance (R_L) and reactance (X_L) are included as shown in Figure 2.2. Such a model which operated under balanced conditions is considered adequate for representing a short line which is typically less than 80km long [11].

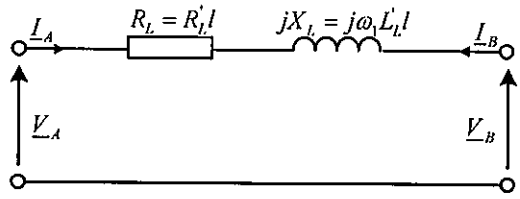

Figure 2.2 Lumped parameter line model

where l is line length, ω_1 is angular fundamental frequency

Under unbalanced conditions, mostly under faults, a three-phase line representation has to be considered. Explicit representation of faulted lines, occurred at the point F, together with equivalent sources behind the line terminal A and B are presented in Figure 2.3(a). Assume as a short transmission line, only series parameters are presented whereas shunt parameters are neglected as illustrated in Figure 2.3(b) [2,7].

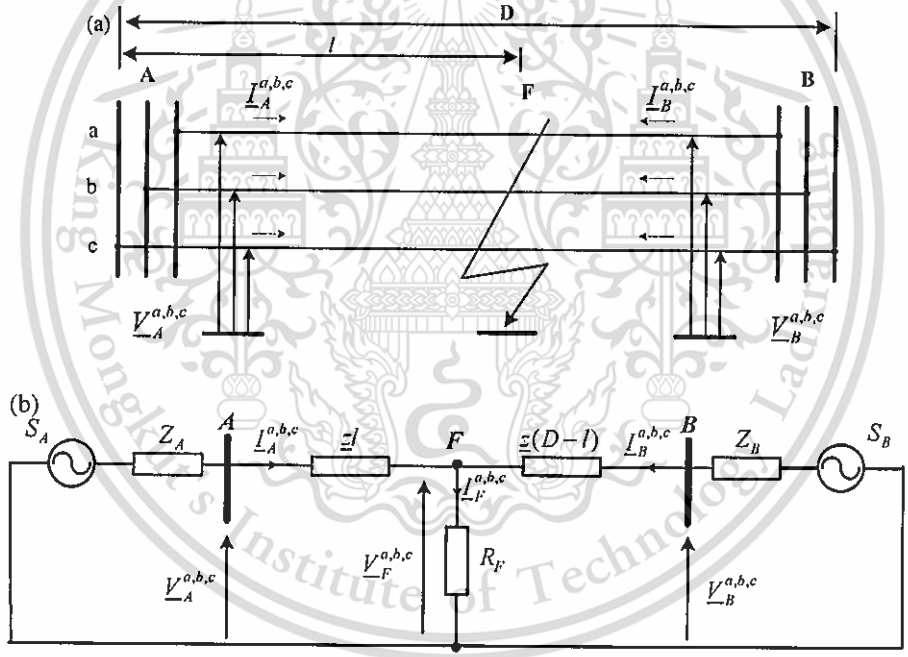

Figure 2.3 (a) Faulted line representation of two terminals transmission line, (b) Circuit diagram of faulted line representation on lumped parameter line model

Generally, line impedance matrix $\underline{z}$ is not symmetrical and identical. To fulfill this, completed transposition of the line is applied by exchanging the conductor positions along the line in order to provide each phase (a, b, and c) occupies each position for one-third of the line length as shown in Figure 2.4.

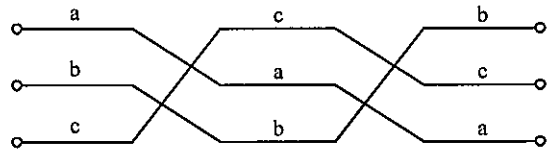

Figure 2.4 Completely transposed section of three-phase line

From this point, the following impedance matrix which contained self-impedances and mutual impedances is currently symmetrical as applied to the completely transposed line.

$$\underline{z} = \begin{bmatrix} \underline{z}_s & \underline{z}_m & \underline{z}_m \\ \underline{z}_m & \underline{z}_s & \underline{z}_m \\ \underline{z}_m & \underline{z}_m & \underline{z}_s \end{bmatrix} \tag{2.1}$$

Self- and mutual impedances can be calculated by the positive- and zero-sequence line impedance as following equations:

$$\underline{z}_s = \frac{\underline{z}_0 + 2\underline{z}_1}{3} \tag{2.2}$$

$$\underline{z}_m = \frac{\underline{z}_0 - \underline{z}_1}{3} \tag{2.3}$$

It is possible to apply the method of symmetrical components which developed by C.L. Fortescue in 1918 to transform phase components to a set of symmetrical components. For instance, the voltages from terminal A can be transformed as:

$$\begin{bmatrix} \underline{V}_{A0} \\ \underline{V}_{A1} \\ \underline{V}_{A2} \end{bmatrix} = \frac{1}{3}\begin{bmatrix} 1 & 1 & 1 \\ 1 & \underline{a} & \underline{a}^2 \\ 1 & \underline{a}^2 & \underline{a} \end{bmatrix}\begin{bmatrix} \underline{V}_{Aa} \\ \underline{V}_{Ab} \\ \underline{V}_{Ac} \end{bmatrix} \tag{2.4}$$

where $\underline{V}_{A0}, \underline{V}_{A1}, \underline{V}_{A2}$ are zero-, positive-, and negative-sequence voltage from side A

$\underline{V}_{Aa}, \underline{V}_{Ab}, \underline{V}_{Ac}$ are voltages from phase a, b, c

$\underline{a} = 1\angle 120° = -0.5 + j0.5\sqrt{3}$ is a complex number with unit magnitude and 120° phase angle

Analogously to Eq. (2.4), the currents from terminal A can be formulated as:

$$\begin{bmatrix} \underline{I}_{A0} \\ \underline{I}_{A1} \\ \underline{I}_{A2} \end{bmatrix} = \frac{1}{3}\begin{bmatrix} 1 & 1 & 1 \\ 1 & \underline{a} & \underline{a}^2 \\ 1 & \underline{a}^2 & a \end{bmatrix}\begin{bmatrix} \underline{I}_{Aa} \\ \underline{I}_{Ab} \\ \underline{I}_{Ac} \end{bmatrix} \tag{2.5}$$

where $\underline{I}_{A0}, \underline{I}_{A1}, \underline{I}_{A2}$ are zero-, positive-, and negative-sequence current from side A

$\underline{I}_{Aa}, \underline{I}_{Ab}, \underline{I}_{Ac}$ are current from phase a, b, c

$\underline{a}$ is defined in Eq. (2.4)

The voltages and currents from terminal B are also transformed as one achieved in Eqs. (2.4) and (2.5), respectively.

2.2.2 Distributed Parameter Line Models

The distributed parameter line models are considered as the characteristic transmission line model which provided more accurate results in the case of medium or long transmission line. This model consists of series *RL* impedance along with shunt admittance. Shunt admittance needs to be taken into account for the leakage current for medium to long transmission lines. The voltages and currents along the line are a function of both the distance *x* and time *t* whose generalized model is depicted in the figure below.

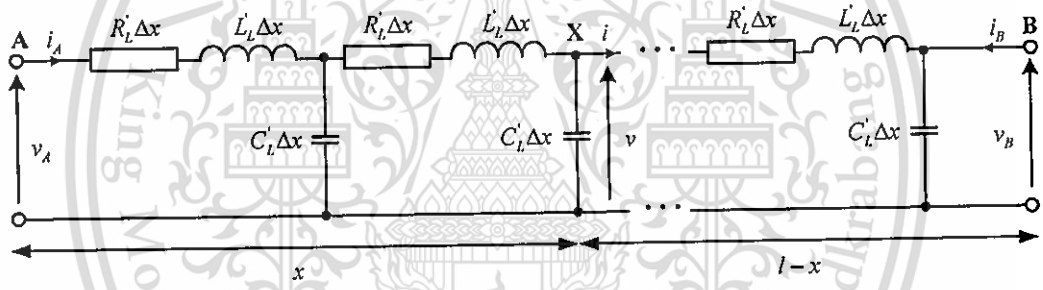

Figure 2.5 Generalized distributed parameter line model

The equivalent π circuit illustrated in Figure 2.6 is applied more commonly for impedance-based fault location algorithm since the distributed parameter line model can be used in phasors as well.

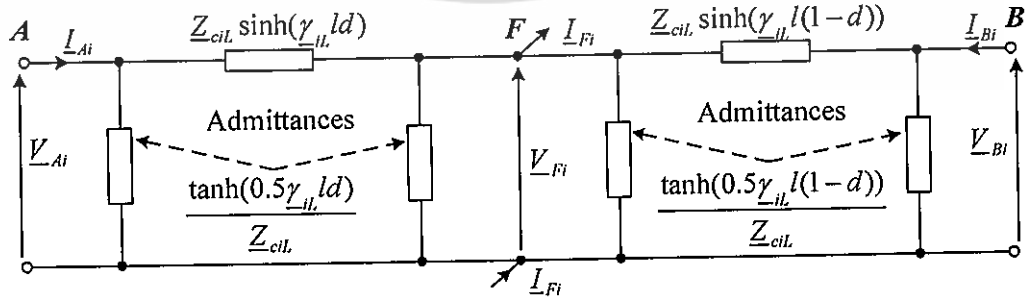

Figure 2.6 Distributed parameter line model for i[th] symmetrical components of faulted line

The presented algorithm in this model is also designed for the fully transposed line as the case using lumped line model. Both the series impedances and shunt admittances are expressed using:

- Surge impedance of line for the ith sequences

$$\underline{Z}_{ci} = \sqrt{\frac{\underline{Z}'_{iL}}{\underline{Y}'_{iL}}} \tag{2.6}$$

where $\underline{Z}'_{iL} = R'_{iL} + j\omega_1 L'_{iL}$ impedance of line for the ith symmetrical component (Ω/km)

$\underline{Y}'_{iL} = G'_{iL} + j\omega_1 C'_{iL}$ admittance of line for the ith symmetrical component (S/km)

$R'_{iL}, L'_{iL}, G'_{iL}, C'_{iL}$ resistance, inductance, conductance, and capacitance of line per kilometer length

- Propagation constant of the line for the ith sequence

$$\underline{\gamma}_{ci} = \sqrt{\underline{Z}'_{iL}\underline{Y}'_{iL}} \tag{2.7}$$

where $\underline{Z}'_{iL}, \underline{Y}'_{iL}$ are defined in Eq. (2.6)

2.3 Time-Frequency Domain Transformation

Voltage and current waveforms are considered as the input to process the symmetrical components based on the phasors concept. They were derived on an assumption that the post-fault state can be considered as a steady-state one. As a result, fault voltages and currents are represented in a form of sinusoidal waveforms. Unfortunately, there are some processes in which containing the DC components with different frequency. Thus, this process is specifically considered in term of transforming the voltage and current waveforms from the time domain to fundamental frequency domain.

2.3.1 Fast Fourier Transform

This section provides only the concepts of the need of using FFT while explicit equations of the determination of fundamental phasors i.e. real part, imaginary part, and phase angle of the fundamental phasor are not included here. FFT is very sensitive to filter the measured signals by coding in Matlab.

When a fault occurs, the voltage and current waveforms become severely distorted due to the presence of higher harmonics and a significant decaying DC

component [12]. The presence of higher harmonics makes the fast estimation of fundamental phasor quantities be very difficult and ultimately affects the performance of the fault location algorithm. The speed and accuracy of which the phasors are calculated play an important role in fast fault locating. Since both algorithms proposed here does not consider to the quality of the phasors' determination, it is known that FFT approach is sensitive to decaying DC components in the fault current. On the other hand, other methods such as an optimal estimation theory [13] can also be used to extract the unknown phasors.

2.3.2 Analog Anti-aliasing Filters Built-in Function in Matlab

Most A/D converters are preceded by a filter that removes frequency components which are beyond its range. In actual practice, sampling is usually higher to provide some margin and make the filtering requirements less critical. The sampling rate must be greater than or equal to two times the highest frequency component in the input signals. If this rule is violated, unwanted signals appear in the frequency band of interest. When selecting a filter, the goal is to provide a cutoff frequency that removes undesired signals from the A/D converter input or at least attenuates them to the point that they do not adversely affect the circuit. An anti-aliasing filter is a low-pass filter that accomplishes this.

In this research, a method of selection and designing filters is not taken into account. The proposed fault location algorithm utilizing synchronized measurement is not considered to apply to analog anti-aliasing filter since it is modeled as the short transmission line which is not adversely affected by shunt capacitances. However, second order Butterworth analog anti-aliasing filters with the cutoff frequency 500 Hz which corresponds to 10^{th} harmonic were applied by built-in function in Matlab to filter the secondary signals of the proposed fault location algorithm utilizing unsynchronized measurement. This is due to the proposed algorithm is considered on the distributed parameter modeled on the long transmission line.

2.4 Existing Fault Location Schemes

Fault location on the transmission line is an attractive and desirable feature in any protection scheme. The advantage is that it was designed to pinpoint the exact location where the fault took place while distance relays installed for protection of transmission line are able to furnish some information on the general area. It does not need to be monitored online on the calculation of the fault distance since it can be performed offline from the recorded data. Fault location algorithm that utilized two-end measurement can have signal data fed from either synchronized sampling

or unsynchronized digital fault recorders, generally known as phasor measurement units (PMUs).

Numerous fault location algorithms have been elaborated and can be broadly categorized as:

- Procedures based on the fundamental frequency voltages and currents, generally known as an impedance-base principle.
- Time-domain based procedures such as traveling wave fault locators
- Non-conventional fault locating procedures such as those based on Artificial Neural Networks (ANNs) [14].

The most popular and widely used in real applications refers to the fundamental frequency based fault location procedures whereas the processes based on travelling-wave are typically more costly due to the high sampling rate requirements.

2.4.1 Review on the Existing Fault Location Algorithms Utilizing Two-End Synchronized Measurement without Line Parameter Requirement

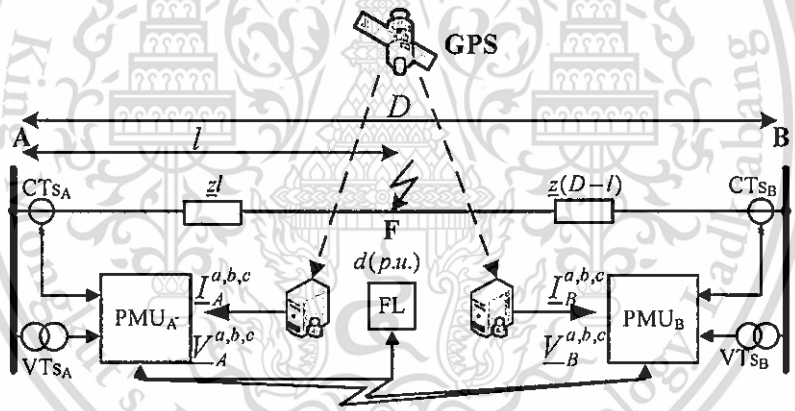

Figure 2.7 Representative diagram of two-end synchronized measurement with the aid of GPS for fault location

Two-end synchronized measurement in Figure 2.7 means a common time reference of the synchronization angle from both terminals is facilitated by the aid of Global Positioning System (GPS). Synchronized sampling of data from both terminals makes the procedures of locating fault to be simple and accurate. Modern PMUs based on GPS can reportedly achieve synchronization accuracy of ±0.5 μs [15].

One-end measurement compared to two-end measurement offer less computation and complexity, but the accurate resulted provided by those algorithms is affected by line loading, fault resistance, and un-transposed line [16,

17]. Thus, two-end fault location algorithms have been proposed with the aim of overcoming the limitations of the one-end fault location techniques and improving the fault location accuracy.

Line parameter elements are only approximately constant which may vary by line loading and weather condition. References [18-20] were proposed to calculate the fault location by synchronized sampling. The disadvantage in these algorithms is the need of line parameters and line length which needed to locate the fault distance. This affected the accuracy due to the uncertainty of the line parameters. However, due to these reasons, other algorithms in [21, 22] proposed without any knowledge of line parameters. These two methods were operated with unsynchronized data sampling by applying the iterative technique to find the distance of line-line fault, but it cannot be used to locate the three-phase fault.

Although the two algorithms stated above have done effectively, the first proposed algorithm in this thesis can be used to locate all fault types without line parameter requirement. Detailed derivation of this algorithm is provided explicitly in Chapter 3.

2.4.2 Review on the Existing Fault Location Algorithms Utilizing Two-End Unsynchronized Measurement

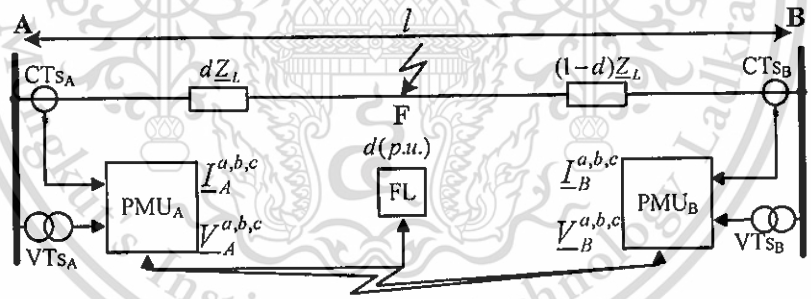

Figure 2.8 Representative diagram of two-end unsynchronized measurement for fault location

Performing synchronized measurement results highly accurate, but the fact remains that GPS assists PMUs are still not as widely adopted as they could be due to economic considerations. In turn, unsynchronized measurement for fault locating in Figure 2.8 appears more attractive in case GPS-based synchronization mechanism is unavailable. Data measurements performed asynchronously do not have a common time reference and consequently, the sampling instants at point A and B

do not coincide. As a result of the mismatched sampling instants, a certain phase shift, δ, exists between the waveforms recorded by the PMUs on either end.

In order to overcome this method, a common time reference has to be identified by accomplishing the analytical synchronization. Conventional analysis on the synchronization operator, which is really needed in the second proposed algorithm, is calculated iteratively [21, 23]. In [24] were developed to avoid such iteration, but the stage of improving the precision of the presented algorithm with considering distributed parameter line model still needed iterative calculation. New algorithm in [25] was integrated to completely avoid iteration, but the determination of the unknown synchronization operator has to be separated between balanced and unbalanced fault. Moreover, the procedure of selecting the valid solution is not reached for all studied cases and continued to another step by comparing the determined synchronization angles with the unique solution of synchronization angle obtained by using the lump line model.

The second proposed algorithm in this thesis is to refine and validate the method for analytical synchronization corresponding to all fault types by taking into account the distributed parameter line model to ensure the high accuracy of the fault location algorithm. Detailed derivation of this algorithm is provided explicitly in Chapter 3.

2.5 Fault Location Error

2.5.1 Accuracy of Fault Location

The definition for the fault location error is given as follows [2]:

$$error(\%) = \frac{|d - d_{actual}|}{l} 100\% \tag{2.8}$$

where d, d_{actual} are the estimated and actual distance to the fault (km or p.u.)

l total line length (km or p.u.)

2.5.2 Factors Affected on the Accuracy of Fault Location

To improve the fault location estimation, it is critical to eliminate, or at least to reduce errors possible for the considered method. It is worth to point out that a particular factor affecting fault location accuracy has to be considered carefully in relation to the analyzed method. Different factors affect the accuracy of fault location method can be listed as follows:

- Inaccurate compensation for the reactance effect in the case of fault location algorithm providing by one-end measurement.

- Inaccurate fault types identification
- Inaccurate line parameters which do not match the actual parameters. Even if the geometry of line conductors is accurately taken for calculating the line impedances, the total line length could be known with some error.
- The uncertainty of the line parameters, specifically for the zero-sequence impedance. This impedance is affected by a soil resistivity, which may be variable under the whole line route, and it is also dependent on weather conditions.
- The insufficient accuracy of the line model in case un-transposed lines are represented as being transposed and line shunt capacitance is not considered.
- The presence of shunt reactors and capacitors or series capacitor compensating devices equipped with metal oxide varistors (MOVs).
- Load-flow unbalance.
- Errors of current and voltage instrument transformers and unfaithful reproduction of the primary signals due to their limited bandwidth.
- Insufficient sampling frequency and bit resolution of A/D system.

2.6 Summary

Considered fault types which may occur on the transmission line are specifically collected and modeled with different modeling i.e. lumped parameter model and distributed parameter line model on two terminals based on synchronized and unsynchronized measurement, respectively. It begins with the right configuration of the proposed algorithm which its models are very important in designing the fault location algorithms. Once the models are made, the method of extraction the input signals is applied to get the fundamental frequency which analyzes every single point or sample of the measured signals. Every concept on how it involves in the proposed algorithm is presented in this chapter and factors affecting the fault location method is a certain problem which should be more consider on eliminating or minimizing.

CHAPTER 3

SYSTEM MODELING AND DETAILED ALGORITHM DERIVATIONS

In this chapter, the solution to the statement of the problems is modeled as a fault location algorithm which classified separately in two different methods. The mathematical models for the proposed algorithms are intended to make the assumption on using synchronized and unsynchronized three-phase voltages and currents from two terminals. Detailed derivation of the proposed algorithms is now formulated in this chapter.

3.1 None Line Parameter Requirement for Fault Location Algorithm Utilizing Two-End Synchronized Measurement

In this section, the proposed algorithm for fault location without line parameter requirement will be presented. Thus, unbalanced and balanced three-phase fault solution will be derived explicitly.

3.1.1 Derivation of Locating Unbalanced Fault

The considered fault location on two terminals of the transmission line is already presented schematically in Figure 2.3(a) in Chapter 2. Unbalanced faults such as single line to ground (SLG), double line (DL), and double line to ground (DLG) were assumed to occur on the overhead transmission line. The fault location is denoted by F, the fault distance (as measured from terminal A) by l, D is the total line length, and subscripts A and B represented as Terminal A and B of the line, respectively. Voltages ($\underline{V}_A^{a,b,c}$ and $\underline{V}_B^{a,b,c}$) and currents ($\underline{I}_A^{a,b,c}$ and $\underline{I}_B^{a,b,c}$) are synchronously measured at both line terminals.

Assuming that the transmission line is considered as a short line which is less than 100 km long, so the shunt capacitance and the shunt conductance can be neglected.

The proposed algorithm is designed for fault distance on a fully transposed single transmission line which has identical line impedance, so symmetrical components appear to be sufficient to fulfill the aim of this presented algorithm. Zero-sequence is not beneficial to consider due to its uncertain impedance data. Consequently, the unbalanced three-phase circuit using lumped parameter line

model from Figure 2.3(b) can be represented by three equivalent circuits as the positive-, negative-, and zero-sequence circuit. As mentioned, only positive- and negative-sequence circuits which contained identical impedance will be used as depicted in Figure 3.1, respectively.

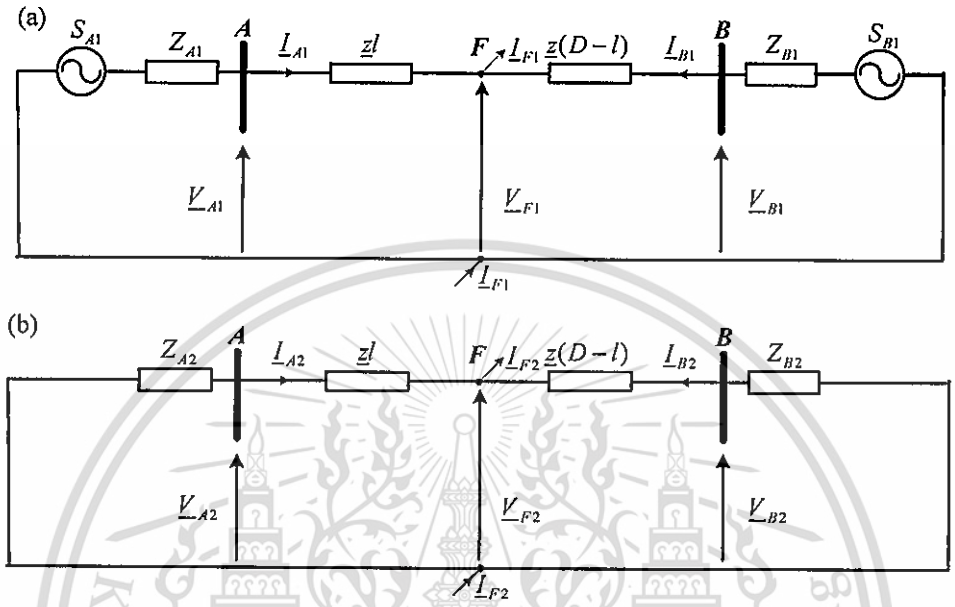

Figure 3.1 Equivalent circuit of single-circuit faulted line (a) positive-sequence and (b) negative-sequence

From figure above, following equations can be expressed as [26]:

$$\underline{V}_{A1} - \underline{zl}\,\underline{I}_{A1} = \underline{V}_{B1} - \underline{z}(D-l)\underline{I}_{B1} \tag{3.1}$$

$$\underline{V}_{A2} - \underline{zl}\,\underline{I}_{A2} = \underline{V}_{B2} - \underline{z}(D-l)\underline{I}_{B2} \tag{3.2}$$

where $\underline{V}_{A1}, \underline{V}_{B1}, \underline{I}_{A1}, \underline{I}_{B1}$ are the positive-sequence voltages and currents in phasor quantities from both terminals

$\underline{V}_{A2}, \underline{V}_{B2}, \underline{I}_{A2}, \underline{I}_{B2}$ are the negative-sequence voltages and currents in phasor quantities from both terminals

$\underline{z}$ is the identical positive- and negative line impedance

Obviously, Eqs. (3.1) and (3.2) have two unknown terms $\underline{zl}$ and $\underline{z}(D-l)$, and it is sufficient to be determined as two unknown variables with two equations provided. Then the unknown terms give two formulae as follows:

$$\underline{zl} = \frac{(\underline{V}_{A1} - \underline{V}_{B1})\underline{I}_{B2} - (\underline{V}_{A2} - \underline{V}_{B2})\underline{I}_{B1}}{\underline{I}_{A1}\underline{I}_{B2} - \underline{I}_{A2}\underline{I}_{B1}} \tag{3.3}$$

$$\underline{z}(D-l)=\frac{(\underline{V}_{A1}-\underline{V}_{B1})\underline{I}_{A2}-(\underline{V}_{A2}-\underline{V}_{B2})\underline{I}_{A1}}{\underline{I}_{A1}\underline{I}_{B2}-\underline{I}_{A2}\underline{I}_{B1}} \tag{3.4}$$

The distance to fault l can be expressed as the percentage of the total line length D by the following expression:

$$l\%=\frac{l}{D}100 \tag{3.5}$$

The stated expression can be formed as below:

$$l\%=\frac{\underline{z}l}{\underline{z}l+\underline{z}(D-l)}100 \tag{3.6}$$

Finally, by including Eqs. (3.3) and (3.4) into Eq. (3.6), the distance to fault can be calculated through the following formula:

$$l\%=\frac{(\underline{V}_{A1}-\underline{V}_{B1})\underline{I}_{B2}-(\underline{V}_{A2}-\underline{V}_{B2})\underline{I}_{B1}}{(\underline{V}_{A1}-\underline{V}_{B1})(\underline{I}_{A2}+\underline{I}_{B2})-(\underline{V}_{A2}-\underline{V}_{B2})(\underline{I}_{A1}+\underline{I}_{B1})} \tag{3.7}$$

Based on the explicit formula above which located the unbalanced fault on the transmission line, the distance to a fault can be obviously obtained without any information of line parameters. Flexible solutions can be obtained if the developed fault location algorithm is not involved with line parameter information.

Basically, it is just needed the processing of the synchronously recorded voltage and current waveforms from both line terminals, identifying their phasor quantities of the fundamental frequency 50 Hz, and determining the positive- and negative- sequence voltage and current components. Then fault location can be calculated precisely which makes this algorithm appear to be simple, accurate, and robust.

3.1.2 Derivation of Locating Balanced Three-Phase Fault

Theoretically, the fault currents and voltages are identical along the three phases during a balanced three-phase fault. It is totally sufficient to use only positive-sequence components in the developed algorithm respected with this fault type. The positive-sequence equivalent circuit is presented in Figure 3.2 which $\underline{V}_F$ represents the fault voltage and R_F is the fault resistance.

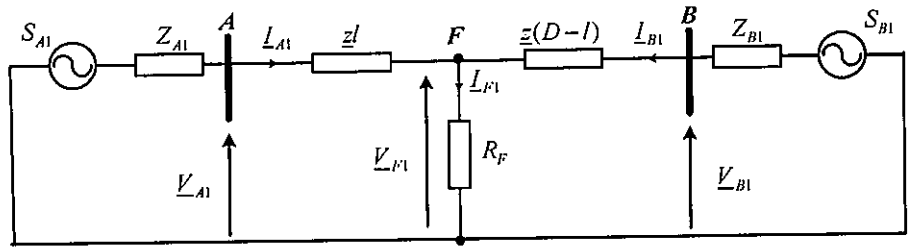

Figure 3.2 Positive-sequence equivalent circuit of single-circuit faulted line

As stated previously, the positive-sequence equivalent circuit illustrated in Figure 3.2 can be written as follows [26]:

$$\underline{V}_{A1} - \underline{z}l\underline{I}_{A1} - \underline{V}_{F1} = 0 \tag{3.8}$$

$$\underline{V}_{B1} - \underline{z}(D-l)\underline{I}_{B1} - \underline{V}_{F1} = 0 \tag{3.9}$$

$$\underline{V}_{F1} = R_F(\underline{I}_{A1} + \underline{I}_{B1}) \tag{3.10}$$

Substituting Eq. (3.10) into Eqs. (3.8) and (3.9) gives two following equations:

$$\underline{z}l = \frac{\underline{V}_{A1}}{\underline{I}_{A1}} - \frac{\underline{I}_{A1} + \underline{I}_{B1}}{\underline{I}_{A1}} R_F \tag{3.11}$$

$$\underline{z}(D-l) = \frac{\underline{V}_{B1}}{\underline{I}_{B1}} - \frac{\underline{I}_{A1} + \underline{I}_{B1}}{\underline{I}_{B1}} R_F \tag{3.12}$$

In this step, the unknown terms reveal with the fault resistance R_F. First, R_F need to be determined in order to find the unknown collinear vectors $\underline{z}l$ and $\underline{z}(D-l)$. Thus, Eqs. (3.11) and (3.12) can be represented in the compact form as follows:

$$\underline{z}l = a_{re} + ja_{im} + (b_{re} + jb_{im})R_F \tag{3.13}$$

$$\underline{z}(D-l) = c_{re} + jc_{im} + (d_{re} + jd_{im})R_F \tag{3.14}$$

where $a_{re} = \mathrm{Re}\left[\frac{\underline{V}_{A1}}{\underline{I}_{A1}}\right]$, $a_{im} = \mathrm{Im}\left[\frac{\underline{V}_{A1}}{\underline{I}_{A1}}\right]$, $b_{re} = \mathrm{Re}\left[-\frac{\underline{I}_{A1} + \underline{I}_{B1}}{\underline{I}_{A1}}\right]$, $b_{im} = \mathrm{Im}\left[-\frac{\underline{I}_{A1} + \underline{I}_{B1}}{\underline{I}_{A1}}\right]$

$c_{re} = \mathrm{Re}\left[\frac{\underline{V}_{B1}}{\underline{I}_{B1}}\right]$, $c_{im} = \mathrm{Im}\left[\frac{\underline{V}_{B1}}{\underline{I}_{B1}}\right]$, $d_{re} = \mathrm{Re}\left[-\frac{\underline{I}_{A1} + \underline{I}_{B1}}{\underline{I}_{B1}}\right]$, $d_{im} = \mathrm{Im}\left[-\frac{\underline{I}_{A1} + \underline{I}_{B1}}{\underline{I}_{B1}}\right]$

Eqs. (3.13) and (3.14) can be grouped their real and imaginary parts separately, so the following expressions hold:

$$\underline{z}l = (a_{re} + b_{re}R_F) + j(a_{im} + b_{im}R_F) \tag{3.15}$$

$$\underline{z}(D-l) = (c_{re} + d_{re}R_F) + j(c_{im} + d_{im}R_F) \tag{3.16}$$

Collinear vectors $\underline{z}l$ and $\underline{z}(D-l)$ lie in the first quadrant of the complex plane in which their real and imaginary parts must be greater than zero and can be transformed into a polar form as they are determined by a vector magnitude and its angle θ. From Eqs. (3.15) and (3.16) the angle θ, which must be located in the range 0-90°, can be determined as expressed in the following formulae:

$$\tan\theta = \frac{a_{im} + b_{im}R_F}{a_{re} + b_{re}R_F} \tag{3.17}$$

$$\tan\theta = \frac{c_{im} + d_{im}R_F}{c_{re} + d_{re}R_F} \tag{3.18}$$

Next, single unknown R_F will be determined by combining Eqs. (3.17) and (3.18) together and used the determined R_F to solve the unknown collinear vectors by the following expression:

$$\frac{a_{im} + b_{im}R_F}{a_{re} + b_{re}R_F} = \frac{c_{im} + d_{im}R_F}{c_{re} + d_{re}R_F} \tag{3.19}$$

It is obvious that from Eq. (3.19) the quadratic equation which solves R_F can be formulated:

$$R_F^2 + mR_F + n = 0 \tag{3.20}$$

where $m = \dfrac{a_{im}d_{re} + b_{im}c_{re} - a_{re}d_{im} - b_{re}c_{im}}{b_{im}d_{re} - b_{re}d_{im}}$

$$n = \frac{a_{im}c_{re} - a_{re}c_{im}}{b_{im}d_{re} - b_{re}d_{im}}$$

Basically, two solutions are obtained from the quadratic equation (3.20):

$$(R_F)_1 = \frac{-m + \sqrt{m^2 - 4n}}{2} \tag{3.21}$$

$$(R_F)_2 = \frac{-m - \sqrt{m^2 - 4n}}{2} \tag{3.22}$$

It is unable to identify the real value of R_F. To perform it, one needed to identify the value of phase angle θ by substituting $(R_F)_1$ and $(R_F)_2$ into Eq. (3.17) which gives the following expressions for phase angle θ:

$$\theta_1 = \arctan \frac{a_{im} + b_{im}(R_F)_1}{a_{re} + b_{re}(R_F)_1} \tag{3.23}$$

$$\theta_2 = \arctan \frac{a_{im} + b_{im}(R_F)_2}{a_{re} + b_{re}(R_F)_2} \tag{3.24}$$

To discriminate the valid solution for angle θ, the value which lies in the first quadrant of the complex plane and the one which is closer to the typical value of the line characteristic (e.g. 80°) should be selected. Thus, the fault resistance R_F corresponding to the selected angle should be selected as the valid solution as well. In the case in which one of the determined fault resistance lies in a quadrant other than the first quadrant, then the other fault resistance is definitely the valid one.

Finally, the selected fault resistance would be included back into Eqs. (3.15) and (3.16). Then substitute them into Eq. (3.6) where this equation is also used in this fault type and already stated in Derivation of Proposed Unbalanced Fault Locating section in order to express the distance to fault in the percentage of the total line length. Consequently, the unknown distance to fault for balanced three-phase fault can be calculated through the following formula:

$$l\% = \frac{(a_{re} + b_{re}(R_F)_i) + j(a_{im} + b_{im}(R_F)_i)}{(a_{re} + b_{re}(R_F)_i) + j(a_{im} + b_{im}(R_F)_i) + (c_{re} + d_{re}(R_F)_i) + j(c_{im} + d_{im}(R_F)_i)} 100 \tag{3.25}$$

where i index representing both solutions of the fault resistance which need to be determined prior to the selecting and substituting in Eq. (3.25)

The presented algorithm has the advantage that it does not require rigorous procedures for determining the fault type or affected phase. For this algorithm, it is sufficient to differentiate between balanced and unbalanced fault which can be achieved by checking whether there is a separation of phase currents for 120°. This feature makes the proposed algorithm robust and flexible.

3.1.3 Flowchart of Proposed Algorithm Based on Two-End Synchronized Measurement

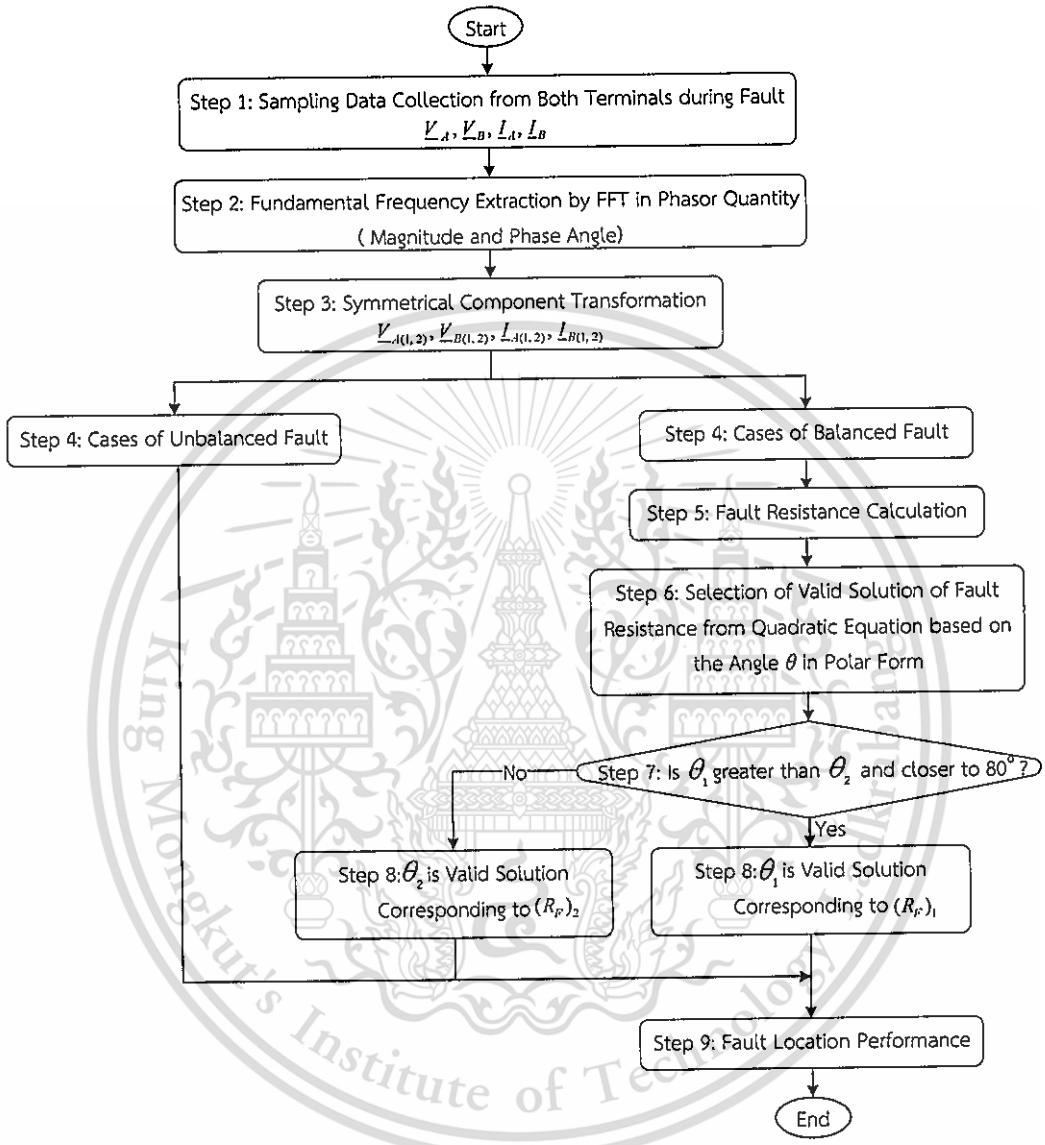

Figure 3.3 Flowchart of proposed algorithm based on two-end synchronized measurement

3.2 Fault Location Algorithm on Long Transmission Line Utilizing Two-End Unsynchronized Measurement

In this section, the second proposed fault location algorithm is derived. Single developed fault location algorithm is presented without identifying the affected phases or selecting the fault types. This makes this algorithm more flexible, robust, and at the same time highly accurate in locating all considered fault types.

3.2.1 Prominent Formula for Locating All Considered Fault Types

Considered two-end unsynchronized measurement diagram for faulted point on the transmission line is already presented in Figure 2.8 in Chapter 2. Current transformers (CTs_A, CTs_B) and voltage transformers (VTs_A, VTs_B) are put at both terminals (A, B) to transform the signals to phasor measurement units (PMUs) in order to get currents ($\underline{I}_A^{a,b,c}, \underline{I}_B^{a,b,c}$) and voltages ($\underline{V}_A^{a,b,c}, \underline{V}_B^{a,b,c}$) in phasor quantities which are the inputs for fault locator device (FL). These PMUs are not associated with GPS, so this kind of measurement was considered as unsynchronized due to no common time reference.

The proposed algorithm is implemented for fault distance on the fully transposed transmission line, so symmetrical components appear to be sufficient to fulfill the aim of this presented algorithm. Zero-sequence is not beneficial to consider due to its uncertain impedance data. Theoretically, according to the sequence component mathematical manipulation, negative-sequence does not contain in the three-phase fault. However, in practice, a perfectly balanced system does not exist. Even if the system is 100% balanced, it does not mean that negative- and zero-sequence do not exist.

In [25] proposed the use of incremental positive-sequence, which is obtained by subtracting the pre-fault quantities from fault quantities, instead of negative-sequence in the case of the determination of synchronization operator in balanced three-phase fault. It is worth to notice that the pre-fault signal is not always in the form of pure sinusoids since the indication of the appearing fault can be observed just before fault occurrence [24]. Thus, the consideration of using the incremental positive-sequence in such cases is unnecessary.

Due to these reasons, positive- and negative-sequence were assumed to be presented in all fault types in order to reduce the manipulation of the determination of the synchronization operator. Therefore, distance to faulted point can be obtained without performing fault type selection of affected phase. The distributed parameter line model utilized with correction factors for symbolizing series and shunt parameter is considered in the equivalent circuit of faulted line for positive- and negative-sequence as presented in Figure 3.4.

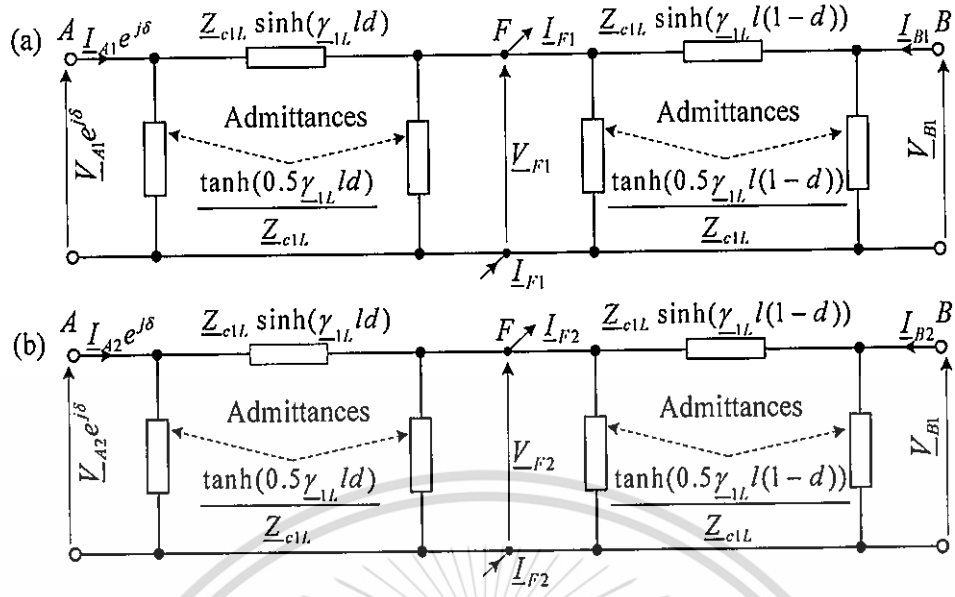

Figure 3.4 Distributed parameter line model of faulted line for (a) positive-sequence and (b) negative-sequence

Since fully transposed overhead line contains the identical impedance and admittance parameters for the positive- and negative-sequence, the surge impedance ($\underline{Z}_{c1L}$) and the propagation constant ($\underline{\gamma}_{1L}$) are also uniform, and positive-sequence is significantly used as shown in Figure 3.4. The voltage and current phasors from terminal B are supposed as the base, whereas those from terminal A are multiplied with the determined synchronization operator ($e^{j\delta}$) where δ is the synchronization angle.

After performing the analytical synchronization with the determined synchronization operator, it would be clearly stated that such measurements become synchronized and then fault distance can be located precisely as the cases of using synchronized measurement by applying the prominent formula [27] in term of positive-sequence as expressed in Eq. (3.26). However, this formula can also perform with negative-sequence.

$$d = \frac{1}{\underline{\gamma}_{1L}}\tanh^{-1}\left(\frac{\underline{V}_{B1}\cosh(\underline{\gamma}_{1L}l) - \underline{Z}_{c1L}\underline{I}_{B1}\sinh(\underline{\gamma}_{1L}l) - \underline{V}_{A1}^{syn.}}{\underline{V}_{B1}\sinh(\underline{\gamma}_{1L}l) - \underline{Z}_{c1L}\underline{I}_{B1}\cosh(\underline{\gamma}_{1L}l) - \underline{Z}_{c1L}\underline{I}_{A1}^{syn.}}\right) \tag{3.26}$$

where $\underline{V}_{A1}^{syn.} = \underline{V}_{A1}e^{j\delta}$ synchronized positive-sequence voltage phasor at terminal A

$\underline{I}_{A1}^{syn.} = \underline{I}_{A1}e^{j\delta}$ synchronized positive-sequence current phasor at terminal A

$e^{j\delta} = \cos(\delta) + j\sin(\delta)$	synchronization operator to be determined
$\underline{Z}_{c1L} = \sqrt{\underline{Z}'_{1L} / \underline{Y}'_{1L}}$	positive-sequence surge impedance
$\underline{\gamma}_{1L} = \sqrt{\underline{Z}'_{1L}\underline{Y}'_{1L}}$	positive-sequence propagation constant
$\underline{Z}'_{1L}$	positive-sequence line impedance (Ω/km)
$\underline{Y}'_{1L}$	positive-sequence line admittance (S/km)
$\underline{V}_{B1}$, $\underline{I}_{B1}$	positive-sequence voltage and current phasors at terminal B
d	distance from terminal A to faulted point F (p.u.)
l	total transmission line length (km)

3.2.2 Determination of the Synchronization Operator

Through the consideration of the distributed parameter line model of faulted line in Figure 3.4, the positive-sequence voltages corresponded to the faulted point F seen from both terminals with superscript A and B can be written as [25]:

$$\underline{V}^{A}_{F1} = \underline{V}_{A1} e^{j\delta} \cosh(\underline{\gamma}_{1L} l d) - \underline{Z}_{c1L} \underline{I}_{A1} e^{j\delta} \sinh(\underline{\gamma}_{1L} l d) \tag{3.27}$$

$$\underline{V}^{B}_{F1} = \underline{V}_{B1} \cosh(\underline{\gamma}_{1L} l(1-d)) - \underline{Z}_{c1L} \underline{I}_{B1} \sinh(\underline{\gamma}_{1L} l(1-d)) \tag{3.28}$$

The following trigonometric identities from Eq. (3.28) can be expressed as:

$$\cosh(\underline{\gamma}_{1L} l(1-d)) = \cosh(\underline{\gamma}_{1L} l)\cosh(\underline{\gamma}_{1L} l d) - \sinh(\underline{\gamma}_{1L} l)\sinh(\underline{\gamma}_{1L} l d) \tag{3.29}$$

$$\sinh(\underline{\gamma}_{1L} l(1-d)) = \sinh(\underline{\gamma}_{1L} l)\cosh(\underline{\gamma}_{1L} l d) - \cosh(\underline{\gamma}_{1L} l)\sinh(\underline{\gamma}_{1L} l d) \tag{3.30}$$

After the rearrangement by providing Eqs. (3.29) and (3.30) into Eq. (3.28), the following equation was obtained as:

$$\underline{V}^{B}_{F1} = \underline{A}_1 \cosh(\underline{\gamma}_{1L} l d) + \underline{B}_1 \sinh(\underline{\gamma}_{1L} l d) \tag{3.31}$$

where $\underline{A}_1 = \underline{V}_{B1} \cosh(\underline{\gamma}_{1L} l) - \underline{Z}_{c1L} \underline{I}_{B1} \sinh(\underline{\gamma}_{1L} l)$

$\underline{B}_1 = -\underline{V}_{B1} \sinh(\underline{\gamma}_{1L} l) + \underline{Z}_{c1L} \underline{I}_{B1} \cosh(\underline{\gamma}_{1L} l)$

By comparing $\underline{V}^{A}_{F1} = \underline{V}^{B}_{F1}$ which corresponded to Eq. (3.27) equal Eq. (3.31), the following equation is represented as:

$$(\underline{C}_1 e^{j\delta} - \underline{A}_1)\cosh(\underline{\gamma}_{1L} l d) + (\underline{D}_1 e^{j\delta} - \underline{B}_1)\sinh(\underline{\gamma}_{1L} l d) = 0 \tag{3.32}$$

where $\underline{A}_1, \underline{B}_1$ are defined in Eq. (3.31)

$$\underline{C}_1 = \underline{V}_{A1}$$

$$\underline{D}_1 = -\underline{Z}_{c1L}\underline{I}_{A1}$$

Once the positive-sequence was derived in Eq. (3.32), the analogous equation for negative-sequence was obtained by:

$$(\underline{C}_2 e^{j\delta} - \underline{A}_2)\cosh(\underline{\gamma}_{1L} ld) + (\underline{D}_2 e^{j\delta} - \underline{B}_2)\sinh(\underline{\gamma}_{1L} ld) = 0 \tag{3.33}$$

where $\underline{A}_2 = \underline{V}_{B2}\cosh(\underline{\gamma}_{1L} l) - \underline{Z}_{c1L}\underline{I}_{B2}\sinh(\underline{\gamma}_{1L} l)$

$$\underline{B}_2 = -\underline{V}_{B2}\sinh(\underline{\gamma}_{1L} l) + \underline{Z}_{c1L}\underline{I}_{B2}\cosh(\underline{\gamma}_{1L} l)$$

$$\underline{C}_2 = \underline{V}_{A2}$$

$$\underline{D}_2 = -\underline{Z}_{c1L}\underline{I}_{A2}$$

As stated, only positive- and negative-sequence are sufficient to determine the synchronization operator. Thus, Eqs. (3.32) and (3.33) are combined to form the equation as follows:

$$(\underline{C}_1 e^{j\delta} - \underline{A}_1)(\underline{D}_2 e^{j\delta} - \underline{B}_2) - (\underline{D}_1 e^{j\delta} - \underline{B}_1)(\underline{C}_2 e^{j\delta} - \underline{A}_2) = 0 \tag{3.34}$$

where $\underline{A}_1, \underline{B}_1, \underline{C}_1, \underline{D}_1$ are defined in Eqs. (3.31) and (3.32)

$\underline{A}_2, \underline{B}_2, \underline{C}_2, \underline{D}_2$ are defined in Eq. (3.33)

From Eq. (3.34), the synchronization operator is obviously determined by solving the quadratic equation in complex form as bellows:

$$\underline{E}(e^{j\delta})^2 + \underline{F}e^{j\delta} + \underline{G} = 0 \tag{3.35}$$

where $\underline{E} = \underline{C}_1\underline{D}_2 - \underline{D}_1\underline{C}_2$

$$\underline{F} = \underline{D}_1\underline{A}_2 + \underline{B}_1\underline{C}_2 - \underline{C}_1\underline{B}_2 - \underline{A}_1\underline{D}_2$$

$$\underline{G} = \underline{A}_1\underline{B}_2 - \underline{B}_1\underline{A}_2$$

in which $\underline{A}_1, \underline{B}_1, \underline{C}_1, \underline{D}_1$ are defined in Eqs. (3.31) and (3.32)

$\underline{A}_2, \underline{B}_2, \underline{C}_2, \underline{D}_2$ are defined in Eq. (3.33)

Basically, two solutions are acquired by the quadratic equation. To distinguish the real value of synchronization operator, the crucial selection was provided in order to perform the analytical synchronization in the next section.

3.2.3 Selection of Valid Solution for the Determined Synchronization Operator

To select the valid solution is to clearly discriminate the magnitude of the determined synchronization operators. One is rejected if its magnitude is not close to unity.

$$(1-\varepsilon) > \left| e^{j\delta_i} \right| > (1+\varepsilon) \tag{3.36}$$

where ε error margin, which is considered as the tolerance of the possible error in synchronization operator determination

i an index representing both solutions of the synchronization operator in which contains the synchronization angle

The possibility in error margin $\varepsilon = 0.01$ was applied in the evaluation section to declare the effectiveness of the proposed method. It is fact that Euler equation provides:

$$e^{j\delta} = \cos(\delta) + j\sin(\delta) \approx 1 \quad (\delta \; close \; to \; 0) \tag{3.37}$$

It is obvious that once the valid solution of the determined synchronization operator is selected, the synchronization angle is followed by the selected valid solution since it is in the phasor quantity. The condition in Eq. (3.36) appears definitely sufficient to perform the synchronization of the initially measured signals in all fault types.

3.2.4 Flowchart for Proposed Algorithm Based on Two-End Unsynchronized Measurement

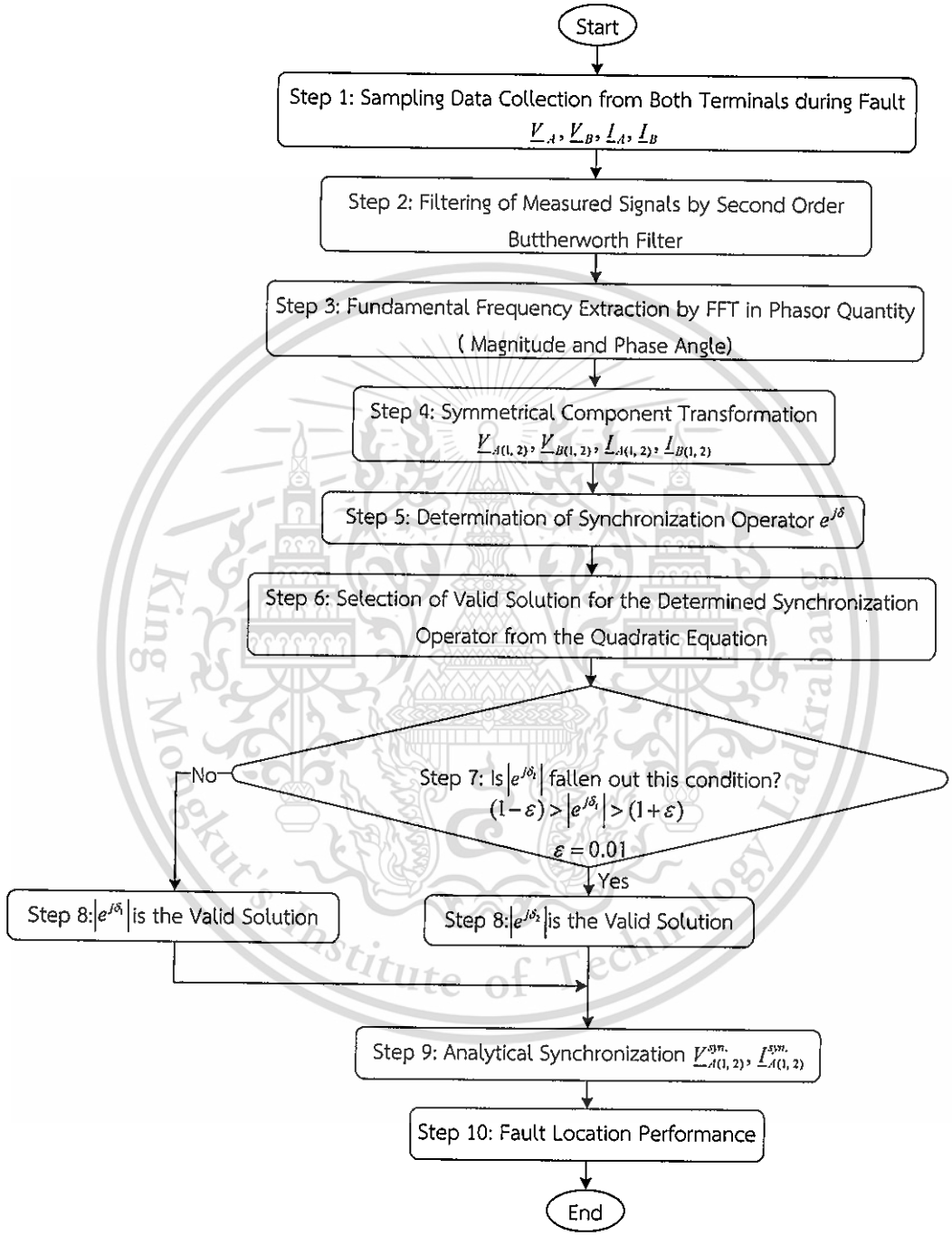

Figure 3.5 Flowchart of proposed algorithm based on two-end unsynchronized measurement

3.3 Summary

The method of finding the distance to faulted point has been derived in this chapter which classified two different algorithms based on synchronized and unsynchronized measurements. None line parameter requirement for fault location algorithm based on two-end synchronized measurement appeared to be simple, robust, and at the same time highly accurate to be implemented in the network. Due to the assumption of locating the fault on the short fully transposed transmission line, lumped line parameter model was used in this presented algorithm. The derivation of this algorithm is explicitly detailed in locating balanced and unbalanced fault covering with simple and low computation based on positive- and negative-sequence component equivalent circuits. The need of line parameters is unnecessary which makes this presented algorithm more flexible while the uncertainty of the line parameters, which is generally affected the accuracy of the fault location estimation, is successfully eliminated.

Unfortunately, due to the economic reasons, the method of using the GPS assisted PMUs is still in limit and cannot adopt as they could be. To refresh the problem, the method using two-end unsynchronized measurement appeared to be more attractive on fault location estimation. Distributed parameter line model is taken into account in this presented algorithm in order to respect the transmission line characteristic corresponded to long fully transposed transmission line. It just needs the common time reference of the measured signals. Only positive- and negative-sequence component equivalent circuits were used simultaneously to determine the synchronization operator. Consequently, the method of identifying the synchronization operator and angle, which are really important to make the analytical synchronization, is provided with the effective selection of the valid solution of the synchronization angle. Once the synchronization angle is selected, the distance to a fault can be performed precisely as the cases using synchronized measurement. This presented algorithm does not require the identifying of the affected phases or fault type selections, so it is flexible, robust, and highly accurate. It is worth to point out that it can be easily implemented into the microprocessor-based protective relays.

CHAPTER 4

PERFORMANCE EVALUATION AND ATP-EMTP SIMULATION RESULTS

This chapter provides the performance evaluation and simulation results of the proposed fault location algorithms which already presented the detailed derivations in Chapter 3. The two terminals system shown in Figure 2.7 is simulated first using synchronized measurement for locating the faults which are artificially implemented in the network. Various fault types with varying the fault resistances and ground resistance in the cases of excluding and including shunt capacitance were tested and evaluated along the entire short transmission line. In the next part, the two terminals system configuration depicted in Figure 2.8 is simulated using unsynchronized measurement for determining the fault distance on the long transmission line. Different fault specifications were tested and evaluated over the entire transmission line. Considered affected factors are also presented in order to investigate how it affected the proposed algorithms. Results of these two proposed algorithms are presented in this chapter and provide high accuracy of the fault location estimation. The results verify the efficacy and robustness of the proposed solution on finding the fault on the transmission line.

4.1 Algorithm Evaluation for Two-End Synchronized Measurement

The presented fault location algorithm has been simulated and validated thoroughly with credible fault data modeling obtained from ATP-EMTP software versatile simulations of fault implemented on the test transmission line containing 400 kV, 100 km long. The parameters of the transmission line and both networks are listed in the Tables 4.1 and 4.2, respectively.

Table 4.1 Transmission line parameters

Parameters	Positive- and negative-sequence	Zero-sequence
Resistance [Ω/km]	0.065	0.195
Inductance [mH/km]	0.95493	2.86479
Capacitance [nF/km]	10.5	5.0

Table 4.2 Parameters of both test networks

Parameters	Terminal A	Terminal B
Line to Line RMS Voltage [kV]	416	400
Phase angle [°]	30	10
Positive-sequence Resistance [Ω]	1.0185892	0.6366183
Positive-sequence Inductance [mH]	50.9395	31.8309
Zero-sequence Resistance [Ω]	2.0371785	1.2732366
Zero-sequence Inductance [mH]	101.8589	60.6618

4.1.1 Evaluation of All Fault Types

SLG, DL, DLG, and 3LG faults were simulated at different locations with a variety of fault resistance and ground resistance from 0Ω to 100Ω along the line. In each case, the fault inception time was set at $t = 23\ ms$. The sampling frequency was $f_s = 6.4\ kHz$. The data window size used for the FFT process to obtain the phasors quantities was $T_{dw} = 20\ ms$ (N=128 samples per data window). It was assumed that the line was loaded before the fault inception and all phasors were in a natural way perfectly synchronized.

4.1.1.1 Cases of Excluding Shunt Capacitance

A SLG fault was simulated at 40 km (observed from terminal A) over 100 km of the total line length with a fault resistance $R_f = 10\Omega$ as for the sample of the result. Figure 4.1 shows the configuration of the SLG fault modeling which taken into account the lumped parameter line model in ATP Draw.

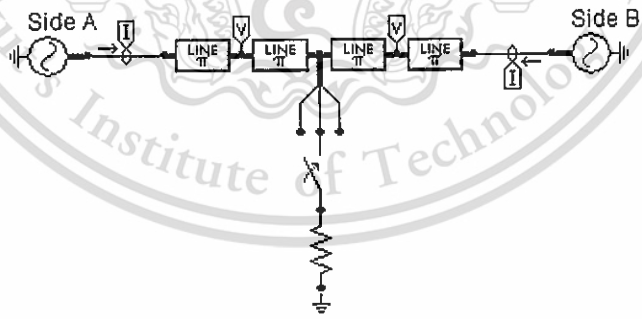

Figure 4.1 SLG fault with lumped parameter line modeling modeled in ATP Draw

Figures 4.2 and 4.3 depicted the simulated voltage and current waveforms at the terminal A and B, respectively. Sampled measurements of these voltages and currents were used as the inputs to the algorithm which developed in Matlab.

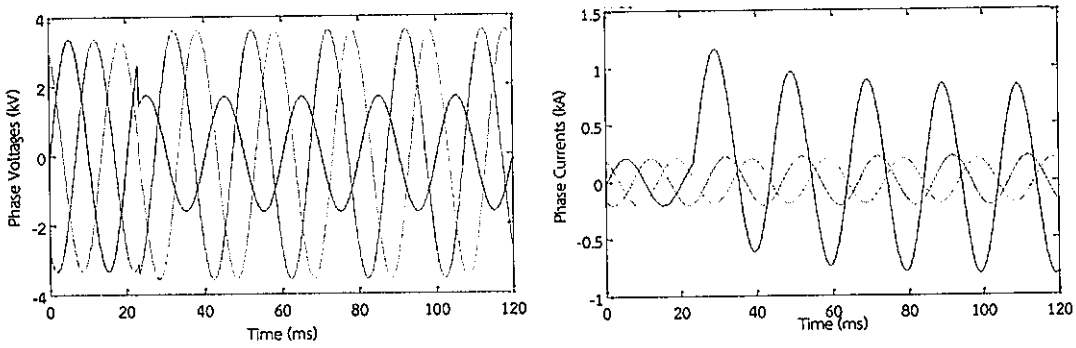

Figure 4.2 Voltage and current waveforms of SLG fault observed from terminal A

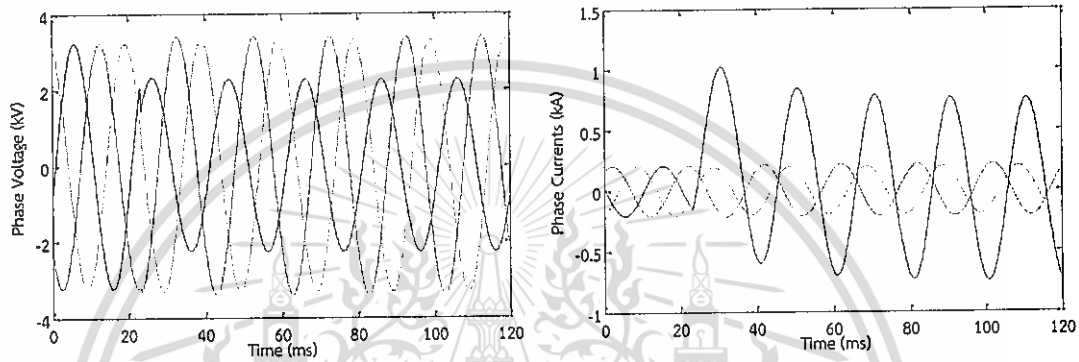

Figure 4.3 Voltage and current waveforms of SLG fault observed from terminal B

Based on the voltages and currents synchronously measured at line terminals, the unknown fault location is calculated using Eq. (3.7), as presented in Figure 4.4.

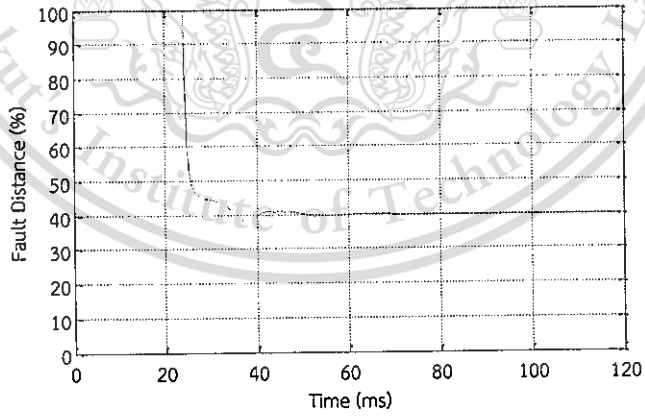

Figure 4.4 SLG fault with $R_f = 10\Omega$ estimated fault location (40 km fault was simulated in ATP-EMTP)

From Figure 4.4, it can be seen that the algorithm accurately determines the fault distance and converges to the solution shortly after the fault inception. The estimated distance to fault averaged over the interval 40-120 ms was 40.0168 km.

Obviously, the errors occurred during the convergence process are due to the presence of the DC components in the fault current. Commonly, since FFT was used in this extraction process, it is known to be sensitive to the decaying of DC components.

Next, a DL fault was also simulated at 40 km (observed from terminal A) over 100 km of the total line length with a fault resistance $R_F = 100\Omega$. Figure 4.5 shows the configuration of the DL fault modeling which taken into account the lumped parameter line model in ATP Draw.

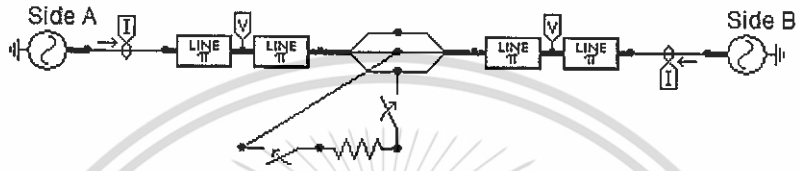

Figure 4.5 DL fault with lumped parameter line modeling modeled in ATP Draw

Figures 4.6 and 4.7 depicted the simulated voltage and current waveforms at the terminal A and B, respectively. Sampled measurements of these voltages and currents were used as the inputs to the algorithm which developed in Matlab.

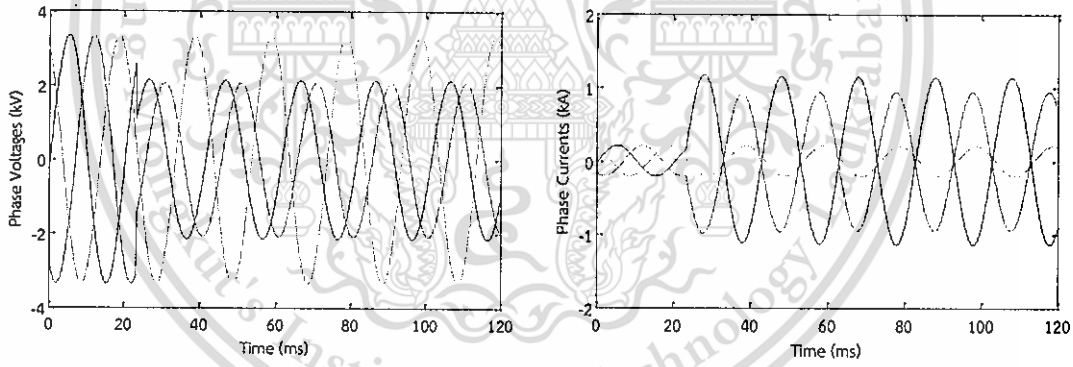

Figure 4.6 Voltage and current waveforms of DL fault observed from terminal A

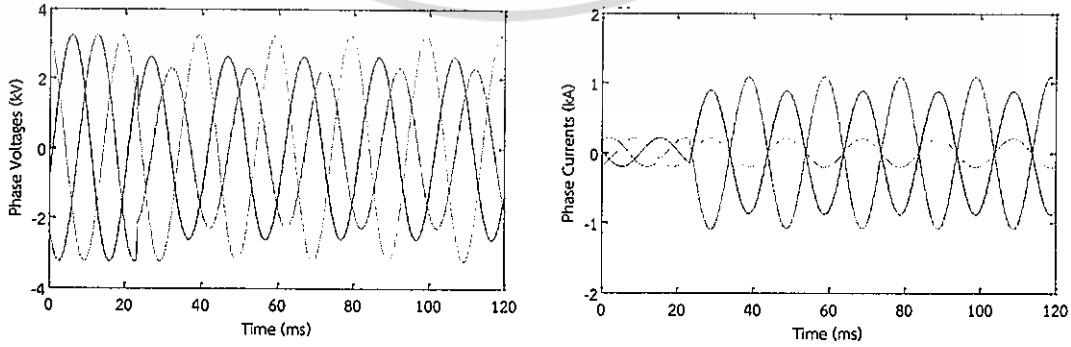

Figure 4.7 Voltage and current waveforms of DL fault observed from terminal B

Based on the voltages and currents synchronously measured at line terminals, the unknown fault location is calculated using Eq. (3.7), as presented in Figure 4.8.

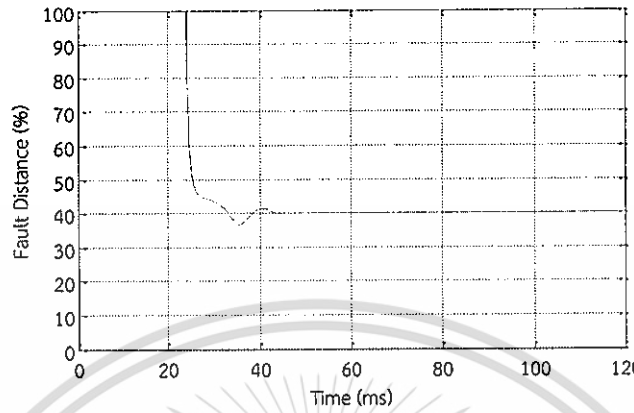

Figure 4.8 DL fault with $R_F = 100\Omega$ estimated fault location (40 km fault was simulated in ATP-EMTP)

From Figure 4.8 it can be seen that the algorithm accurately determines the fault distance and converges to the solution shortly after the fault inception. The estimated distance to fault averaged over the interval 40-120 ms was 40.0023 km.

Beside above fault types, a DLG fault was also simulated at 40 km (observed from terminal A) over 100 km of the total line length with a fault resistance $R_F = 1\Omega$, $R_g = 100\Omega$ as the case of DL fault. Figure 4.9 shows the configuration of the DLG fault modeling which taken into account the lumped parameter line model in ATP Draw.

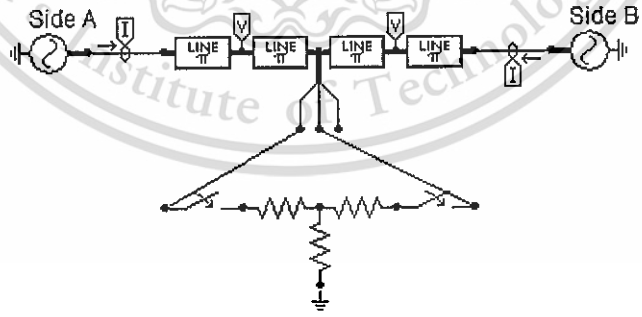

Figure 4.9 DLG fault with lumped parameter line modeling modeled in ATP Draw

Figures 4.10 and 4.11 depicted the simulated voltage and current waveforms at the terminal A and B, respectively. Sampled measurements of these voltages and currents were used as the inputs to the algorithm which developed in Matlab.

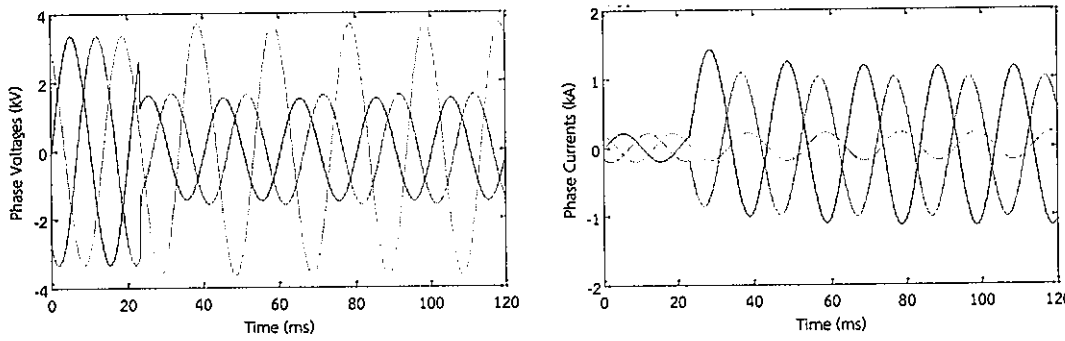

Figure 4.10 Voltage and current waveforms of DLG fault observed from terminal A

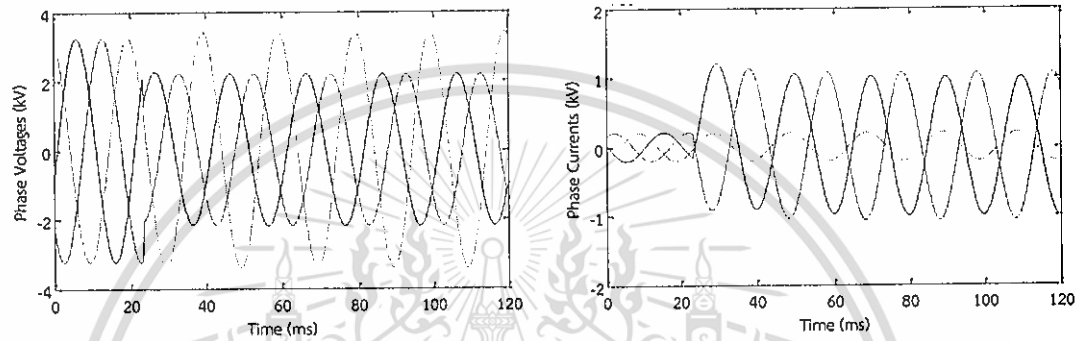

Figure 4.11 Voltage and current waveforms of DLG fault observed from terminal B

Based on the voltages and currents synchronously measured at line terminals, the unknown fault location is calculated using Eq. (3.7), as presented in Figure 4.12.

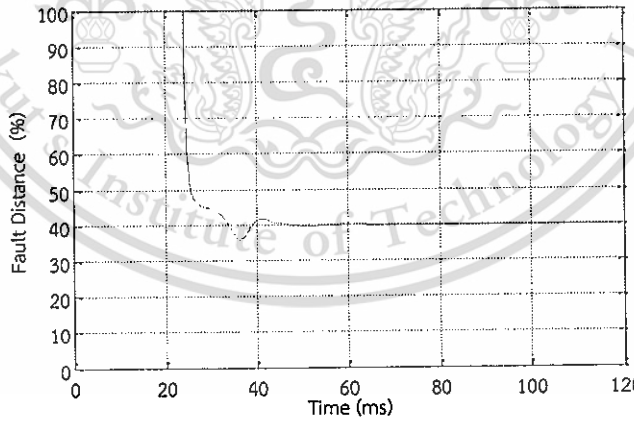

Figure 4.12 DLG fault with $R_F = 1\Omega$, $R_g = 100\Omega$ estimated fault location (40 km fault was simulated in ATP-EMTP)

From Figure 4.12, it can be seen that the algorithm accurately determines the fault distance and converges to the solution shortly after the fault inception. The estimated distance to fault averaged over the interval 40-120 ms was 40.0062 km.

The last fault type, a 3LG fault was also simulated at 40 km (observed from terminal A) over 100 km of the total line length with a fault resistance $R_F = 1\Omega$, $R_g = 1\Omega$. Figure 4.13 shows the configuration of the 3LG fault modeling which taken into account the lumped parameter line model in ATP Draw.

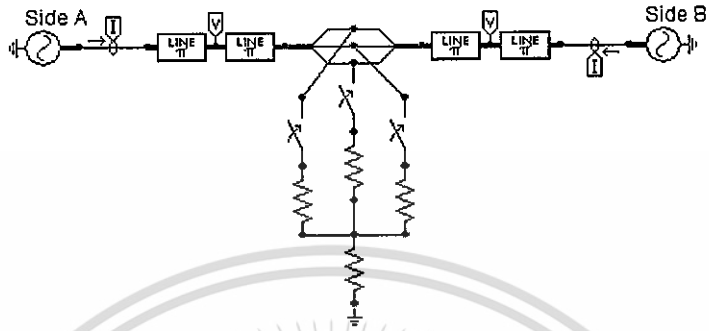

Figure 4.13 3LG fault with lumped parameter line modeling modeled in ATP Draw

Figures 4.14 and 4.15 depicted the simulated voltage and current waveforms at the terminal A and B, respectively. Sampled measurements of these voltages and currents were used as the inputs to the algorithm which developed in Matlab.

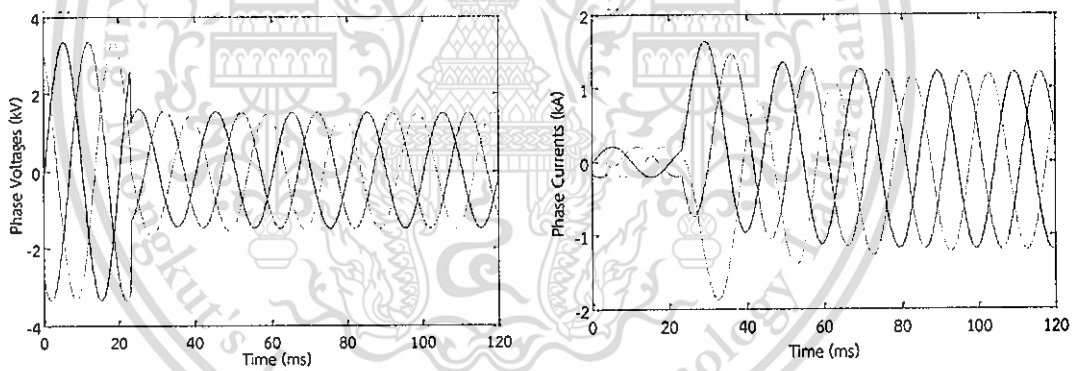

Figure 4.14 Voltage and current waveforms of 3LG fault observed from terminal A

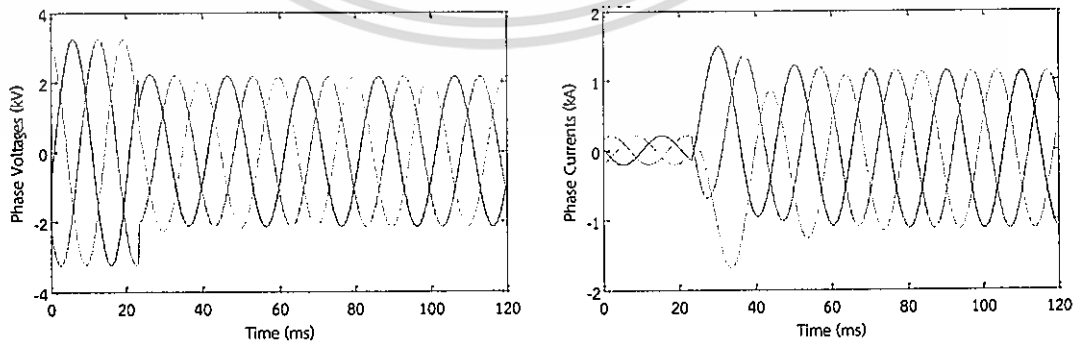

Figure 4.15 Voltage and current waveforms of 3LG fault observed from terminal B

As mentioned previously in the algorithm derivation of Chapter 3, fault resistance R_F needs to be determined and selected as valid one first in order to substitute it into the collinear vectors $\underline{z}l$ and $\underline{z}(D-l)$. Since the fault resistance R_F is determined by solving the quadratic equation, there are two solutions obtained from it. The simple method is just investigated on the value of angle θ which lies in the first quadrant of the complex plane and the one which is closer to the typical value of the line characteristic should be selected. The determined phase angles θ_1 and θ_2 compiled by substituting the fault resistance $(R_F)_1$ and $(R_F)_2$, respectively are depicted in Figure 4.16.

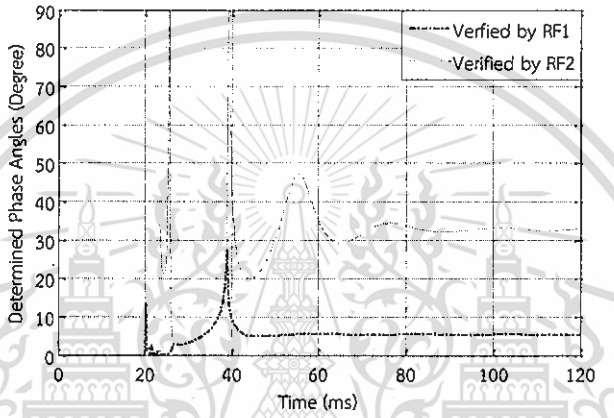

Figure 4.16 Determined phase angles verified two solutions of fault resistance obtained from quadratic equation

From this figure, the valid solution is clearly demonstrated as selecting the phase angle θ_2 which is corresponded to $(R_F)_2$. This value is closer to the typical value of line characteristic (e.g. 80) while another solution differs very much from the valid one. Then fault distance is calculated using Eq. (3.25) as presented in Figure 4.17.

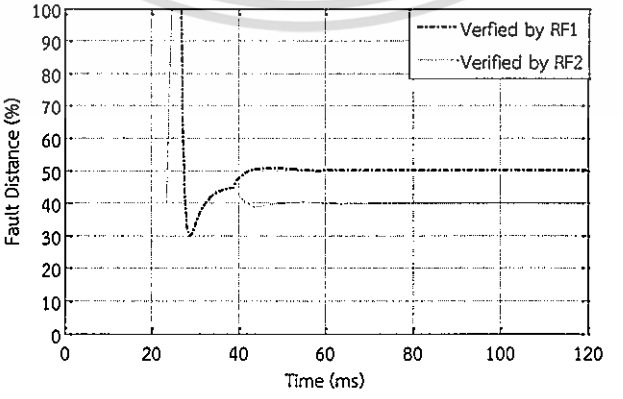

Figure 4.17 3LG fault with $R_F = 1\Omega$, $R_g = 1\Omega$ estimated fault location (40 km fault was simulated in ATP-EMTP)

It is worth to notice that phase angle θ_2 is not always the valid solution; it depends on the value of phase angle which is closer to the typical value of line characteristic. From Figure 4.17, it can be seen that the algorithm accurately determines the fault distance and converges to the solution shortly after the fault inception. The estimated distance to fault averaged over the interval 40-120 ms was 39.9812 km.

In order to further demonstrate the algorithm's efficiency, unbalanced faults and balanced three-phase faults are assumed to occur at different points along the line were simulated. The results in percentage for the various fault locations are presented from Figures 4.18 to 4.21. Based on the results, it can be verified that accurate results were obtained over the range of transmission line.

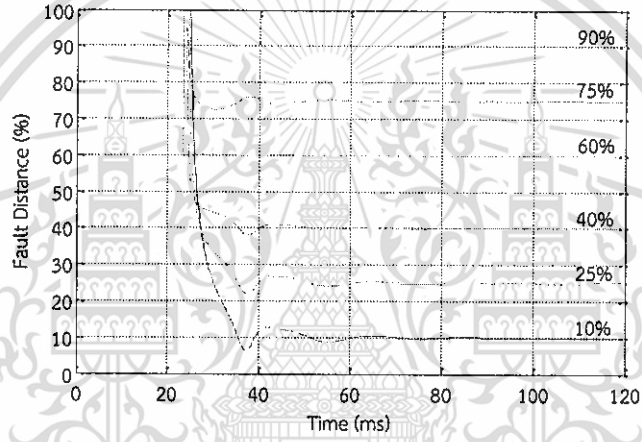

Figure 4.18 Various SLG fault with $R_f = 10\Omega$ estimated fault location over the range of transmission line

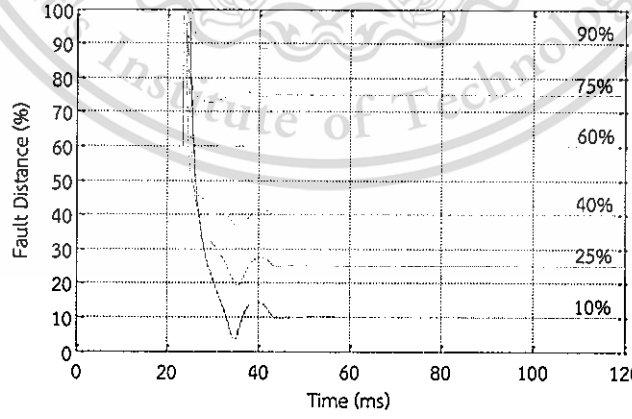

Figure 4.19 Various DL fault with $R_f = 100\Omega$ estimated fault location over the range of transmission line

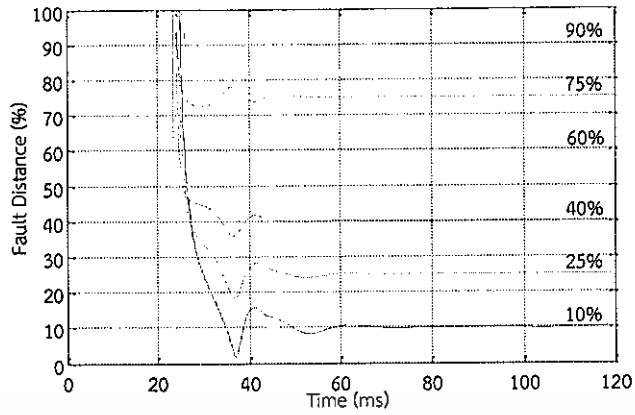

Figure 4.20 Various DLG fault with $R_F = 1\Omega$, $R_g = 100\Omega$ estimated fault location over the range of transmission line

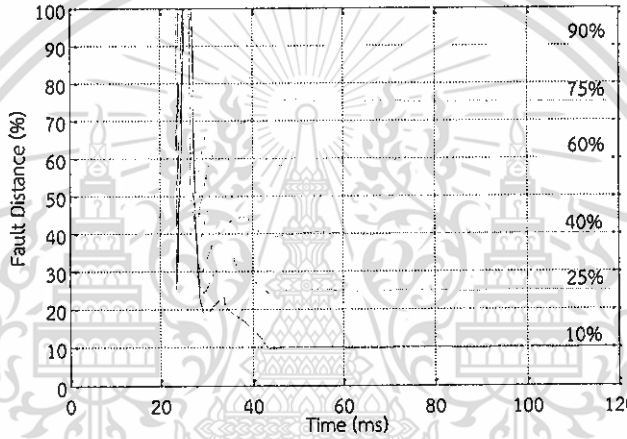

Figure 4.21 Various 3LG fault with $R_F = 1\Omega$, $R_g = 1\Omega$ estimated fault location over the range of transmission line

The results for a variety of the unbalanced faults and balanced three-phase faults with different locations and fault resistances by excluding line capacitance in the modeling are gathered in Table 4.3. Results for 66 simulation tests have been presented. The errors presented in the results have been calculated as a percentage of the entire line length by using Eq. (2.8) and averaged over the interval 40-120 ms.

From Table 4.3 it can be concluded that the algorithm maintained a high level of accuracy in locating all fault types with varying the fault location as well as fault resistance. The error of the estimation for faults occurred in the middle of the line are relatively smaller than those occurred close to line terminal. It is obvious that the effect of fault resistance changed the amplitude of voltages and currents, but the flexibility of the proposed algorithm is more robust since it is not involved with line parameters. Additionally, it is unaffected by fault resistance varied from 0Ω to 100Ω. The maximum error does not exceed 0.0637%

Table 4.3 Fault location error [%] for all fault types excluding line capacitance

Fault Types	Fault distance [%]					
	10	25	40	60	75	90
SLG, $R_F = 0\Omega$	0.0453	0.0298	0.0173	0.0015	0.0117	0.0281
SLG, $R_F = 10\Omega$	0.0444	0.0290	0.0168	0.0015	0.0114	0.0276
SLG, $R_F = 100\Omega$	0.0337	0.0216	0.0125	0.0011	0.0081	0.0199
DL, $R_F = 0\Omega$	0.0043	0.0250	0.0084	0.0004	0.0019	0.0065
DL, $R_F = 100\Omega$	0.0081	0.0053	0.0024	0.0001	0.0002	0.0028
DLG, $R_F = 1\Omega$, $R_g = 0\Omega$	0.0637	0.0250	0.0084	0.0004	0.0019	0.0147
DLG, $R_F = 1\Omega$, $R_g = 100\Omega$	0.0466	0.0182	0.0063	0.0004	0.0002	0.0049
3LG, $R_F = 1\Omega$, $R_g = 0\Omega$	0.0076	0.0163	0.0205	0.0137	0.0107	0.0051
3LG, $R_F = 1\Omega$, $R_g = 1\Omega$	0.0084	0.0158	0.0188	0.0334	0.0058	0.0026
3LG, $R_F = 1\Omega$, $R_g = 10\Omega$	0.0029	0.0032	0.0009	0.0010	0.0022	0.0022
3LG, $R_F = 1\Omega$, $R_g = 100\Omega$	0.0084	0.0158	0.0188	0.0334	0.0058	0.0026

4.1.1.2 Cases of Including Shunt Capacitance

In the derivation of the algorithm, the shunt capacitance was assumed to be neglected, but a realistic Pi-model in ATP-EMTP including line capacitance was used to simulate all fault types. This may cause some errors in fault location estimation. All fault types have been tested and validated in order to show the efficiency of the proposed algorithm as the case of excluding line capacitance. The way of excluding and including line capacitance is just changed the input value of the lumped RLC Pi-equivalent 3 phase model in ATP-EMTP, so the configurations of all fault types are originally maintained as the case of excluding line capacitance.

A SLG fault was simulated again at 40 km (observed from terminal A) over 100 km of the total line length with a fault resistance $R_F = 10\Omega$ in considering the line capacitance in the modeling. Figures 4.22 and 4.23 depicted the simulated voltage and current waveforms at the terminal A and B, respectively. Consequently, these waveforms will be used as the inputs for the developed algorithm in Matlab.

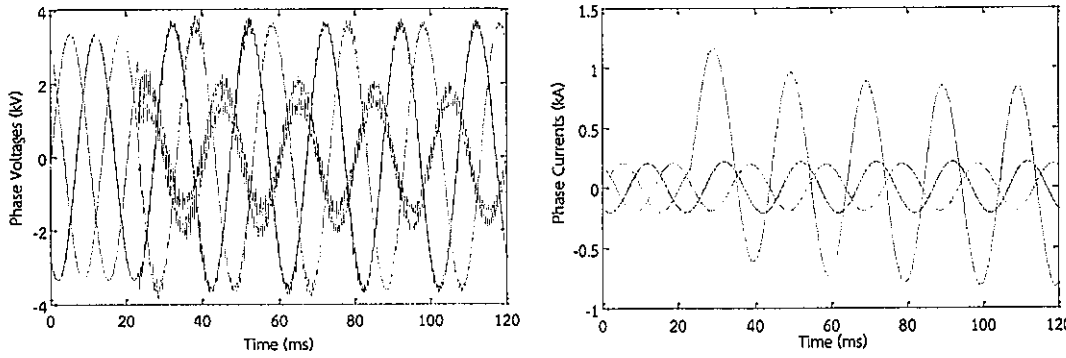

Figure 4.22 Voltage and current waveforms of SLG fault captured from terminal A

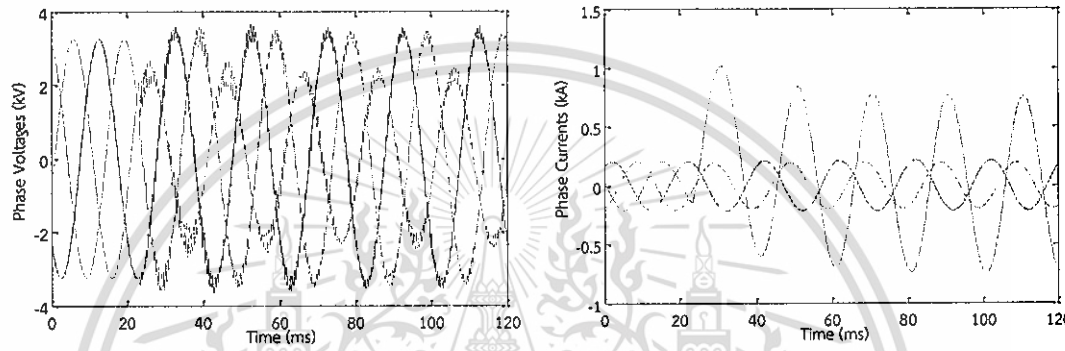

Figure 4.23 Voltage and current waveforms of SLG fault captured from terminal B

Based on the voltages and currents synchronously measured at line terminals, the unknown fault location is calculated using Eq. (3.7), as presented in Figure 4.24.

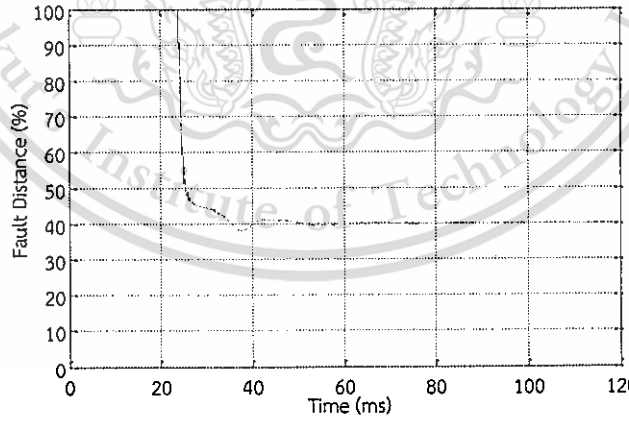

Figure 4.24 SLG fault with $R_f = 10\Omega$ estimated fault location (40 km fault was simulated in ATP-EMTP)

From Figure 4.24, it can be seen that the algorithm accurately determines the fault distance and converges to the solution shortly after the fault inception even shunt capacitance is also considered in the modeling. The estimated distance to

fault averaged over the interval 40-120 ms was 40.0333 km. Basically, it depends on the quality of the method for phasors extraction, while FFT was used in this extraction and it is known to be very sensitive the decaying DC component.

Next, a DL fault, in this case, was also simulated at 40 km (observed from terminal A) over 100 km of the total line length with a fault resistance $R_F = 100\Omega$. The procedure of locating fault is totally the same as the previous case. This proposed algorithm is robust since it needs only the voltage and current waveforms synchronously measured from both terminals as illustrated in Figures 4.25 and 4.26.

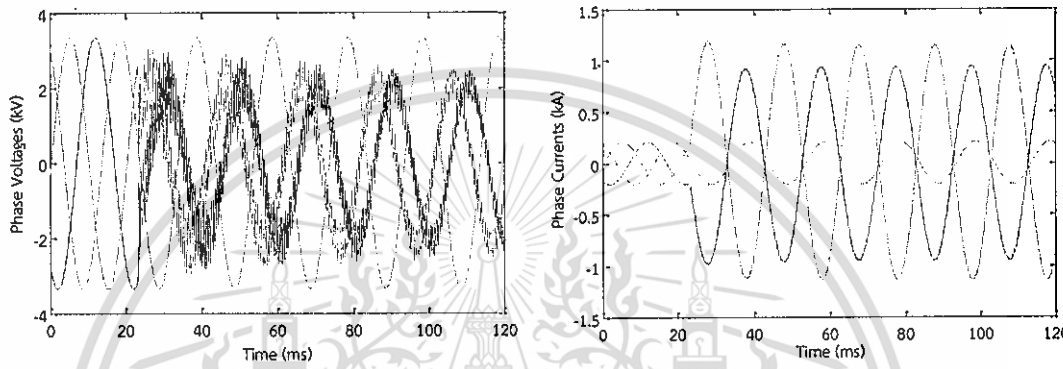

Figure 4.25 Voltage and current waveforms of DL fault captured from terminal A

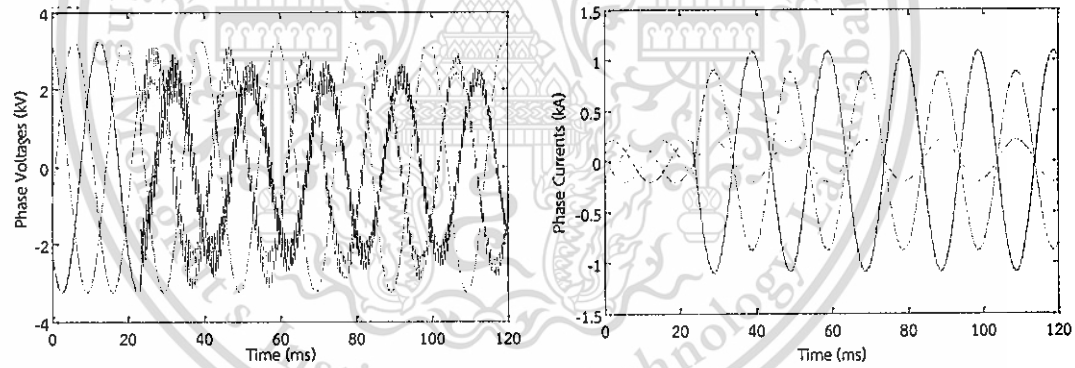

Figure 4.26 Voltage and current waveforms of DL fault captured from terminal B

Based on the voltages and currents synchronously measured at line terminals, the unknown fault location is calculated using Eq. (3.7), as presented in Figure 4.27. From Figure 4.27 it can be seen that the algorithm accurately determines the fault distance and converges to the solution shortly after the fault inception. The estimated distance to fault averaged over the interval 40-120 ms was 40.0141 km

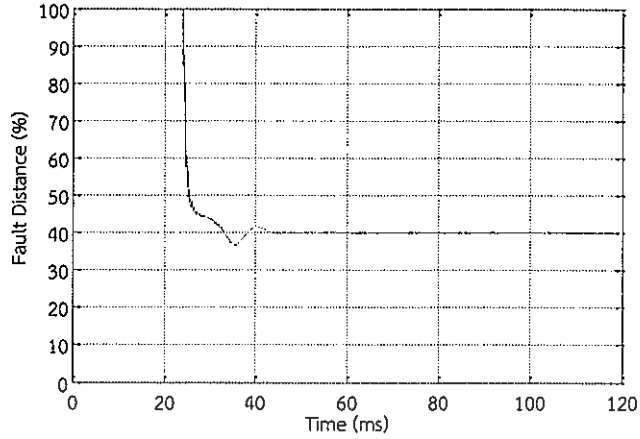

Figure 4.27 DL fault with $R_F = 100\Omega$ estimated fault location (40 km fault was simulated in ATP-EMTP)

As mentioned, all fault types need to be considered in this case, so a DLG fault with fault resistance $R_F = 1\Omega$, $R_g = 100\Omega$ was also simulated at 40 km (observed from terminal A) over 100 km of the total line length. Figures 4.28 and 4.29 depicted the simulated voltage and current waveforms at the terminal A and B, respectively.

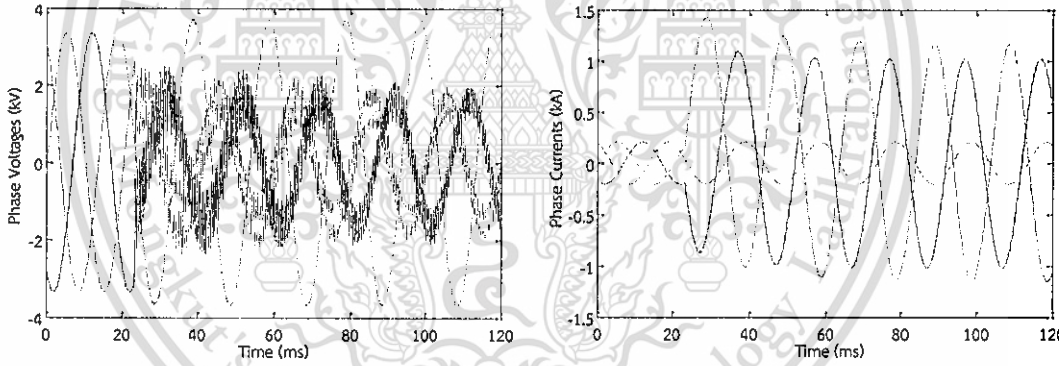

Figure 4.28 Voltage and current waveforms of DLG fault captured from terminal A

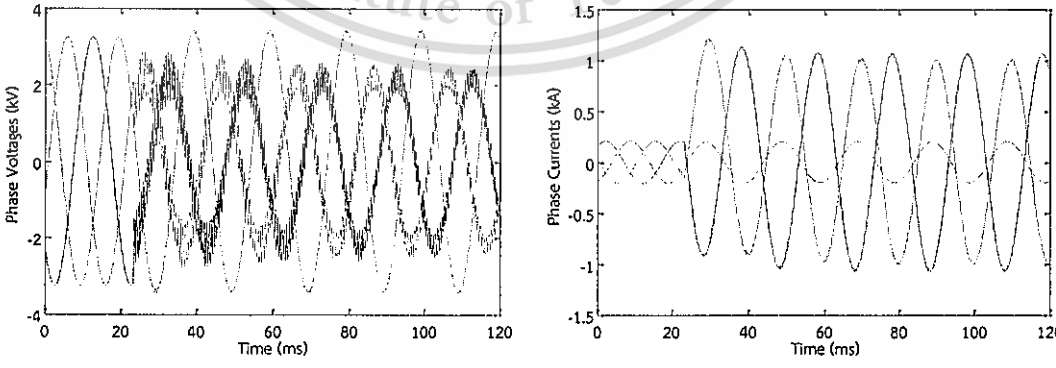

Figure 4.29 Voltage and current waveforms of DLG fault captured from terminal B

Based on the voltages and currents synchronously measured at line terminals, the unknown fault location is calculated using Eq. (3.7), as presented in Figure 4.30.

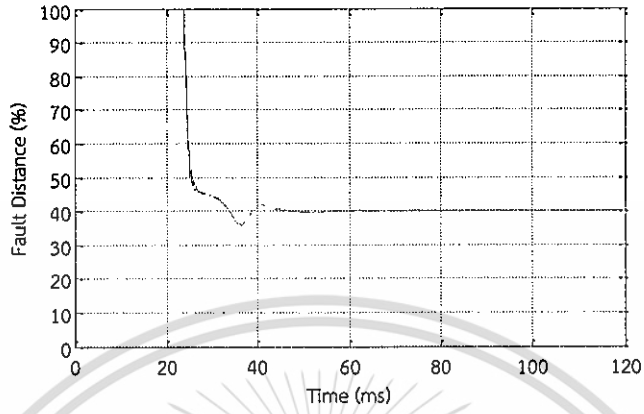

Figure 4.30 DLG fault with $R_F = 1\Omega$, $R_g = 100\Omega$ estimated fault location (40 km fault was simulated in ATP-EMTP)

From Figure 4.30, it can be seen that the algorithm accurately determines the fault distance and converges to the solution shortly after the fault inception. The estimated distance to fault averaged over the interval 40-120 ms was 40.0228 km.

The last fault type which considered in this case is a 3LG fault with fault resistance $R_F = 1\Omega$, $R_g = 1\Omega$ which was also simulated at 40 km (observed from terminal A) over 100 km of the total line length as same as all the cases in order to see how fault resistance make changes in the voltage and current waveforms. Figures 4.31 and 4.32 depicted the simulated voltage and current waveforms at the terminal A and B, respectively.

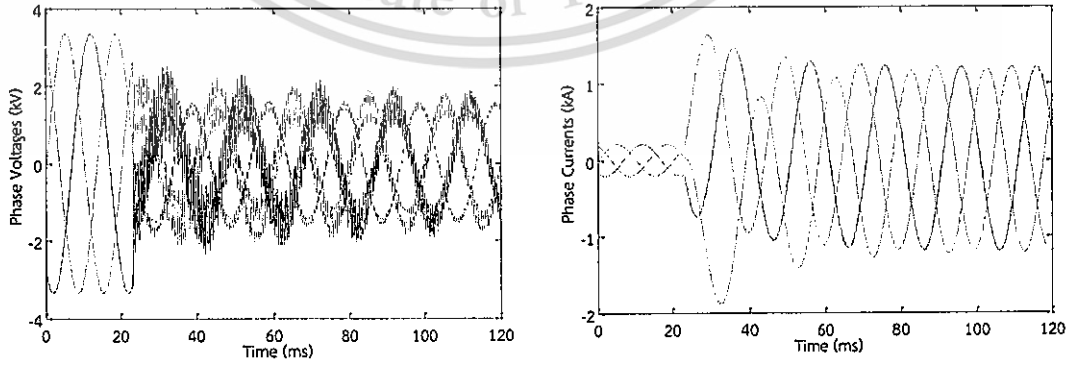

Figure 4.31 Voltage and current waveforms of 3LG fault captured from terminal A

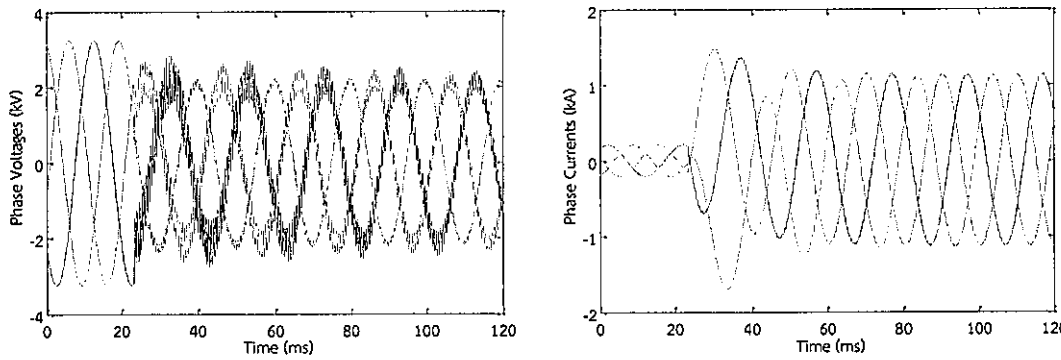

Figure 4.32 Voltage and current waveforms of 3LG fault captured from terminal B

The determined phase angles θ_1 and θ_2 compiled by substituting the fault resistance $(R_F)_1$ and $(R_F)_2$, respectively are depicted in Figure 4.33.

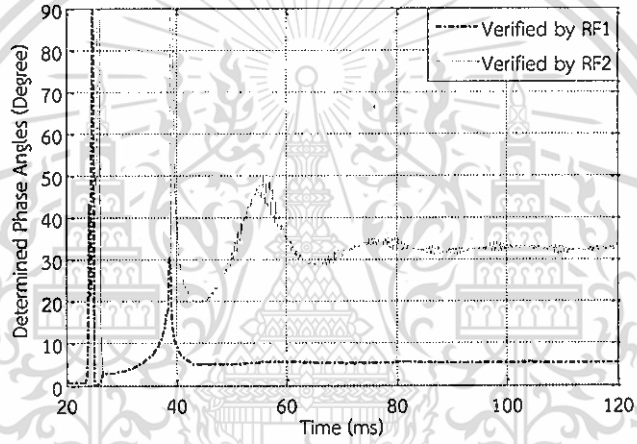

Figure 4.33 Determined phase angles verified two solutions of fault resistance obtained from quadratic equation

From this figure, the valid solution is clearly demonstrated as selecting the phase angle θ_2 which is corresponded to $(R_F)_2$. This value is closer to the typical value of line characteristic (e.g. 80°) while another solution differs very much from the valid one. Then fault distance is calculated using Eq. (3.25) as presented in Figure 4.34.

From Figure 4.34, it can be seen that the algorithm accurately determines the fault distance and converges to the solution shortly after the fault inception. The estimated distance to fault averaged over the interval 40-120 ms was 39.9570 km.

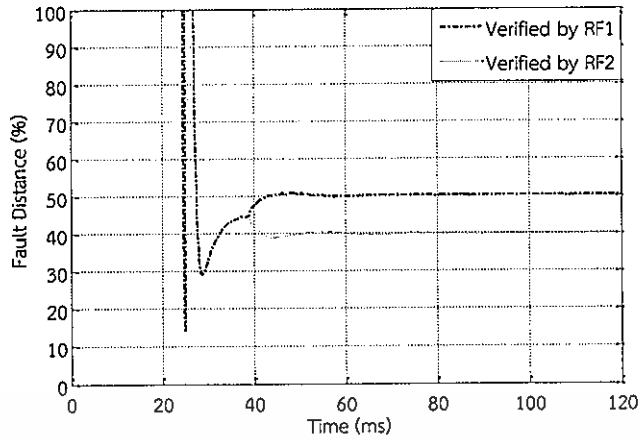

Figure 4.34 3LG fault with $R_F = 1\Omega$, $R_g = 1\Omega$ estimated fault location (40 km fault was simulated in ATP-EMTP)

The results for a variety of the unbalanced faults and balanced three-phase faults with different locations and fault resistances by including line capacitance in the modeling are gathered in Table 4.4. The same amount of results for 66 simulation tests has been presented as the case of excluding shunt capacitance. The errors presented in the results have been calculated as a percentage of the entire line length by using Eq. (2.8) and averaged over the interval 40-120 ms. The maximum error does not exceed 0.121%.

Table 4.4 Fault location error [%] for all fault types including line capacitance

Fault Types	Fault distance [%]					
	10	25	40	60	75	90
SLG, $R_F = 0\Omega$	0.1210	0.0717	0.0337	0.0151	0.0543	0.0983
SLG, $R_F = 10\Omega$	0.1201	0.0710	0.0333	0.0152	0.0539	0.0978
SLG, $R_F = 100\Omega$	0.1092	0.0635	0.0289	0.0155	0.0507	0.0902
DL, $R_F = 0\Omega$	0.0703	0.0392	0.0157	0.0163	0.0408	0.0772
DL, $R_F = 100\Omega$	0.0665	0.0366	0.0141	0.0165	0.0425	0.0735
DLG, $R_F = 1\Omega$, $R_g = 0\Omega$	0.1371	0.0665	0.0249	0.0162	0.0408	0.0565
DLG, $R_F = 1\Omega$, $R_g = 100\Omega$	0.1064	0.0505	0.0228	0.0162	0.0425	0.0663
3LG, $R_F = 1\Omega$, $R_g = 0\Omega$	0.0366	0.0559	0.0424	0.0450	0.0145	0.0206
3LG, $R_F = 1\Omega$, $R_g = 1\Omega$	0.0394	0.0576	0.0430	0.0178	0.0147	0.0208
3LG, $R_F = 1\Omega$, $R_g = 10\Omega$	0.0914	0.0946	0.0807	0.0177	0.0350	0.0573
3LG, $R_F = 1\Omega$, $R_g = 100\Omega$	0.0393	0.0576	0.0429	0.0178	0.0147	0.0207

From Table 4.4 it can be concluded that the algorithm maintained a high level of accuracy in locating all fault types with varying the fault location as well as fault resistance even the shunt capacitance is considered in the modeling. It can be noticed from the simulated trial tests as follows:

- If faults occurred in the middle of the line as the sample cases shown above, the fault currents from both terminals are approximately the same as the errors caused by shunt capacitance. Thus, the errors are relatively small.
- If faults occurred close to either line terminal, there is a bigger difference in fault currents from each line terminal and the errors caused by shunt capacitance also differ. If the fault is closed to the terminal A, the line capacitance has a much smaller influence on the fault current than it has on the fault current from terminal B. This leads to larger errors for faults occurred closer to line terminal.

4.1.2 Investigation on Additive White Gaussian Noise (AWGN)

In reality, the non-linear effects on instrument transformers and errors introduced during A/D conversion are factors which would be adversely affected the accuracy of the fault location. Since this algorithm is based on the synchronized measured voltages and currents, it needs to use fast communication channels between two synchronized measurement units installed at the line terminal which can be introduced by some irritate noises. Noise ratio 40dB is considered as the severe noise introduced in the network. AWGN whose signal-to-noise ratio (SNR) 40dB was randomly added to all simulation tests by Matlab. Noise is added to all voltage and current waveforms from both terminals, but Figure 4.35 shows only the first steady state cycle of original voltage waveforms from terminal A and added noise in order to clearly see the irritated noise.

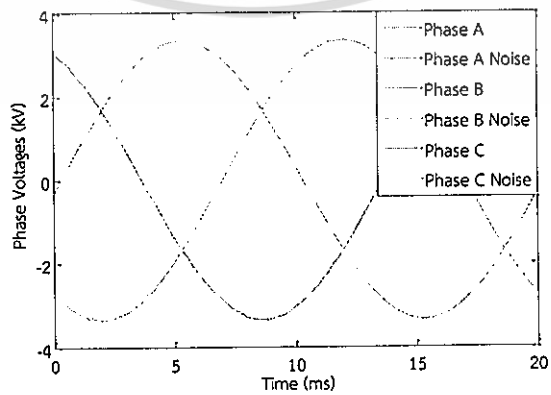

Figure 4.35 Original and added noise for the 1st cycle of voltages from terminal A

The procedure of locating the fault still maintains the same steps as shown in the samples of all fault types. This is showed only the final results after severe noise is considered. The errors presented in the results have been calculated by Eq. (2.8). Results obtained for this investigation used the average value of 10-time simulations in each case as given in Tables 4.5 and 4.6 which corresponded to cases of excluding and including line capacitance, respectively.

From these tables, it can be seen that the accuracy of the proposed algorithm in locating all fault types still applicable even considering with severe noise artificially implemented in the network. The maximum error for cases excluding and including shunt capacitance does not exceed 0.2685% and 0.3419%, respectively.

Table 4.5 Fault location error [%] for all fault types considering severe noise ratio 40dB in case of excluding line capacitance

Fault Types	Fault distance [%]					
	10	25	40	60	75	90
SLG, $R_F = 0\Omega$	0.1985	0.1213	0.0701	0.0043	0.0371	0.0762
SLG, $R_F = 10\Omega$	0.2041	0.1207	0.0707	0.0058	0.0408	0.0758
SLG, $R_F = 100\Omega$	0.2180	0.1324	0.0759	0.0079	0.0462	0.0948
DL, $R_F = 0\Omega$	0.1182	0.1224	0.0605	0.0029	0.0204	0.0591
DL, $R_F = 100\Omega$	0.1117	0.0707	0.0431	0.0040	0.0278	0.0622
DLG, $R_F = 1\Omega$, $R_g = 0\Omega$	0.2640	0.1219	0.0576	0.0039	0.0217	0.0285
DLG, $R_F = 1\Omega$, $R_g = 100\Omega$	0.2685	0.1376	0.0650	0.0037	0.0213	0.0129
3LG, $R_F = 1\Omega$, $R_g = 0\Omega$	0.1281	0.0666	0.0183	0.0838	0.1353	0.1504
3LG, $R_F = 1\Omega$, $R_g = 1\Omega$	0.1204	0.0555	0.0055	0.1862	0.1354	0.1530
3LG, $R_F = 1\Omega$, $R_g = 10\Omega$	0.0765	0.0099	0.0743	0.0119	0.1666	0.1586
3LG, $R_F = 1\Omega$, $R_g = 100\Omega$	0.1206	0.0555	0.0055	0.1840	0.1372	0.1536

Table 4.6 Fault location error [%] for all fault types considering severe noise ratio 40dB in case of including line capacitance

Fault Types	Fault distance [%]					
	10	25	40	60	75	90
SLG, $R_F = 0\Omega$	0.2804	0.1681	0.0831	0.0144	0.0838	0.1455
SLG, $R_F = 10\Omega$	0.2841	0.1666	0.0837	0.0116	0.0808	0.1495
SLG, $R_F = 100\Omega$	0.2986	0.1768	0.0948	0.0082	0.0889	0.1627
DL, $R_F = 0\Omega$	0.1916	0.1170	0.0605	0.0134	0.0637	0.1276
DL, $R_F = 100\Omega$	0.1920	0.1148	0.0571	0.0122	0.0696	0.1287
DLG, $R_F = 1\Omega$, $R_g = 0\Omega$	0.3419	0.1666	0.0773	0.0134	0.0711	0.1001

DLG, $R_F = 1\Omega$, $R_g = 100\Omega$	0.3073	0.1521	0.0779	0.0132	0.0592	0.0840
3LG, $R_F = 1\Omega$, $R_g = 0\Omega$	0.0991	0.0267	0.0041	0.0526	0.0964	0.1250
3LG, $R_F = 1\Omega$, $R_g = 1\Omega$	0.0896	0.0142	0.0188	0.1508	0.1169	0.1311
3LG, $R_F = 1\Omega$, $R_g = 10\Omega$	0.0119	0.1028	0.1538	0.0069	0.1349	0.1045
3LG, $R_F = 1\Omega$, $R_g = 100\Omega$	0.0900	0.0072	0.0180	0.1506	0.1323	0.1159

4.1.3 Investigation on Synchronization Error

As mentioned, this algorithm implements with the perfectly synchronized measurements. A SLG fault with fault resistance $R_F = 10\Omega$ was tested over the range of the entire line by considering the time delay (t_d) of the synchronized data sampling which varied from 10 μs to 500 μs from both terminals. The errors presented in the results have been calculated by Eq. (2.8) and averaged over the interval 40-120 ms.

Two different scenarios have been proposed to investigate on the synchronization error which is considered as one of the affected factors to the algorithm based on synchronized measurements. To demonstrate the tolerance of the presented algorithm with the non-ideal synchronization, firstly, all measured signals from terminal A were artificially delayed by 10 μs to 500 μs (0.18° to 9°) which corresponded to 1 to 50 samples in 50 Hz digitalized at 100 kHz. In addition, another scenario has been offered by setting all measured signals from terminal B delayed from 10 μs to 500 μs as well. Results for this investigation have been collected in Tables 4.7 and 4.8.

From Tables 4.7 and 4.8 it can be concluded that the fault location error was appeared to be higher by the fault occurred close to the end of the terminals, and it was lower by the fault approached to the middle. For $t_d \leq 20$ μs, the fault location error is totally acceptable, while $t_d > 20$ μs would not be considered as acceptable due to the high errors of the estimated faults occurred at the end of line terminals.

Table 4.7 Fault location error [%] considering synchronization error delayed from terminal A

Time Delay (t_d), [μs]	Fault distance [%]					
	10	25	40	60	75	90
10	0.3996	0.2845	0.1445	0.0145	0.0792	0.1685
20	0.8043	0.5744	0.319	0.0358	0.1717	0.3748
30	1.2224	0.8741	0.4994	0.0577	0.2676	0.5884
40	1.6546	1.1841	0.686	0.0803	0.3668	0.8095
50	2.1013	1.5049	0.8791	0.1037	0.4696	1.0385

60	2.5634	1.837	1.0791	0.128	0.5761	1.2758
70	3.0413	2.181	1.2865	0.1531	0.6866	1.5218
80	3.5358	2.5377	1.5015	0.1793	0.8011	1.7769
90	4.0473	2.9076	1.7247	0.2065	0.9198	2.0418
100	4.5761	3.2915	1.9565	0.2349	1.0431	2.3167
200	7.9912	8.0989	4.8851	0.6136	2.5763	5.7680
500	58.609	13.553	23.150	9.3205	12.857	37.579

Table 4.8 Fault location error [%] considering synchronization error delayed from terminal B

Time Delay (t_d), [μs]	Fault distance [%]					
	10	25	40	60	75	90
10	0.3684	0.2647	0.1878	0.0263	0.0967	0.224
20	0.7333	0.5259	0.3450	0.0459	0.1802	0.4107
30	1.0871	0.7791	0.4975	0.0651	0.2610	0.5913
40	1.4303	1.0247	0.6454	0.0838	0.3391	0.7663
50	1.7634	1.2630	0.7890	0.1021	0.4146	0.9357
60	2.0867	1.4944	0.9285	0.1201	0.4876	1.0998
70	2.4006	1.7191	1.0640	0.1378	0.5583	1.2589
80	2.7057	1.9375	1.1958	0.1551	0.6267	1.4131
90	3.0022	2.1497	1.3240	0.1722	0.6929	1.5626
100	3.2905	2.3562	1.4487	0.1890	0.7569	1.7077
200	5.7885	4.1481	2.5367	0.3477	1.2953	2.9455
500	10.6372	7.6716	4.7421	0.8090	2.1530	5.1424

4.2 Algorithm Evaluation for Two-End Unsynchronized Measurement

This presented fault location algorithm has been simulated and validated thoroughly with credible fault data modeling obtained from ATP-EMTP software versatile simulations of fault implemented on the test transmission line containing 400 kV, 300 km long. The parameters of both networks and transmission line are listed in Table 4.9.

Table 4.9 Parameters of the test networks

Components	Parameters	
Terminal A	RMS Voltage	416 kV
	Phase Shift Angle	α_A =30°
	$\underline{Z}_{1SA}$	(1.312+j15.0) Ω
	$\underline{Z}_{0SA}$	(2.334+j26.6) Ω
Terminal B	RMS Voltage	400 kV
	Phase Shift Angle	α_B =10°
	$\underline{Z}_{1SB}$	(2.624+j30.0) Ω
	$\underline{Z}_{0SB}$	(4.668+j53.2) Ω
Transmission line from A to B	$\underline{Z}'_{1L}$	(0.0276+j0.3151) Ω/km
	$\underline{Z}'_{0L}$	(0.2750+j1.0265) Ω/km
	$\underline{C}'_{1L}$	13.0 nF/km
	$\underline{C}'_{0L}$	8.5 nF/km
	l	300 km

4.2.1 Verification of Synchronization Performance

In order to clearly demonstrate the method of determination of synchronization angles, the simulation of the test network is performed in normal condition. Healthy phase voltages and currents from terminal A are depicted in Figure 4.36. Very similar waveforms are obtained from terminal B.

Basically, the measured signals obtained from ATP-EMTP simulations are perfectly synchronized. To demonstrate the effectiveness of the presented algorithm, all measured signals from terminal A were artificially delayed by 18° (actual value) which firmly tallies to 10 samples in 50 Hz digitalized at 10 kHz. The calculated synchronization angles during steady-state operation, using Eq. (3.35), are shown in Figure 4.37.

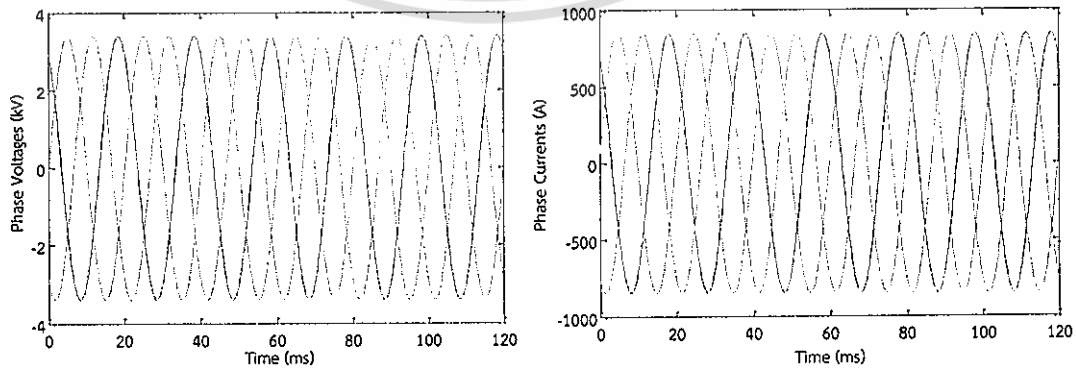

Figure 4.36 Healthy phase voltages and currents observed from terminal A

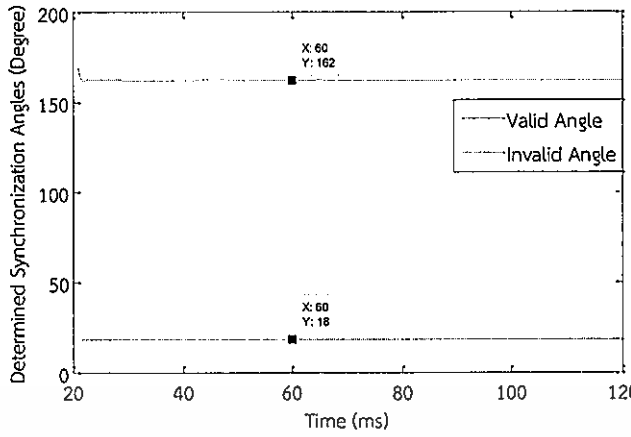

Figure 4.37 Calculated synchronization angles

From Figure 4.37 it can be confirmed that the developed algorithm starts with the quite accurate determination of the synchronization angle. This is the first approach to fulfilling the aim of finding fault on the long transmission line. Once the analytical synchronization is made, the unknown fault location is calculated as the cases of using synchronized measurement.

4.2.2 Evaluation of All Fault Types

SLG, DLG, and 3LG faults were simulated at different locations with a variety of fault resistance as well as ground resistance from 1Ω to 50Ω along the line. The represented models were depicted in Figure 2.1(a), (c), and (d). The sampling frequency was set $f_s = 10\ kHz$. The data window size used for FFT process to obtain the phasors quantities was $T_{dw} = 20\ ms$ (N = 200 samples per data window). It was assumed that the line was loaded and the fault inception time was set at $t = 40\ ms$ in all considered cases. The CTs and VTs were deliberately modeled as errorless instrument transformers. Second order Butterworth analog anti-aliasing filters designed for 500 Hz of the cutoff frequency which agrees to 10^{th} harmonic were applied by built-in function in Matlab to filter the secondary signals of the CTs and VTs.

The fault location estimation is performed in per unit (p.u.) value which complies with the given parameters of the test network. Compared to the first proposed algorithm, the presented algorithm in this section is taken into account the distributed parameter line model to ensure the high accuracy of locating faults on the long transmission line. This is so the effect of shunt capacitance is not a big deal.

To illustrate the procedures of locating a fault in this configuration, a SLG fault, as for the sample of the result, was simulated to be taken place at 0.3 p.u. (observed from terminal A) over 1 p.u. corresponded to 300 km of the total line

length with a fault resistance $R_f = 50\Omega$. The configuration of the SLG fault modeling in ATP Draw is presented in the Figure 4.38.

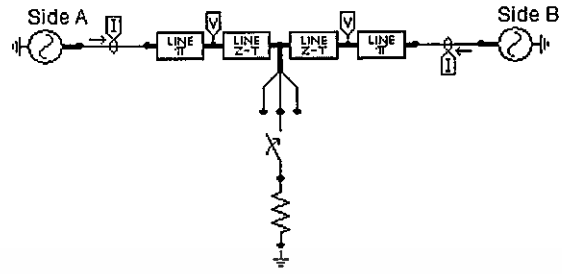

Figure 4.38 SLG fault with distributed parameter line modeling modeled in ATP Draw

The procedures for locating faults in this presented algorithm are not much different from the previous one. It just needs to do the analytical synchronization of the measured signals from both terminals. Figures 4.39 and 4.40 depicted the simulated voltage and current waveforms at the terminal A and B, respectively. Sampled measurements of these voltages and currents were used as the inputs to the algorithm which developed in Matlab.

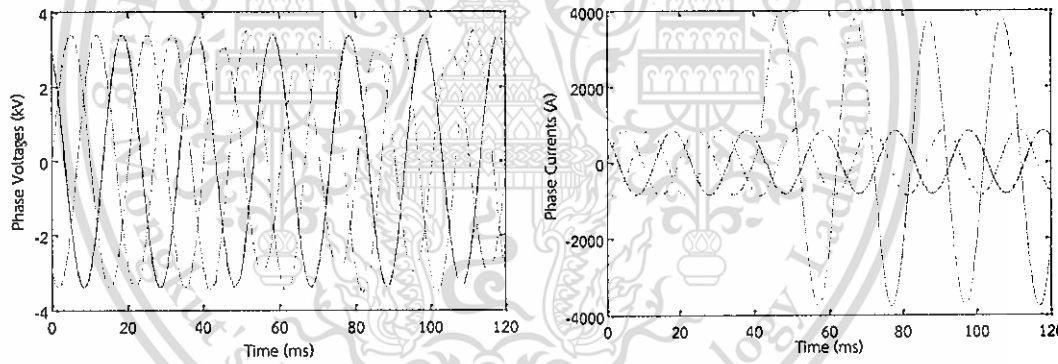

Figure 4.39 Simulated Voltages and currents of SLG fault seen from terminal A

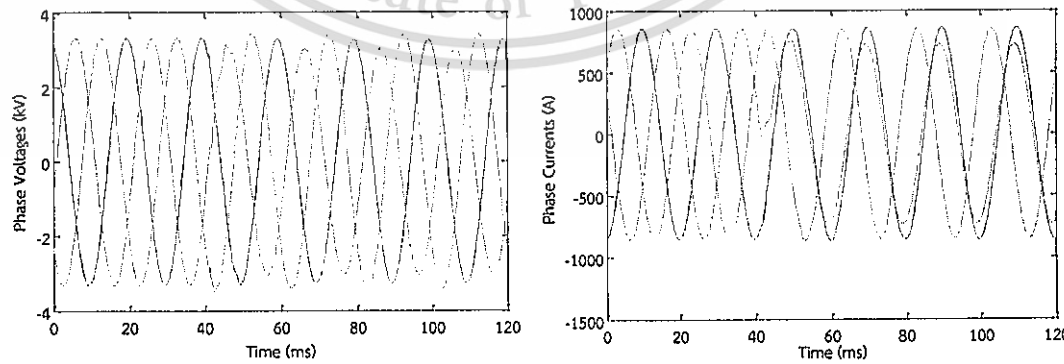

Figure 4.40 Simulated Voltages and currents of SLG fault seen from terminal B

As mentioned previously, all measured signals from terminal A were intentionally delayed by 18° (actual value) in order to show the strength of the

presented algorithm in determining the synchronization operator and angle in even faulted condition. The calculated and selected the valid synchronization operators and angles using Eqs. (3.35) and (3.36), respectively, in faulted condition are illustrated in Figure 4.41.

From Figure 4.41 it is worth to notice that the algorithm was able to carry out data synchronization during power system transients. The method of selection of the determined synchronization operator is quite reliable with the proposed tolerance of the possible error $\varepsilon = 0.01$.

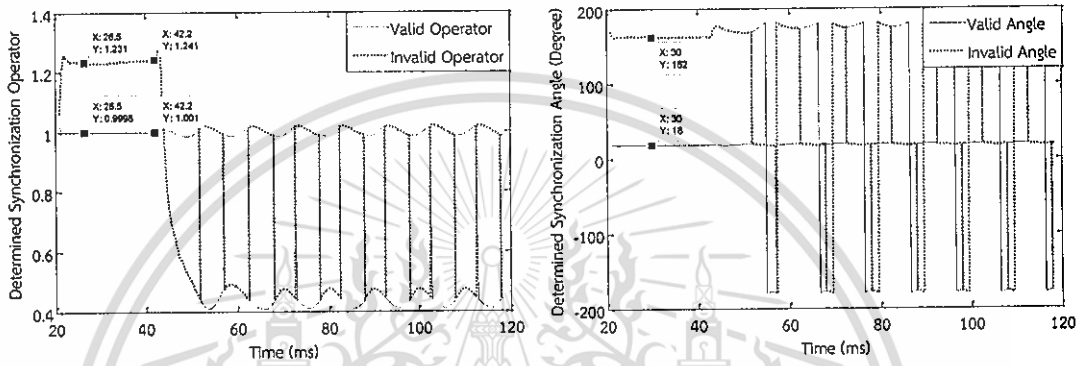

Figure 4.41 Calculated synchronization operators and angles in SLG fault

After performing the analytical synchronization, all measured signals appeared as synchronized from both terminals as the case using synchronized measurement. Then the fault location is calculated using Eq. (3.26) as plotted in Figure 4.42.

From Figure 4.42 the fault detection scheme successfully identified the faulted point just only one power cycle after the fault inception. This clearly demonstrates the robustness of the proposed algorithm.

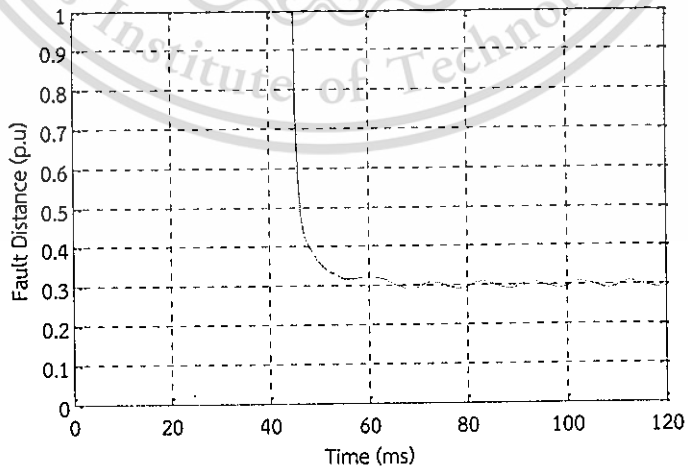

Figure 4.42 SLG fault with $R_F = 50\Omega$ estimated fault location (0.3 p.u. fault was simulated in ATP-EMTP)

Another fault type, a DLG fault was also simulated at 0.3 p.u. as the case of SLG fault (observed from terminal A) over 1 p.u. with a fault resistance $R_F = 1\Omega$, $R_g = 50\Omega$. The configuration of the DLG fault modeling in ATP Draw is presented in the Figure 4.43.

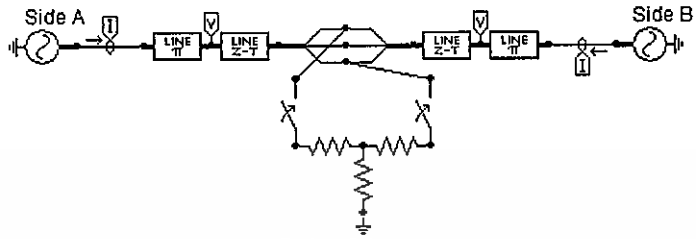

Figure 4.43 DLG fault with distributed parameter line modeling modeled in ATP Draw

Figures 4.44 and 4.45 depicted the simulated voltage and current waveforms corresponded to a DLG fault seen at the terminal A and B, respectively.

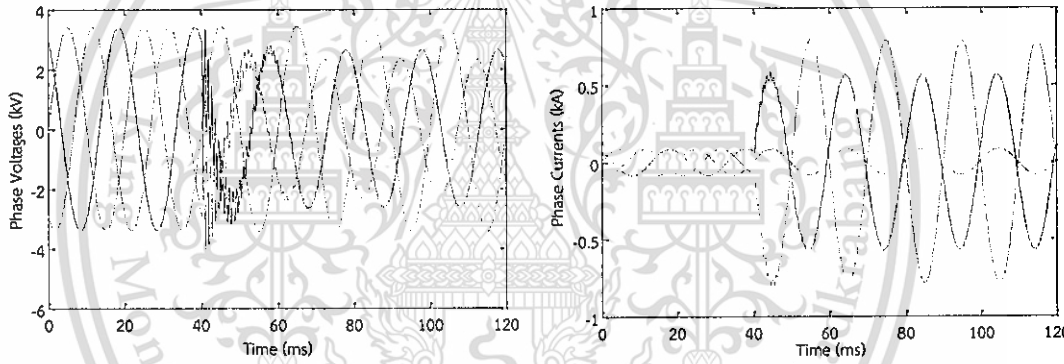

Figure 4.44 Simulated Voltages and currents of DLG fault seen from terminal A

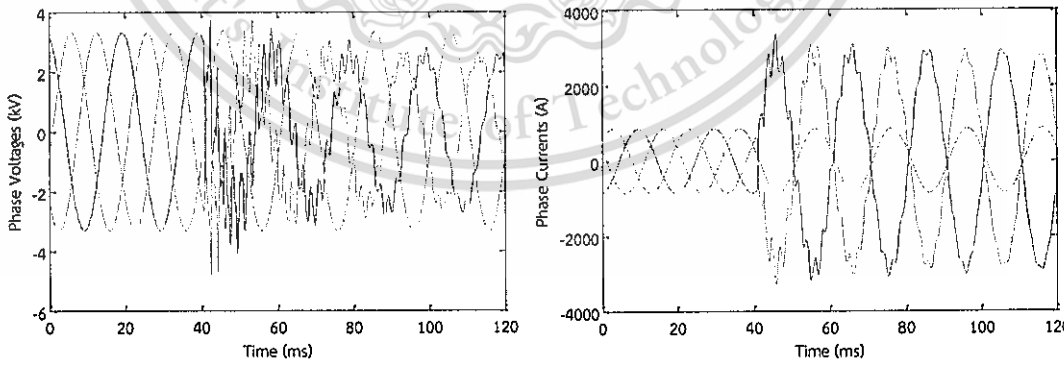

Figure 4.45 Simulated Voltages and currents of DLG fault seen from terminal B

Power systems are subjected to high-speed transients that fade away within the span of a few fundamental power cycles. It is worth to point out that good accuracy of fault location is achieved and appeared mainly due to the limited ability of the applied filter (second order Butterworth analog anti-aliasing with cutoff

frequency 500 Hz) and method of phasors extraction (FFT process) to filter out the transient distortions from the processed signals. Figures 4.46 and 4.47 depicted the voltage and current waveforms after applying the filters from the secondary signals of the CTs and VTs on terminal A and B.

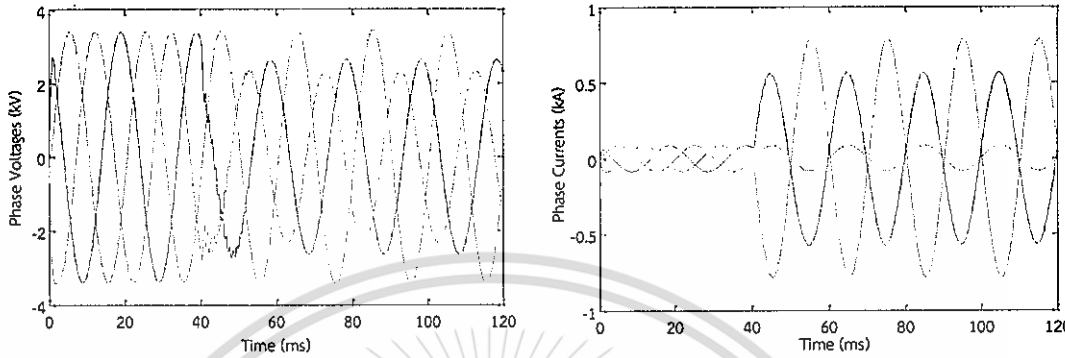

Figure 4.46 Filtered Voltages and currents of DLG fault from terminal A

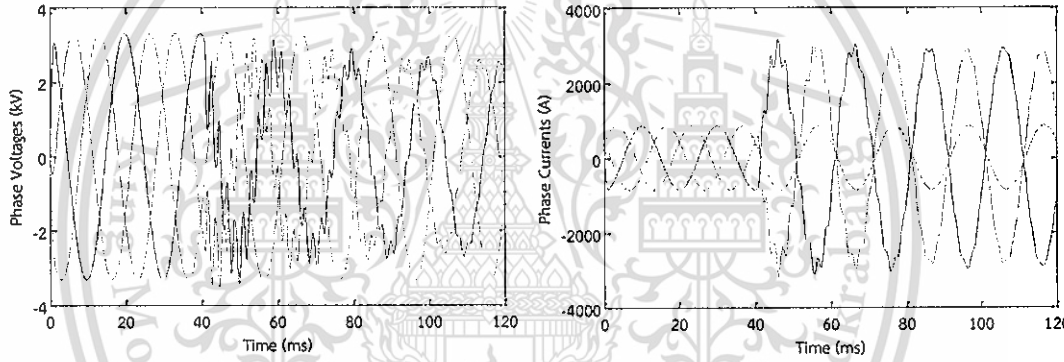

Figure 4.47 Filtered Voltages and currents of DLG fault from terminal B

The calculated and selected the valid synchronization operators and angles using Eqs. (3.35) and (3.36), respectively, in faulted condition are illustrated in Figure 4.48.

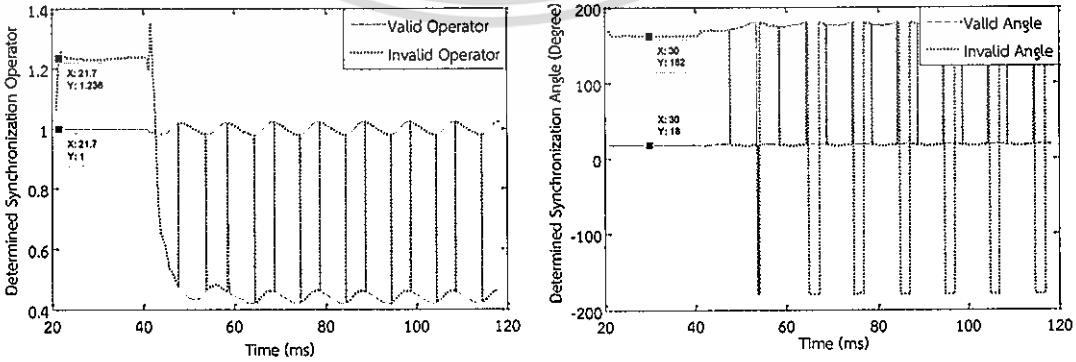

Figure 4.48 Calculated synchronization operators and angles in DLG fault

After performing the analytical synchronization, the unknown fault location is calculated using Eq. (3.26) and precisely identified as illustrated in Figure 4.49.

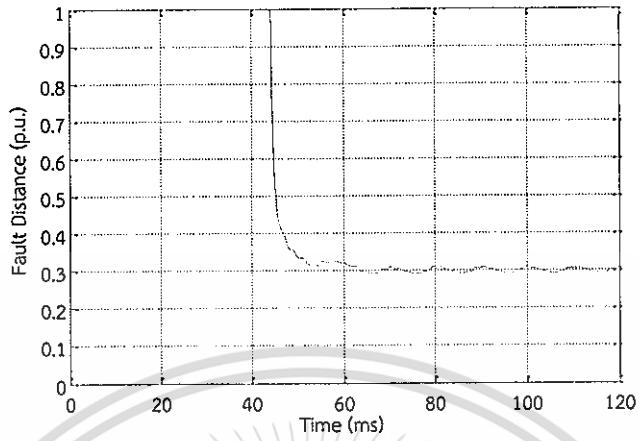

Figure 4.49 DLG fault with $R_F = 1\Omega$, $R_g = 50\Omega$ estimated fault location (0.3 p.u. fault was simulated in ATP-EMTP)

The last considered fault type, a 3LG fault was also simulated at 0.3 p.u. (observed from terminal A) over 1 p.u. with a fault resistance $R_F = 1\Omega$, $R_g = 50\Omega$. The configuration of the DLG fault modeling in ATP Draw is presented in the Figure 4.50.

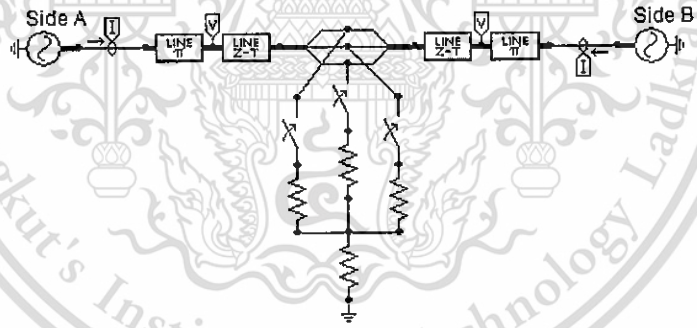

Figure 4.50 3LG fault with distributed parameter line modeling modeled in ATP Draw

Figures 4.51 and 4.52 depicted the simulated voltage and current waveforms corresponded to 3LG fault seen at the terminal A and B, respectively.

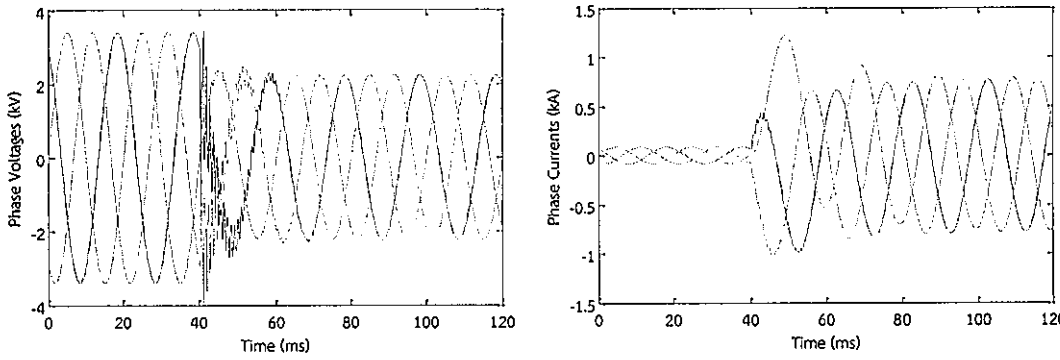

Figure 4.51 Simulated Voltages and currents of 3LG fault seen from terminal A

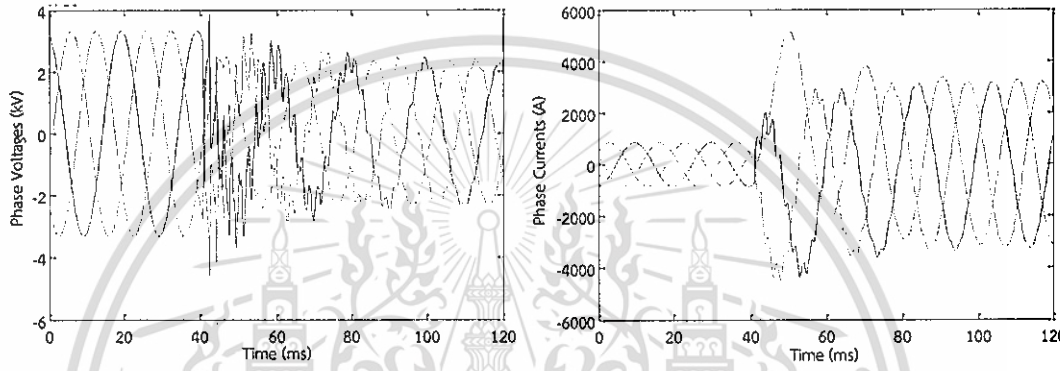

Figure 4.52 Simulated Voltages and currents of 3LG fault seen from terminal B

Figures 4.53 and 4.54 depicted the voltage and current waveforms after filtering out the distortion caused by the transients from the secondary signals of the CTs and VTs on terminal A and B.

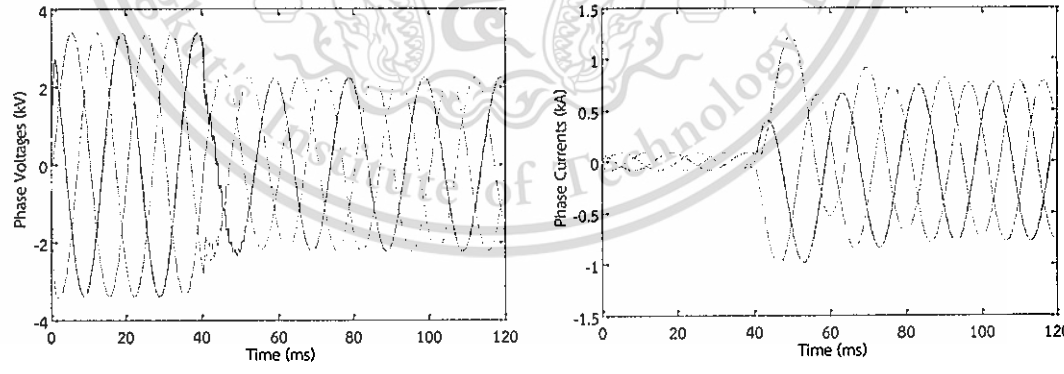

Figure 4.53 Filtered Voltages and currents of 3LG fault from terminal A

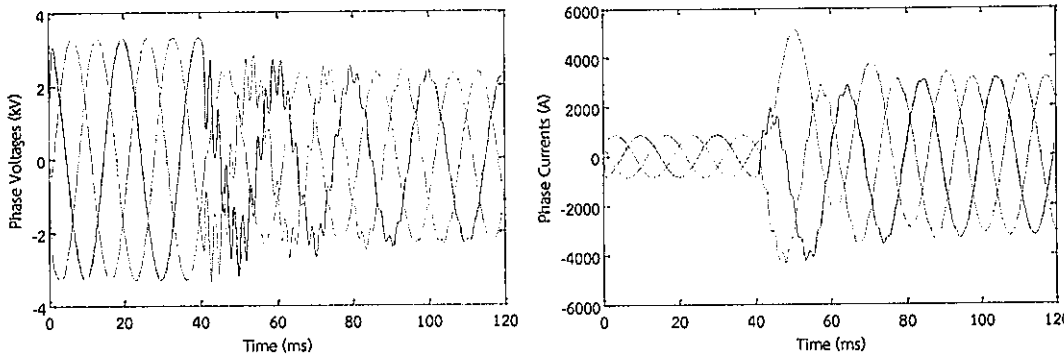

Figure 4.54 Filtered Voltages and currents of 3LG fault from terminal B

The calculated and selected the valid synchronization operators and angles using Eqs. (3.35) and (3.36), respectively, in faulted condition are plotted in Figure 4.55.

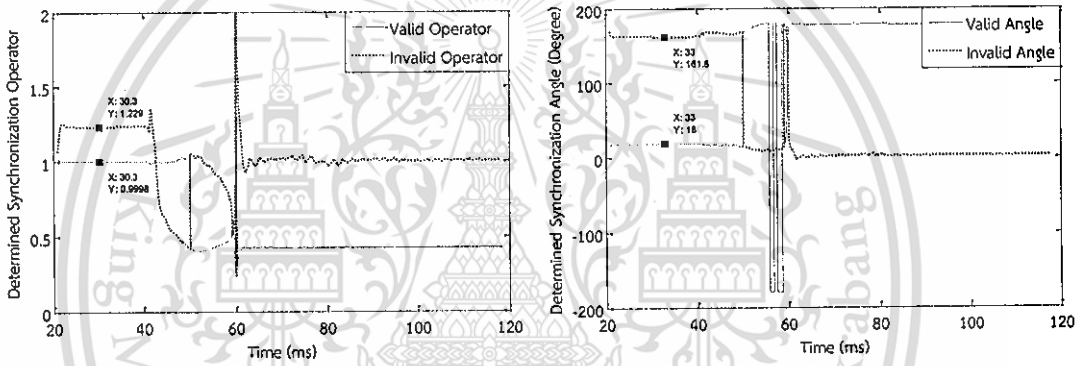

Figure 4.55 Calculated synchronization operators and angles in 3LG fault

Once the valid solution of synchronization angle is selected, the analytical synchronization is performed. Then unknown fault location is calculated using Eq. (3.26) and precisely identified as depicted in Figure 4.56.

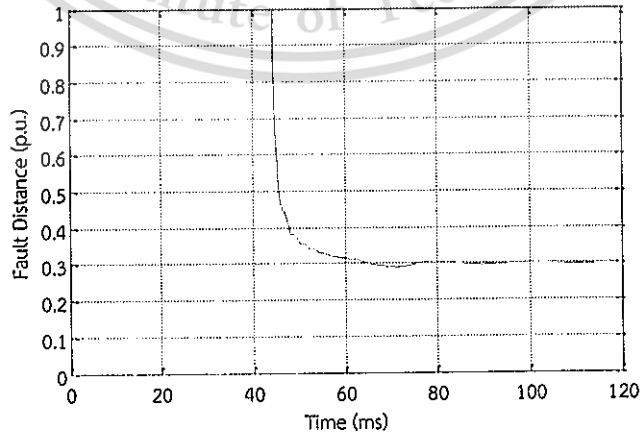

Figure 4.56 3LG fault with $R_F = 1\Omega$, $R_g = 50\Omega$ estimated fault location (0.3 p.u. fault was simulated in ATP-EMTP)

From Figure 4.56 the presented algorithm successfully identified the faulted point on the test network and agreed well with the expected theoretical results. All considered fault types have been successfully tested and located as presented in the samples.

In order to further demonstrate the algorithm's efficiency, results for 54 simulations with different scenarios have been proposed and gathered in Tables 4.10-4.12, respectively. In these tables, a variety of different fault specifications i.e. fault types, fault resistances and ground resistances which are the certain factors affected to fault location algorithm have been considered over the entire line length. The verifications of the fault distance were averaged over the interval 100-120 ms.

Table 4.10 Evaluation of SLG fault verified by using positive-sequence with $\delta_{actual} = 18^{\circ}$

Fault Distance	Determined Synchronization Operators and Synchronization Angles								Verified Fault Distance			
	$R_F = 1\Omega$				$R_F = 50\Omega$				$R_F = 1\Omega$		$R_F = 50\Omega$	
[p.u.]	$\lvert e^{j\delta_1}\rvert$	$\lvert e^{j\delta_2}\rvert$	δ_1 [°]	δ_2 [°]	$\lvert e^{j\delta_1}\rvert$	$\lvert e^{j\delta_2}\rvert$	δ_1 [°]	δ_2 [°]	d [p.u.]	error [%]	d [p.u.]	error [%]
0.1	1.0002	1.2363	17.9864	162.1161	1.0002	1.2363	17.9864	162.1161	0.1012	0.12	0.1004	0.04
0.2	1.0002	1.2333	17.9864	162.1219	1.0002	1.2333	17.9864	162.1219	0.2006	0.06	0.2000	0.00
0.3	1.0001	1.2311	17.9865	162.1260	1.0001	1.2311	17.9865	162.1260	0.3004	0.04	0.3000	0.00
0.4	1.0001	1.2298	17.9866	162.1282	1.0001	1.2298	17.9866	162.1283	0.4003	0.03	0.4001	0.01
0.5	1.0001	1.2293	17.9867	162.1287	1.0001	1.2293	17.9867	162.1288	0.5003	0.03	0.5002	0.02
0.6	1.0001	1.2297	17.9868	162.1275	1.0001	1.2297	17.9868	162.1277	0.6002	0.02	0.6003	0.03
0.7	1.0001	1.2309	17.9870	162.1252	1.0001	1.2309	17.9869	162.1253	0.7001	0.01	0.7004	0.04
0.8	1.0001	1.2330	17.9872	162.1224	1.0001	1.2331	17.9871	162.1222	0.7999	0.01	0.8005	0.05
0.9	1.0002	1.2361	17.9873	162.1195	1.0002	1.2361	17.9872	162.1188	0.8996	0.04	0.9005	0.05

Table 4.11 Evaluation of DLG fault verified by using positive-sequence with $\delta_{actual} = 18^{\circ}$

Fault Distance	Determined Synchronization Operators and Synchronization Angles								Verified Fault Distance			
	$R_F = 1\Omega, R_g = 1\Omega$				$R_F = 1\Omega, R_g = 50\Omega$				$R_F = 1\Omega, R_g = 1\Omega$		$R_F = 1\Omega, R_g = 50\Omega$	
[p.u.]	$\lvert e^{j\delta_1}\rvert$	$\lvert e^{j\delta_2}\rvert$	δ_1 [°]	δ_2 [°]	$\lvert e^{j\delta_1}\rvert$	$\lvert e^{j\delta_2}\rvert$	δ_1 [°]	δ_2 [°]	d [p.u.]	error [%]	d [p.u.]	error [%]
0.1	1.0002	1.2363	17.9864	162.1161	1.0002	1.2363	17.9864	162.1161	0.1004	0.04	0.1007	0.07
0.2	1.0002	1.2333	17.9864	162.1224	1.0002	1.2333	17.9864	162.1224	0.2002	0.02	0.2002	0.02
0.3	1.0001	1.2311	17.9864	162.1300	1.0001	1.2311	17.9864	162.1300	0.3002	0.02	0.3002	0.02
0.4	1.0001	1.2297	17.9861	162.1438	1.0001	1.2297	17.9861	162.1438	0.4002	0.02	0.4002	0.02
0.5	1.0001	1.2291	17.9854	162.1665	1.0001	1.2291	17.9854	162.1665	0.5002	0.02	0.5003	0.03
0.6	1.0001	1.2293	17.9840	162.1959	1.0001	1.2293	17.9840	162.1960	0.6002	0.02	0.6003	0.03
0.7	1.0000	1.2305	17.9817	162.2246	1.0000	1.2305	17.9817	162.2246	0.7002	0.02	0.7004	0.04
0.8	1.0000	1.2330	17.9784	162.2314	1.0000	1.2330	17.9784	162.2313	0.8002	0.02	0.8004	0.04
0.9	1.0000	1.2367	17.9749	162.2135	1.0000	1.2367	17.9748	162.2131	0.9002	0.02	0.9005	0.05

Table 4.12 Evaluation of 3LG fault verified by using positive-sequence with $\delta_{actual} = 18^{\circ}$

Fault Distance	Determined Synchronization Operators and Synchronization Angles								Verified Fault Distance			
	$R_F = 1\Omega, R_g = 1\Omega$				$R_F = 1\Omega, R_g = 50\Omega$				$R_F = 1\Omega, R_g = 1\Omega$		$R_F = 1\Omega, R_g = 50\Omega$	
[p.u.]	$\lvert e^{j\delta_1} \rvert$	$\lvert e^{j\delta_2} \rvert$	δ_1 [°]	δ_2 [°]	$\lvert e^{j\delta_1} \rvert$	$\lvert e^{j\delta_2} \rvert$	δ_1 [°]	δ_2 [°]	d [p.u.]	error [%]	d [p.u.]	error [%]
0.1	1.0002	1.2363	17.9864	162.1161	1.0002	1.2363	17.9864	162.1161	0.1001	0.01	0.1001	0.01
0.2	1.0002	1.2333	17.9864	162.1224	1.0002	1.2333	17.9864	162.1224	0.2001	0.01	0.2001	0.01
0.3	1.0001	1.2311	17.9864	162.1299	1.0001	1.2311	17.9864	162.1299	0.3001	0.01	0.3001	0.01
0.4	1.0001	1.2297	17.9862	162.1432	1.0001	1.2297	17.9862	162.1432	0.4000	0.00	0.4000	0.00
0.5	1.0001	1.2290	17.9855	162.1651	1.0001	1.2290	17.9855	162.1651	0.4999	0.01	0.4999	0.01
0.6	1.0001	1.2292	17.9843	162.1937	1.0001	1.2292	17.9843	162.1937	0.5998	0.02	0.5998	0.02
0.7	1.0000	1.2303	17.9823	162.2222	1.0000	1.2303	17.9823	162.2222	0.6997	0.03	0.6997	0.03
0.8	1.0000	1.2328	17.9794	162.2314	1.0000	1.2328	17.9794	162.2314	0.7997	0.03	0.7997	0.03
0.9	1.0000	1.2365	17.9762	162.2180	1.0000	1.2365	17.9762	162.2180	0.8996	0.04	0.8996	0.04

Based on the condition in Eq. (3.36), synchronization operators and angles are successfully selected as valid solution which is close to actual value, 18°, whereas another solution differs very much from it. The relative error of the synchronization angle does not exceed 0.02°. This shows the strength of the presented algorithm which starts with quite accurate identification of the synchronization angle. Once the synchronization operator is determined, the fault distance is calculated by using Eq. (3.26) and provided the high level of accuracy in locating all fault types as given from Tables 4.10-4.12.

It is obvious that errors occurred during the convergence are due to the presence of the DC components in the fault current. Commonly, since FFT was used in this extraction process, it is known to be sensitive to the decaying of DC components. The relative error of the distance to fault in all cases does not exceed 0.12%. Based on evaluative results, it can be concluded that the proposed algorithm is unaffected by fault resistance and ground resistance for all fault types.

4.2.3 Investigation on Additive White Gaussian Noise (AWGN)

The use of PMUs in the reality can be disturbed by noise. This includes electronic noise even some external events that affect the measured phenomenon. Noise ratio 40dB is considered as the severe noise introduced in the network. AWGN whose SNR is 40dB has been added to voltages and currents from both terminals by Matlab. The error presented in the results obtained for this condition have been used the averaged value of 10-time simulations within interval 100-120 ms in each case as given in Table 4.13.

Table 4.13 Fault location error [%] for all considered fault type evaluation with considering AWGN

Fault Distance [p.u.]	Verified Fault Distance Error [%]					
	SLG	DLG	3LG	SLG	DLG	3LG
	$R_F = 1\Omega$	$R_F = 1\Omega$, $R_g = 1\Omega$		$R_F = 50\Omega$	$R_F = 1\Omega$, $R_g = 50\Omega$	
0.1	0.123	0.044	0.013	0.054	0.066	0.013
0.2	0.057	0.020	0.011	0.007	0.021	0.012
0.3	0.041	0.018	0.010	0.002	0.018	0.010
0.4	0.037	0.020	0.000	0.004	0.021	0.001
0.5	0.035	0.022	0.006	0.025	0.031	0.006
0.6	0.017	0.023	0.015	0.028	0.032	0.018
0.7	0.004	0.024	0.024	0.048	0.039	0.027
0.8	0.014	0.022	0.032	0.049	0.041	0.031
0.9	0.037	0.020	0.040	0.052	0.050	0.040

From Table 4.13, it can be concluded that the algorithm still maintained a high level of accuracy in locating all fault types even the effect of severe noise in the network has been considered and maximum error does not more than 0.123%.

4.2.4 Investigation on Phase Shift Angle

Phase shift angle from both terminals which considered as one of the affected factors was further investigated in order to ensure the efficiency of the presented algorithm. Phase shift angle was changed by setting the terminal B as delayed (α_B =-10°, -20°, -30°), leading (α_B =10°, 20°, 30°), and no phase shift angle ($\alpha_A = \alpha_B = 0°$) to the terminal A.

4.2.4.1 Terminal B Delayed by (α_B =-10°, -20°, -30°) to Terminal A

Tables 4.14-4.19 show the results of all fault types considering different phase shift angles which were set the terminal B as delayed to the terminal A. The errors presented in the results have been averaged over the interval 100-120 ms.

From Tables 4.14-4.19, it can be confirmed that the high accuracy of the presented algorithm is still applicable even delayed phase shift angles from terminal B are considered. The maximum error of fault distance and determined synchronization angle in all cases do not exceed 0.08% and 0.03°, respectively.

Table 4.14 Determination of synchronization operators and angles in SLG fault with $R_F = 10\Omega$, $\alpha_A = 0°$, $\delta_{actual} = 18°$ in considering delayed phase shift angles

Fault Distance	Determined Synchronization Operators and Synchronization Angles											
	$\alpha_B = -10°$				$\alpha_B = -20°$				$\alpha_B = -30°$			
d [p.u.]	$\lvert e^{j\delta_1} \rvert$	$\lvert e^{j\delta_2} \rvert$	δ_1 [°]	δ_2 [°]	$\lvert e^{j\delta_1} \rvert$	$\lvert e^{j\delta_2} \rvert$	δ_1 [°]	δ_2 [°]	$\lvert e^{j\delta_1} \rvert$	$\lvert e^{j\delta_2} \rvert$	δ_1 [°]	δ_2 [°]
0.1	1.0002	1.4749	17.9863	162.1051	1.0002	1.2363	17.9864	162.1161	1.4399	1.0000	161.9393	17.9859
0.2	1.0001	1.4738	17.9864	162.1068	1.0002	1.2333	17.9864	162.1220	1.4746	1.0000	161.8771	17.9864
0.3	1.0001	1.4730	17.9865	162.1081	1.0001	1.2311	17.9865	162.1263	1.5003	1.0000	161.8302	17.9865
0.4	1.0001	1.4725	17.9866	162.1093	1.0001	1.2297	17.9866	162.1295	1.5169	1.0000	161.7968	17.9865
0.5	1.0001	1.4724	17.9868	162.1107	1.0001	1.2292	17.9867	162.1322	1.5240	1.0000	161.7746	17.9862
0.6	1.0001	1.4725	17.9869	162.1127	1.0001	1.2294	17.9868	162.1346	1.5218	1.0000	161.7631	17.9857
0.7	1.0001	1.4731	17.9871	162.1155	1.0001	1.2306	17.9870	162.1369	1.5099	1.0000	161.7635	17.9853
0.8	1.0001	1.4740	17.9872	162.1192	1.0001	1.2327	17.9871	162.1385	1.4879	1.0000	161.7823	17.9848
0.9	1.0001	1.4755	17.9873	162.1227	1.0001	1.2359	17.9871	162.1378	1.4547	0.9999	161.8299	17.9845

Table 4.15 Verification of the fault distance in SLG fault with $R_F = 10\Omega$, $\alpha_A = 0°$ $\delta_{actual} = 18°$ in considering delayed phase shift angles

Fault Distance	Verified Fault Distance					
	$\alpha_B = -10°$		$\alpha_B = -20°$		$\alpha_B = -30°$	
d [p.u.]	d [p.u.]	error [%]	d [p.u.]	error [%]	d [p.u.]	error [%]
0.1	0.1008	0.08	0.1008	0.08	0.1006	0.06
0.2	0.2003	0.03	0.2004	0.04	0.2002	0.02
0.3	0.3002	0.02	0.3003	0.03	0.3003	0.03
0.4	0.4002	0.02	0.4003	0.03	0.4003	0.03
0.5	0.5002	0.02	0.5004	0.04	0.5004	0.04
0.6	0.6002	0.02	0.6004	0.04	0.6004	0.04
0.7	0.7003	0.03	0.7004	0.04	0.7004	0.04
0.8	0.8003	0.03	0.8004	0.04	0.8003	0.03
0.9	0.9003	0.03	0.9004	0.04	0.9002	0.02

Table 4.16 Determination of synchronization operators and angles in DLG fault with $R_F = 1\Omega$, $R_g = 10\Omega$, $\alpha_A = 0°$, $\delta_{actual} = 18°$ in considering delayed phase shift angles

Fault Distance	Determined Synchronization Operators and Synchronization Angles											
	$\alpha_B = -10°$				$\alpha_B = -20°$				$\alpha_B = -30°$			
d [p.u.]	$\lvert e^{j\delta_1} \rvert$	$\lvert e^{j\delta_2} \rvert$	δ_1 [°]	δ_2 [°]	$\lvert e^{j\delta_1} \rvert$	$\lvert e^{j\delta_2} \rvert$	δ_1 [°]	δ_2 [°]	$\lvert e^{j\delta_1} \rvert$	$\lvert e^{j\delta_2} \rvert$	δ_1 [°]	δ_2 [°]
0.1	1.0002	1.4749	17.9863	162.1051	1.0002	1.2363	17.9864	162.1161	1.4399	1.0000	161.9393	17.9859
0.2	1.0001	1.4738	17.9864	162.1068	1.0002	1.2333	17.9864	162.1220	1.4745	1.0000	161.8740	17.9864
0.3	1.0001	1.4731	17.9863	162.1088	1.0001	1.2311	17.9864	162.1295	1.5002	1.0000	161.8021	17.9866
0.4	1.0001	1.4726	17.9860	162.1114	1.0001	1.2298	17.9861	162.1414	1.5163	1.0000	161.6892	17.9866
0.5	1.0001	1.4725	17.9851	162.1140	1.0001	1.2294	17.9854	162.1601	1.5225	1.0000	161.5099	17.9864
0.6	1.0001	1.4729	17.9832	162.1137	1.0001	1.2298	17.9839	162.1829	1.5188	1.0000	161.2656	17.9860
0.7	1.0001	1.4738	17.9802	162.1056	1.0001	1.2312	17.9816	162.2029	1.5051	1.0000	160.9853	17.9852

0.8	1.0001	1.4753	17.9760	162.0820	1.0001	1.2336	17.9784	162.2025	1.4813	1.0000	160.7813	17.9837
0.9	1.0001	1.4771	17.9715	162.0473	1.0001	1.2371	17.9751	162.1803	1.4474	1.0000	160.7116	17.9820

Table 4.17 Verification of the fault distance in DLG fault with $R_F = 1\Omega$, $R_g = 10\Omega$ $\alpha_A = 0^\circ$, $\delta_{actual} = 18^\circ$ in considering delayed phase shift angles

Fault Distance	Verified Fault Distance					
	$\alpha_B = -10^\circ$		$\alpha_B = -20^\circ$		$\alpha_B = -30^\circ$	
d [p.u.]	d [p.u.]	error [%]	d [p.u.]	error [%]	d [p.u.]	error [%]
0.1	0.1004	0.04	0.1004	0.04	0.1004	0.04
0.2	0.1999	0.01	0.2000	0.00	0.2000	0.00
0.3	0.2999	0.01	0.2999	0.01	0.2999	0.01
0.4	0.3998	0.02	0.3998	0.02	0.3998	0.02
0.5	0.4998	0.02	0.4998	0.02	0.4998	0.02
0.6	0.5998	0.02	0.5998	0.02	0.5997	0.03
0.7	0.6998	0.02	0.6998	0.02	0.6996	0.04
0.8	0.7999	0.01	0.7997	0.03	0.7996	0.04
0.9	0.8999	0.01	0.8997	0.03	0.8995	0.05

Table 4.18 Determination of synchronization operators and angles in 3LG fault with $R_F = 1\Omega$, $R_g = 10\Omega$, $\alpha_A = 0^\circ$, $\delta_{actual} = 18^\circ$ in considering delayed phase shift angles

Fault Distance	Determined Synchronization Operators and Synchronization Angles											
	$\alpha_B = -10^\circ$				$\alpha_B = -20^\circ$				$\alpha_B = -30^\circ$			
d [p.u.]	$\lvert e^{j\delta_1}\rvert$	$\lvert e^{j\delta_2}\rvert$	δ_1 [°]	δ_2 [°]	$\lvert e^{j\delta_1}\rvert$	$\lvert e^{j\delta_2}\rvert$	δ_1 [°]	δ_2 [°]	$\lvert e^{j\delta_1}\rvert$	$\lvert e^{j\delta_2}\rvert$	δ_1 [°]	δ_2 [°]
0.1	1.0002	1.4749	17.9863	162.1051	1.0002	1.2363	17.9864	162.1161	1.4399	1.0000	161.9393	17.9859
0.2	1.0001	1.4738	17.9864	162.1068	1.0002	1.2333	17.9864	162.1220	1.4746	1.0000	161.8740	17.9864
0.3	1.0001	1.4730	17.9864	162.1088	1.0001	1.2311	17.9864	162.1299	1.5007	1.0000	161.7990	17.9866
0.4	1.0001	1.4726	17.9861	162.1126	1.0001	1.2297	17.9862	162.1432	1.5182	1.0000	161.6764	17.9865
0.5	1.0001	1.4725	17.9853	162.1175	1.0001	1.2290	17.9855	162.1651	1.5276	1.0000	161.4766	17.9862
0.6	1.0000	1.4729	17.9837	162.1215	1.0001	1.2292	17.9843	162.1937	1.5288	1.0000	161.2007	17.9857
0.7	1.0000	1.4740	17.9810	162.1202	1.0000	1.2303	17.9823	162.2222	1.5215	1.0000	160.8817	17.9847
0.8	1.0000	1.4758	17.9772	162.1054	1.0000	1.2328	17.9794	162.2314	1.5030	1.0000	160.6471	17.9833
0.9	1.0000	1.4782	17.9730	162.0797	1.0000	1.2365	17.9762	162.2180	1.4723	1.0000	160.5582	17.9816

Table 4.19 Verification of the fault distance in 3LG fault with $R_F = 1\Omega$, $R_g = 10\Omega$ $\alpha_A = 0^\circ$, $\delta_{actual} = 18^\circ$ in considering delayed phase shift angles

Fault Distance	Verified Fault Distance					
	$\alpha_B = -10^\circ$		$\alpha_B = -20^\circ$		$\alpha_B = -30^\circ$	
d [p.u.]	d [p.u.]	error [%]	d [p.u.]	error [%]	d [p.u.]	error [%]
0.1	0.1001	0.01	0.1001	0.01	0.1001	0.01
0.2	0.2001	0.01	0.2001	0.01	0.2001	0.01
0.3	0.3001	0.01	0.3001	0.01	0.3001	0.01

0.4	0.4000	0.00	0.4000	0.00	0.4001	0.01
0.5	0.4999	0.01	0.4999	0.01	0.500	0.00
0.6	0.5998	0.02	0.5998	0.02	0.5999	0.01
0.7	0.6997	0.03	0.6997	0.03	0.6998	0.02
0.8	0.7997	0.03	0.7997	0.03	0.7997	0.03
0.9	0.8996	0.04	0.8996	0.04	0.8996	0.04

4.2.4.2 Terminal B Leading by (α_B =10°, 20°, 30°) to Terminal A

Tables 4.20-4.25 show the results of all fault types considering different phase shift angles which were set the terminal B as leading to the terminal A. The errors presented in the results have been averaged over the interval 100-120 ms.

From Tables 4.20-4.25, it can be confirmed that the high accuracy of the presented algorithm is still applicable even delayed phase shift angles from terminal B are considered. The maximum error of fault distance and determined synchronization angle in all cases do not exceed 0.06% and 0.138°, respectively.

Table 4.20 Determination of synchronization operators and angles in SLG fault with $R_F = 10\Omega$, $\alpha_A = 0°$, $\delta_{actual} = 18°$ in considering leading phase shift angles

Fault Distance	Determined Synchronization Operators and Synchronization Angles											
	$\alpha_B = 10°$				$\alpha_B = 20°$				$\alpha_B = 30°$			
d [p.u.]	$\lvert e^{j\delta_1}\rvert$	$\lvert e^{j\delta_2}\rvert$	δ_1 [°]	δ_2 [°]	$\lvert e^{j\delta_1}\rvert$	$\lvert e^{j\delta_2}\rvert$	δ_1 [°]	δ_2 [°]	$\lvert e^{j\delta_1}\rvert$	$\lvert e^{j\delta_2}\rvert$	δ_1 [°]	δ_2 [°]
0.1	1.0000	3.8652	17.9845	162.0952	0.9998	5.6028	17.9753	-17.8746	0.8613	1.0004	-17.8354	17.9213
0.2	1.0000	3.8691	17.9850	162.0921	0.9998	5.5907	17.9784	-17.8721	0.8616	1.0003	-17.8542	17.9402
0.3	1.0000	3.8719	17.9856	162.0899	0.9999	5.5822	17.9809	-17.8705	0.8618	1.0002	-17.8670	17.9534
0.4	1.0000	3.8737	17.9861	162.0889	0.9999	5.5772	17.9828	-17.8690	0.8619	1.0002	-17.8729	17.9608
0.5	1.0000	3.8743	17.9865	162.0898	0.9999	5.5758	17.9839	-17.8671	0.8620	1.0001	-17.8713	17.9622
0.6	1.0000	3.8740	17.9869	162.0930	0.9999	5.5781	17.9841	-17.8643	0.8621	1.0001	-17.8625	17.9578
0.7	1.0000	3.8727	17.9870	162.0987	0.9998	5.5840	17.9831	-17.8607	0.8620	1.0001	-17.8478	17.9479
0.8	0.9999	3.8705	17.9869	162.1067	0.9997	5.5934	17.9810	-17.8567	0.8619	1.0002	-17.8302	17.9334
0.9	0.9999	3.8673	17.9863	162.1157	0.9996	5.6061	17.9773	-17.8544	0.8616	1.0003	-17.8140	17.9152

Table 4.21 Verification of the fault distance in SLG fault with $R_F = 10\Omega$, $\alpha_A = 0°$ $\delta_{actual} = 18°$ in considering leading phase shift angles

Fault Distance	Verified Fault Distance					
	$\alpha_B = 10°$		$\alpha_B = 20°$		$\alpha_B = 30°$	
d [p.u.]	d [p.u.]	error [%]	d [p.u.]	error [%]	d [p.u.]	error [%]
0.1	0.1006	0.06	0.1004	0.04	0.1005	0.05
0.2	0.2000	0.00	0.1998	0.02	0.1999	0.01
0.3	0.2999	0.01	0.2996	0.04	0.2997	0.03
0.4	0.3999	0.01	0.3996	0.04	0.3996	0.04
0.5	0.4999	0.01	0.4996	0.04	0.4996	0.04

0.6	0.5999	0.01	0.5996	0.04	0.5996	0.04
0.7	0.6999	0.01	0.6996	0.04	0.6997	0.03
0.8	0.8000	0.00	0.7997	0.03	0.7999	0.01
0.9	0.9001	0.01	0.8998	0.02	0.9001	0.01

Table 4.22 Determination of synchronization operators and angles in DLG fault with $R_F = 1\Omega$, $R_g = 10\Omega$, $\alpha_A = 0^\circ$, $\delta_{actual} = 18^\circ$ in considering leading phase shift angles

Fault Distance	Determined Synchronization Operators and Synchronization Angles											
	$\alpha_B = 10^\circ$				$\alpha_B = 20^\circ$				$\alpha_B = 30^\circ$			
d [p.u.]	$\lvert e^{j\delta_1}\rvert$	$\lvert e^{j\delta_2}\rvert$	δ_1 [°]	δ_2 [°]	$\lvert e^{j\delta_1}\rvert$	$\lvert e^{j\delta_2}\rvert$	δ_1 [°]	δ_2 [°]	$\lvert e^{j\delta_1}\rvert$	$\lvert e^{j\delta_2}\rvert$	δ_1 [°]	δ_2 [°]
0.1	1.0000	3.8652	17.9845	162.0952	0.9998	5.6028	17.9753	-17.8746	0.8613	1.0004	-17.8354	17.9213
0.2	1.0000	3.8691	17.9850	162.0921	0.9998	5.5908	17.9783	-17.8723	0.8616	1.0003	-17.8546	17.9402
0.3	1.0000	3.8720	17.9853	162.0888	0.9999	5.5824	17.9804	-17.8724	0.8618	1.0003	-17.8711	17.9531
0.4	1.0000	3.8740	17.9849	162.0838	0.9999	5.5781	17.9805	-17.8776	0.8621	1.0002	-17.8904	17.9592
0.5	1.0000	3.8754	17.9832	162.0738	0.9999	5.5785	17.9775	-17.8926	0.8626	1.0003	-17.9212	17.9575
0.6	1.0000	3.8765	17.9793	162.0543	0.9999	5.5841	17.9702	-17.9234	0.8635	1.0005	-17.9723	17.9469
0.7	1.0000	3.8776	17.9729	162.0200	0.9999	5.5955	17.9580	-17.9762	0.8648	1.0008	-18.0527	17.9271
0.8	0.9999	3.8787	17.9640	161.9683	0.9998	5.6127	17.9418	-18.0523	0.8666	1.0012	-18.1617	17.8997
0.9	0.9999	3.8791	17.9545	161.9101	0.9998	5.6338	17.9245	-18.1363	0.8684	1.0016	-18.2756	17.8686

Table 4.23 Verification of the fault distance in DLG fault with $R_F = 1\Omega$, $R_g = 10\Omega$ $\alpha_A = 0^\circ$, $\delta_{actual} = 18^\circ$ in considering leading phase shift angles

Fault Distance	Verified Fault Distance					
	$\alpha_B = 10^\circ$		$\alpha_B = 20^\circ$		$\alpha_B = 30^\circ$	
d [p.u.]	d [p.u.]	error [%]	d [p.u.]	error [%]	d [p.u.]	error [%]
0.1	0.1003	0.03	0.1003	0.03	0.1003	0.03
0.2	0.1999	0.01	0.1999	0.01	0.1999	0.01
0.3	0.2998	0.02	0.2998	0.02	0.2999	0.01
0.4	0.3998	0.02	0.3998	0.02	0.3999	0.01
0.5	0.4999	0.01	0.4998	0.02	0.5000	0.00
0.6	0.5999	0.01	0.5999	0.01	0.6001	0.01
0.7	0.7000	0.00	0.7000	0.00	0.7003	0.03
0.8	0.8001	0.01	0.8001	0.01	0.8005	0.05
0.9	0.9002	0.02	0.9002	0.02	0.9006	0.06

Table 4.24 Determination of synchronization operators and angles in 3LG fault with $R_F = 1\Omega$, $R_g = 10\Omega$, $\alpha_A = 0°$, $\delta_{actual} = 18°$ in considering leading phase shift angles

Fault Distance	Determined Synchronization Operators and Synchronization Angles											
	$\alpha_B = 10°$				$\alpha_B = 20°$				$\alpha_B = 30°$			
d [p.u.]	$\lvert e^{j\delta_1}\rvert$	$\lvert e^{j\delta_2}\rvert$	δ_1 [°]	δ_2 [°]	$\lvert e^{j\delta_1}\rvert$	$\lvert e^{j\delta_2}\rvert$	δ_1 [°]	δ_2 [°]	$\lvert e^{j\delta_1}\rvert$	$\lvert e^{j\delta_2}\rvert$	δ_1 [°]	δ_2 [°]
0.1	1.0000	3.8652	17.9845	162.0952	0.9998	5.6028	17.9753	-17.8746	0.8613	1.0004	-17.8354	17.9213
0.2	1.0000	3.8691	17.9850	162.0921	0.9998	5.5908	17.9783	-17.8723	0.8616	1.0003	-17.8546	17.9402
0.3	1.0000	3.8721	17.9853	162.0888	0.9999	5.5825	17.9804	-17.8724	0.8618	1.0003	-17.8697	17.9528
0.4	1.0000	3.8742	17.9851	162.0856	0.9999	5.5784	17.9807	-17.8750	0.8622	1.0002	-17.8852	17.9582
0.5	1.0000	3.8758	17.9835	162.0788	0.9999	5.5792	17.9778	-17.8858	0.8628	1.0003	-17.9081	17.9549
0.6	0.9999	3.8774	17.9801	162.0651	0.9998	5.5856	17.9708	-17.9094	0.8637	1.0005	-17.9477	17.9421
0.7	0.9999	3.8792	17.9742	162.0396	0.9998	5.5982	17.9591	-17.9522	0.8652	1.0007	-18.0153	17.9202
0.8	0.9998	3.8815	17.9659	161.9986	0.9997	5.6167	17.9431	-18.0175	0.8670	1.0011	-18.1166	17.8919
0.9	0.9998	3.8829	17.9568	161.9503	0.9996	5.6388	17.9257	-18.0939	0.8687	1.0015	-18.2342	17.8620

Table 4.25 Verification of the fault distance in 3LG fault with $R_F = 1\Omega$, $R_g = 10\Omega$ $\alpha_A = 0°$, $\delta_{actual} = 18°$ in considering leading phase shift angles

Fault Distance	Verified Fault Distance					
	$\alpha_B = 10°$		$\alpha_B = 20°$		$\alpha_B = 30°$	
d [p.u.]	d [p.u.]	error [%]	d [p.u.]	error [%]	d [p.u.]	error [%]
0.1	0.1001	0.01	0.1001	0.01	0.1001	0.01
0.2	0.2001	0.01	0.2001	0.01	0.2001	0.01
0.3	0.3000	0.00	0.3000	0.00	0.3000	0.00
0.4	0.4000	0.00	0.3999	0.01	0.3999	0.01
0.5	0.4999	0.01	0.4998	0.02	0.4998	0.02
0.6	0.5998	0.02	0.5997	0.03	0.5997	0.03
0.7	0.6997	0.03	0.6997	0.03	0.6996	0.04
0.8	0.7996	0.04	0.7996	0.04	0.7996	0.04
0.9	0.8996	0.04	0.8996	0.04	0.8995	0.05

4.2.4.3 No Phase Shift Angle ($\alpha_A = \alpha_B = 0°$) from Both Terminals

Tables 4.26-4.27 show the results of all fault types considering no phase shift angle from both terminals which are the last case of the verification of the presented fault location algorithm. The errors presented in the results have been averaged over the interval 100-120 ms.

From Tables 4.26-4.27, it can be confirmed that the high accuracy of the presented algorithm is still applicable even no phase shift angle from both terminals is considered. The maximum error of fault distance and determined synchronization angle in all cases do not exceed 0.07% and 0.03°, respectively.

Table 4.26 Determination of synchronization operators and angles in all fault types with $\alpha_A = \alpha_B = 0°$, $\delta_{actual} = 18°$ in considering no phase shift angles

Fault Distance	Determined Synchronization Operators and Synchronization Angles											
	SLG, $R_F = 10\Omega$				DLG, $R_F = 1\Omega, R_g = 10\Omega$				3LG, $R_F = 1\Omega, R_g = 10\Omega$			
d [p.u.]	$\lvert e^{j\delta_1}\rvert$	$\lvert e^{j\delta_2}\rvert$	δ_1 [°]	δ_2 [°]	$\lvert e^{j\delta_1}\rvert$	$\lvert e^{j\delta_2}\rvert$	δ_1 [°]	δ_2 [°]	$\lvert e^{j\delta_1}\rvert$	$\lvert e^{j\delta_2}\rvert$	δ_1 [°]	δ_2 [°]
0.1	1.0001	1.9599	17.9859	162.1006	1.0001	1.9599	17.9859	162.1006	1.0001	1.9599	17.9859	162.1006
0.2	1.0001	1.9599	17.9861	162.1005	1.0001	1.9599	17.9861	162.1005	1.0001	1.9599	17.9861	162.1005
0.3	1.0001	1.9599	17.9863	162.1005	1.0001	1.9599	17.9861	162.1002	1.0001	1.9599	17.9861	162.1005
0.4	1.0001	1.9599	17.9865	162.1008	1.0001	1.9600	17.9857	162.0989	1.0001	1.9600	17.9859	162.1002
0.5	1.0000	1.9599	17.9868	162.1020	1.0000	1.9603	17.9845	162.0946	1.0000	1.9604	17.9848	162.0985
0.6	1.0000	1.9600	17.9870	162.1044	1.0000	1.9608	17.9820	162.0838	1.0000	1.9611	17.9826	162.0925
0.7	1.0000	1.9602	17.9872	162.1083	1.0000	1.9617	17.9778	162.0616	1.0000	1.9624	17.9788	162.0780
0.8	1.0000	1.9605	17.9874	162.1138	1.0000	1.9631	17.9719	162.0235	0.9999	1.9643	17.9735	162.0498
0.9	1.0000	1.9610	17.9873	162.1197	1.0000	1.9646	17.9657	161.9774	0.9999	1.9665	17.9677	162.0135

Table 4.27 Verification of the fault distance in all fault types with $\alpha_A = \alpha_B = 0°$ $\delta_{actual} = 18°$ in considering no phase shift angles

Fault Distance	Verified Fault Distance					
	SLG, $R_F = 10\Omega$		DLG, $R_F = 1\Omega, R_g = 10\Omega$		3LG, $R_F = 1\Omega, R_g = 10\Omega$	
d [p.u.]	d [p.u.]	error [%]	d [p.u.]	error [%]	d [p.u.]	error [%]
0.1	0.1007	0.07	0.1003	0.03	0.1001	0.01
0.2	0.2002	0.02	0.1999	0.01	0.2001	0.01
0.3	0.3001	0.01	0.2998	0.02	0.3001	0.01
0.4	0.4000	0.00	0.3998	0.02	0.4000	0.00
0.5	0.5001	0.01	0.4998	0.02	0.4999	0.01
0.6	0.6001	0.01	0.5999	0.01	0.5998	0.02
0.7	0.7001	0.01	0.6999	0.01	0.6997	0.03
0.8	0.8002	0.02	0.8000	0.00	0.7996	0.04
0.9	0.9003	0.03	0.9001	0.01	0.8996	0.04

4.3 Summary

Performance evaluation and simulation results of the proposed algorithms have been presented in this chapter in order to show the success of the solution to the statement of the problems. Rigorous evaluation has been performed with all considered cases in the presented algorithms and provided highly accurate to the fault location estimation on the short and long transmission line based on synchronized and unsynchronized measurement, respectively. This proved the effectiveness and robustness of the proposed fault location algorithms which can identify the faulted point over the entire line length. Additionally, fault resistance and ground resistance have been varied to ensure its effects on the proposed algorithm. As the result, these algorithms are unaffected by fault resistance and

ground resistance. AWGN whose SNR is 40dB has been artificially added to the measured signals from both terminals to indicate the reality of the measured phenomenon which can be disturbed by noise. However, this severe noise still maintains the high accuracy in locating all fault types. Since the first algorithm is based on synchronized measurement, investigation on the synchronization error has been considered. Time delay greater than 20 μs would not be considered as acceptable due to the high errors of the estimated faults occurred at the end of line terminals. Reversely, the second proposed algorithm is more attractive for economic reasons and can overcome the non-ideal synchronization of the algorithm based on synchronized measurement. Its effectiveness is come up with the quite accurate determination of the synchronization angle which needed to make the analytical synchronization. Once this approach is achieved, fault location estimation is performed precisely as the cases using synchronized measurement. Different phase shift angles from both terminals are also considered as delayed, leading, and no phase shift angle from terminal B to terminal A. Based on the results collected in the tables, it can be proved that this presented algorithm still provided the high accuracy in locating all fault types even phase shift angle is varied. This shows the performance of the proposed algorithm with considering the affected factors on the fault location estimation.

CHAPTER 5

CONCLUSIONS AND RECOMMENDATIONS FOR FUTURE WORK

An effective and accurate fault location estimation technique can greatly improve the operation of a power system and provide useful information for fault analysis. It was designed to provide a rapid and reliable indication of the general faulted area rather than furnish fault distance estimates with pin-point accuracy. Impedance-based fault location methods are considered as effective and economical, and the two-end data measurement provides far more accurate results compared to one-end data measurement. In this thesis, the solution to the statement of problems is modeled as fault location algorithms which propose two alternative simple fault location algorithms for two-end short and long transmission line based on synchronized and unsynchronized measurement, respectively.

A part of this work, a parameters-free algorithm using two-end synchronized measurement for fault location on short transmission line modeled with lump parameter line modeling has been presented. It does not require the line parameters to determine the distance to a fault; making it robust, accurate, and reliable. The algorithm is based on the synchronously measured voltages and currents and used the FFT which implemented in Matlab to obtain the phasor quantities. The performed testing and evaluation with the fault data obtained from ATP-EMTP simulations have been proved satisfactory performance and high accuracy of the presented fault algorithm. Through algorithms testing on unbalanced faults and balanced three-phase faults with varying fault location and fault resistances, it was proved that the algorithm efficiently and accurately determines fault locations and it is unaffected by fault resistance. Additionally, the algorithm was also noticed to maintain a high accuracy even severe noise ratio 40dB was implemented. Non-ideal synchronization with time delay greater than 20 μs would produce the adverse errors in fault location estimation. This means data synchronization between both terminals is another issue that demands careful consideration.

To overcome this problem and fulfill the economic reasons, an impedance-based algorithm for fault location on the fully transposed transmission line by processing two-end unsynchronized measurement has been presented in another part of this thesis. The distributed parameter line model is strictly taken into account

to ensure the high accuracy of the presented algorithm. The proposed algorithm is formulated in term of phasors of the symmetrical components. Only positive- and negative-sequence components were used simultaneously to determine the unknown synchronization operator and angle for all fault types. Thus, analytical determination of synchronization operator of the inputs can be accomplished non-iteratively by solving the quadratic equation in phasor quantity which contains an absolute value of magnitude for synchronization operator and phase for synchronization angle. The procedure of selecting the valid solution has been provided to sufficiently discriminate the real synchronization operator among two solutions, and it is definitely reliable for all trial tests. Consequently, the unknown fault location is calculated precisely as the case of using synchronized measurement after making the analytical synchronization. Through overall algorithm testing and evaluation with the credible fault data modeling obtained from ATP-EMTP simulations, the accuracy of the presented algorithm is very high and definitely acceptable. Based on all successful trial tests, it can be proved that the algorithm is unaffected by fault location, fault resistance, phase shift angle, and still maintained the high accuracy even adding severe noise AWGN ratio 40dB.

The main contributions of this thesis can be summarized as follows:

- Fault location problem on the transmission line is solved: the solution to the statement of problems is modeled as fault location algorithms that work principally with synchronized and unsynchronized measurement.
- Two fault location algorithms are developed for two fundamental power system topologies: short and long transmission line entitled by none line parameter requirement for fault location algorithm based on two-end synchronized measurement; and two-end unsynchronized data sampling for fault location algorithm on the long transmission line.
- The high accuracy of the proposed fault location algorithms are not affected by fault location, fault type, high fault resistance, noise added, and the pre-fault power flow direction (phase shift angle). Data synchronization problem from both terminals is solved by the second proposed algorithm which can be considered as more attractive to the first proposed algorithm.
- The works done in this thesis have been presented in two conference papers submitted to the 9th International Symposium on EMC and Transients in Infrastructures and International Student Session (ISET/ISS) which was held on 26-27 November 2015, Pattaya, Chonburi, Thailand; and the International Conference of Electrical Engineering 2016 (ICEE2016) which was held on 3-7 July 2016, Okinawa Jichikaikan, Okinawa, Japan.

Future work on the topic of transmission line fault location could focus on the designing algorithms to work with a un-transposed transmission line which should be considered to be more challenge to this presented work. Transposition of transmission lines ensures that the sequence components of the line's impedance are not mutually coupled which enables the circuit sequence networks to be dealt with independently. Un-transposed lines have the effect of inducing inter-network coupling between sequence impedances which convolutes the fault location process. It would be necessary to resort to phase voltage, current, and distributed impedance parameters when designing fault locators for un-transposed lines.

Additionally, these proposed algorithms should have been tested with the real implemented transmission lines in Thailand or other countries to ensure its strength on the real application rather than in simulations. The data presented in this work have been collected from the well-known IEEE transaction on power delivery which is really common for other authors to use it as the simulations and validations of their proposed algorithms on fault location estimation.

REFERENCES

[1] Das R., Novosel D., "Review of fault location techniques for transmission and sub-transmission lines," *Proceedings of 54th Annual Georgia Tech Protective Relaying Conference* (CD–ROM), 2000.

[2] IEEE Std C37.114, "IEEE guide for determining fault location on AC transmission and distribution lines," **IEEE Power Engineering Society Publ., New York**, 2005.

[3] Izykowski J., "Fault location on power transmission lines," *The Technical University of Wroclaw Press, Wroclaw, Poland*, 2008.

[4] Sachdev M.S., "Advancement in microprocessor based protection and communication," *IEEE Tutorial Course, IEEE PES, IEEE Catalog Number: 97TP120-0*, 1997.

[5] Cook V., "Analysis of Distance Protection," *Research Studies Press Ltd., John Wiley & Sons, Inc., New York*, 1985.

[6] Eriksson L., Saha M.M., Rockefeller G.D., "An accurate fault locator with compensation for apparent reactance in the fault resistance resulting from remote-end infeed," *IEEE Transactions on Power Apparatus and Systems*, 104(2), pp. 424–436, 1985.

[7] Korejwo E., Synal B., Trojak J., "Short HV transmission lines problems," *Proceedings of 2nd Int. Conf. on Development in Power System Protection, IEE CP185, London*, pp. 196–200, 1980.

[8] Paul M. Anderson, "Analysis of Faulted Power Systems," *the Institute of Electrical and Electronics Engineers, Inc.*, 1995.

[9] Dommel H.W., "Electro-Magnetic Transients Program (EMTP)," *BPA, Portland, Oregon, USA*, 1986.

[10] Maun J-C., Philppot L., Coemans J. et al., "Power system modelling for the design of advanced fault locators and line protections," *Proceedings of the IEEE/KTH Stockholm Power Tech Conference, Stockholm*, paper SPT IC 12–01–0381, pp. 394–399, 1995.

[11] Glover J.D., Sarma M., "Power System Analysis and Design," *PWS Publishing Company, Boston*, 1994.

[12] Ching-Shan C., Chih-Wen L., and Jiang J.A., "Application of combined adaptive Fourier filtering technique and fault detector to fast distance protection," *IEEE Transactions on Power Delivery*, vol. 21, no. 2, pp. 619- 626, April 2006.

[13] Terzija V., "Improved recursive Newton type algorithm for frequency and spectra estimation in power systems," *IEEE Transactions on Instrumentation and Measurement*, 52, (5), pp. 1654–1659, 2003.

[14] Osman A.H., Abdelazim T., and Malik O.P., "Transmission line distance relaying using on-line trained neural networks," *IEEE Transactions on Power Delivery,* vol. 20, no. 2, pp. 1257- 1264, April 2005.

[15] Saha M.M., Izykowski J., and Rosolowski E., "Fault Location on Power Networks", *Springer-Verlag London Limited Publications*, 2010.

[16] Takagi K., Yomakoshi Y., Yamaura M., Kondow R., Matsushima T., "Development of a new type fault locator using the one terminal voltage and current data," *IEEE Transactions Power Apparatus and Systems*, PAS-101, pp. 2892–2898, 1982.

[17] Djuric´ M., Radojevic´ Z., Terzija V., "Distance protection and fault location utilizing only phase current phasors," *IEEE Transactions on Power Delivery*, vol. 13, pp. 1020–1026, 1998.

[18] Jiang J-A., Lin Y-H., Yang J-Z., Too T-M., Liu C-W., "An adaptive PMU based fault detection/location technique for transmission lines. II. PMU implementation and performance evaluation," *IEEE Transactions on Power Delivery*, vol. 15, no. 4, pp. 1136-1146, Oct. 2000.

[19] Gopalakrishnan A., Kezunovic M., McKenna S.M., Hamai D.M., "Fault location using the distributed parameter transmission line model," *IEEE Transactions on Power Delivery*, vol. 15, no. 4, pp. 1169-1174, Oct. 2000.

[20] Ahsaee M.G., Sadeh J., "A Novel Fault-Location Algorithm for Long Transmission Lines Compensated by Series FACTS Devices," *IEEE Transactions on Power Delivery*, vol. 26, no. 4, pp. 2299-2308, Oct. 2011.

[21] Liao Y., Elangovan S., "Unsynchronized two-terminal transmission line fault-location without using line parameters," *IEE Proceedings - Generation Transmission and Distribution*, 153, (6), pp. 639–643, 2006.

[22] Liao Y., Kang N., "Fault-location algorithms without utilizing line parameters based on the distributed parameter line model," *IEEE Transactions on Power Delivery*, 24, (2), pp. 579–584, 2009.

[23] Liao Y., "Unsynchronized fault location based on distributed parameter line model," *Electric Power Components System*, vol. 35, no. 9, pp. 1061–1077, 2007.

[24] Izykowski J., Molag R., Rosolowski E., and Saha M.M., "Accurate location of faults on power transmission lines with use of two-end unsynchronized measurements," *IEEE Transactions on Power Delivery*, vol. 21, no. 2, pp. 627–633, Apr. 2006.

[25] Izykowski J., Rosolowski E., Balcerek P., Fulczyk M., and Saha M.M., "Accurate noniterative fault-location algorithm utilizing two-end unsynchronized

measurements," *IEEE Transactions on Power Delivery*, vol. 26, no. 2, pp. 547–554, Apr. 2011.

[26] Preston G., Radojević Z.M., Kim C.H., Terzija V., "New settings free fault location algorithm based on synchronized sampling," *IET ,Generation, Transmission, and Distribution*, vol. 5, no. 3, pp. 376-383, Mar. 2011.

[27] Johns A.T., Jamali S., "Accurate fault location technique for power transmission lines," *IEE Proceedings*, vol. 137, no. 6, pp. 395-402, Nov. 1990.

BIOGRAPHY

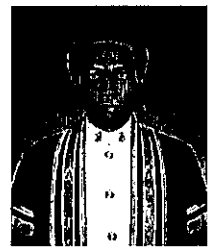

PERSONAL INFORMATION

Name:	Mr. Daro Din
Date of Birth:	April 4th, 1990
Born:	Kandal, Cambodia
Nationality:	Cambodian
Current Address:	Veng Sreng Street, Chom Chao, Dangkor, Phnom Penh, Cambodia
E-mail:	daro_din@ymail.com

EDUCATIONS

Bachelor Degree

Thesis	Optimal Switching in Power Distribution System by Using Reclosers and Sectionalizers
Major:	Electrical and Electronic Engineering
Year:	2009-2014
Department:	Electrical and Energy Engineering
University:	Institute of Technology of Cambodia, Phnom Penh, Cambodia

Master Degree

Major:	Computing in Engineering Systems
Year:	2014-2016
Laboratory:	High Voltage Engineering Laboratory, Department of Electrical Engineering, Faculty of Engineering
College:	International College
University:	King Mongkut's Institute of Technology Ladkrabang (KMITL), Bangkok, Thailand

Research Interests

Power System Analysis, Fault Location on Transmission Line

LIST OF PUBLICATIONS

1. D. Din and P. Yutthagowith, "None Line Parameter Requirement for Fault Location Algorithm Based on Two-End Synchronous Measurements," **The 9th International Symposium on EMC and Transients in Infrastructures and International Student Session (ISET/ISS)**, Pattaya, Chonburi, Thailand, 26-27 November 2015, ISS-04, pp. 14-18.
2. Daro DIN and Peerawut YUTTHAGOWITH, "Two-End Unsynchronized Data Sampling for Fault Location Algorithm on Long Transmission Line," **The International Conference on Electrical Engineering 2016 (ICEE2016)**, Paper ID. 90158, Okinawa Jichikaikan, Okinawa, Japan, 03-07 July 2016.

ISET / ISS 2015 – PATTAYA

The 9th International Symposium on EMC and Transients in Infrastructures

The 11th International Student Session

26 - 27 November 2015
Ambassador City Jomtien, Chonburi, Thailand

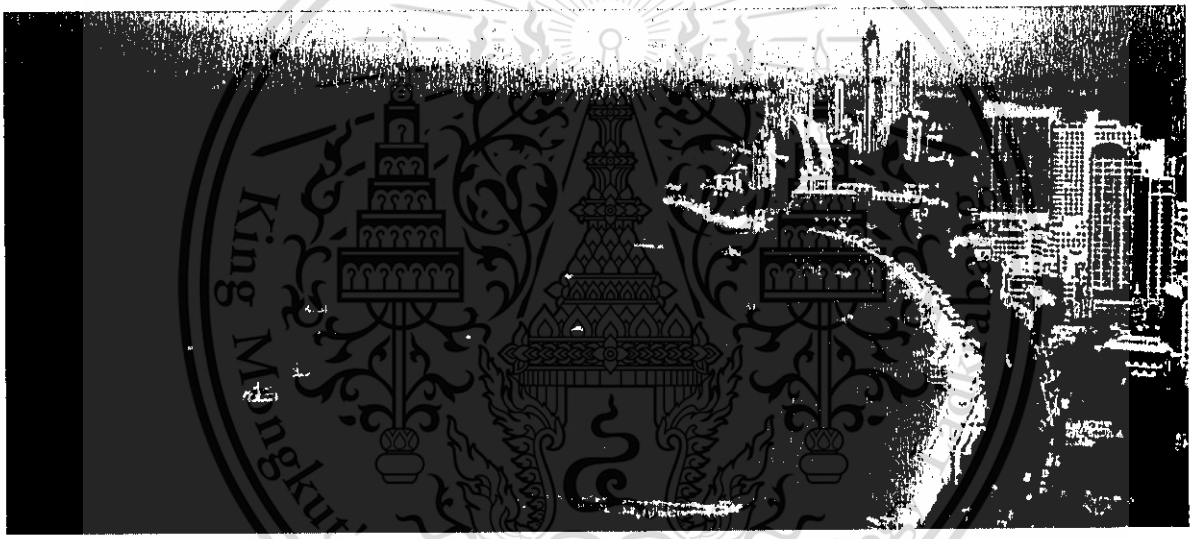

Organized by

King Mongkut's Institute of Technology Ladkrabang, Bangkok, Thailand

In Cooperation with

Doshisha University, Kyoto, Japan

Chubu University, Kasugai, Japan

Tsuruoka National College of Technology, Tsuruoka, Japan

University of Bologna, Bologna, Italy

Seoul National University, Seoul, Korea

Federal Institute of Technology Lausanne, Switzerland

None Line Parameter Requirement for Fault Location Algorithm Based on Two-End Synchronous Measurements

D. Din and P. Yutthagowith

Abstract—**This paper presents a new algorithm for locating faults in two-terminal transmission lines. It is unconventional from other fault location algorithms since it does not involve with the use of any line parameters. The voltages and currents from all terminals are considered as inputs and synchronization is needed. Fast Fourier Transform (FFT) was used to extract the voltages and currents in phasor quantities. Consequently, the fault location is determined. The proposed algorithm has been tested and validated thoroughly with reliable fault data obtained from ATP-EMTP simulations. The significant results with various fault types and conditions including severe Additive White Gaussian Noise (AWGN) ratio 40dB and synchronization error analysis are reported and discussed.**

Keywords—**ATP-EMTP, Additive White Gaussian Noise, Fault location, Fast Fourier Transform, Synchronous measurements**

I. Introduction

IRREGULAR situations in power system can occur unexpectedly due to the fault on transmission line. Reliable and effective algorithms for locating the fault on overhead transmission line have become an essential part of modern transmission line protection schemes.

Numerous fault location algorithms have been developed for decades. A number of approaches using data from two-end terminals are more complex, but it reaches to the accurate estimation of the unknown fault location [1, 2]. References [3] and [4] were proposed to calculate the fault location by synchronous and asynchronous data sampling, respectively. The disadvantage in these algorithms is the need of line parameters and line length to locate the fault distance. These affect the accuracy in the algorithms since the line parameters may differ by line loading and weather conditions. However, due to their uncertainty, another algorithms in [5, 6] were proposed without any knowledge of line parameters. These two methods were operated with asynchronous data sampling by applying iterative technique to find the distance of line-line fault, but it cannot be used to locate balanced three-phase fault. Although the two algorithms stated above have done effectively, the proposed algorithm used in this paper can be used to locate all fault types.

The aim of the presented paper is to validate a new numerical algorithm, which determines the distance to the fault on transmission line without any knowledge of line parameters, by processing synchronized two-end measurements of voltages and currents in the phasor quantities and transform it to sequence components. The flexibility of this proposed algorithm still maintained the accuracy of the fault distance by adding the severe Additive White Gaussian Noise (AWGN) ratio 40dB.

II. Detailed Derivation of Proposed Algorithm

In this section, the proposed algorithm for fault location without line parameter will be presented. Thus, unbalanced faults and balanced three phase faults solution will be derived explicitly.

A. Unbalanced Fault Approach

The considered fault location on two terminals of the transmission line is presented schematically in Fig. 1. The fault location is denoted by F, the fault distance (as measured from local terminal) by l, D is the total line length, and subscripts L and R represent as Local and Remote terminal of the line, respectively. Voltage ($\underline{V}_L^{a,b,c}$ and $\underline{V}_R^{a,b,c}$) and currents ($\underline{I}_L^{a,b,c}$ and $\underline{I}_R^{a,b,c}$) are synchronously measured at both line terminals.

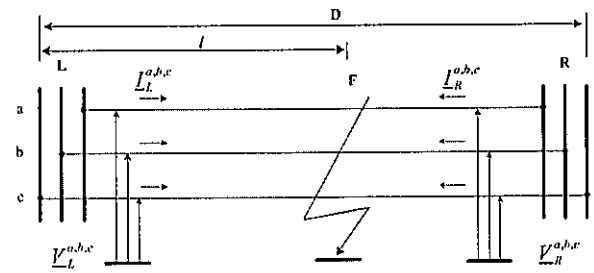

Fig. 1 Faulted line representation of two terminals transmission line

D. Din is with the International College, King Mongkut's Institute of Technology Ladkrabang, Bangkok, Thailand, 10520 (daro_din@ymail.com)
P. Yutthagowith is with the Department of Electrical Engineering, Faculty of Engineering, King Mongkut's Institute of Technology Ladkrabang, Bangkok, Thailand, 10520 (kypeeraw@kmitl.ac.th).

Assuming that the transmission line is considered as short line which is less than 100 km long, so the shunt capacitance and the shunt conductance can be neglected [7].

The presented algorithm is designed for locating faults on a transposed transmission line which has identical line impedance, thus the circuit from Fig. 1 can be represented by three equivalent circuits as the positive- (p-), negative- (n-), and zero- (0-) sequence circuit. Only p- and n- sequence circuits will be used as presented in Figs. 2 and 3, respectively.

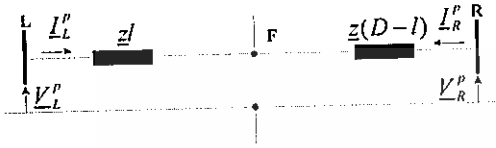

Fig. 2 Positive- sequence equivalent circuit of the faulted line

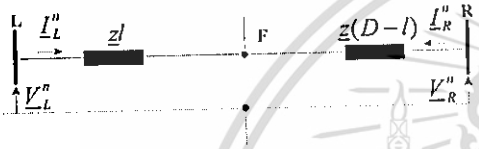

Fig. 3 Negative- sequence equivalent circuit of the faulted line

From figures above, following equations can be expressed as [8]

$$\underline{V}_L^p - \underline{z}l\underline{I}_L^p = \underline{V}_R^p - \underline{z}(D-l)\underline{I}_R^p \quad (1)$$

$$\underline{V}_L^n - \underline{z}l\underline{I}_L^n = \underline{V}_R^n - \underline{z}(D-l)\underline{I}_R^n \quad (2)$$

where $\underline{V}_L^{p,n}$, $\underline{V}_R^{p,n}$, $\underline{I}_L^{p,n}$, $\underline{I}_R^{p,n}$ are the p- and n- sequence voltage and current in phasor quantities from both line terminals, respectively; $\underline{z}$ is the p- and n- sequence line impedance.

Obviously, (1) and (2) has two unknown terms $\underline{z}l$ and $\underline{z}(D-l)$, and it is sufficient to be determined.

Then the unknown terms gives two formulae as following

$$\underline{z}l = \frac{(\underline{V}_L^p - \underline{V}_R^p)\underline{I}_R^n - (\underline{V}_L^n - \underline{V}_R^n)\underline{I}_R^p}{\underline{I}_L^p\underline{I}_R^n - \underline{I}_L^n\underline{I}_R^p} \quad (3)$$

$$\underline{z}(D-l) = \frac{(\underline{V}_L^p - \underline{V}_R^p)\underline{I}_L^n - (\underline{V}_L^n - \underline{V}_R^n)\underline{I}_L^p}{\underline{I}_L^p\underline{I}_R^n - \underline{I}_L^n\underline{I}_R^p} \quad (4)$$

The distance to the fault l can be expressed as the percentage of the total line length D by the following expression

$$l\% = \frac{l}{D}100 \quad (5)$$

The stated expression can be formed as below

$$l\% = \frac{\underline{z}l}{\underline{z}l + \underline{z}(D-l)}100 \quad (6)$$

So far, by including (3) and (4) into (6), the distance to the fault can be calculated through the following formula

$$l\% = \frac{(\underline{V}_L^p - \underline{V}_R^p)\underline{I}_R^n - (\underline{V}_L^n - \underline{V}_R^n)\underline{I}_R^p}{(\underline{V}_L^p - \underline{V}_R^p)(\underline{I}_L^n + \underline{I}_R^n) - (\underline{V}_L^n - \underline{V}_R^n)(\underline{I}_L^p + \underline{I}_R^p)}100 \quad (7)$$

Based on explicit formula above which located the unbalanced fault on the transmission line, the distance to the fault solution can obviously be obtained without any information of line parameters.

Basically, it is just needed the processing of the synchronously recorded voltage and current waveforms from both line terminals, identifying their phasor quantities of the common frequency 50 Hz, and determining the p- and n- sequence voltage and current components.

B. Balanced Three-Phase Fault Approach

The fault currents and voltages are identical along the three phases during a balanced three-phase fault. Theoretically, n- and 0- sequence components do not contain in this fault type. Thus, only p- sequence equivalent circuit is used in the developed algorithm as presented in Fig. 4.

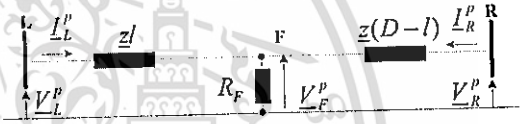

Fig. 4 Positive- sequence equivalent circuit of the faulted line

As stated, the p- sequence can be written as follows [8]

$$\underline{V}_L^p - \underline{z}l\underline{I}_L^p - \underline{V}_F^p = 0 \quad (8)$$

$$\underline{V}_R^p - \underline{z}(D-l)\underline{I}_R^p - \underline{V}_F^p = 0 \quad (9)$$

$$\underline{V}_F^p = R_F(\underline{I}_L^p + \underline{I}_R^p) \quad (10)$$

Substituting (10) into (8) and (9) gives two following equations

$$\underline{z}l = \frac{\underline{V}_L^p}{\underline{I}_L^p} - \frac{\underline{I}_L^p + \underline{I}_R^p}{\underline{I}_L^p}R_F \quad (11)$$

$$\underline{z}(D-l) = \frac{\underline{V}_R^p}{\underline{I}_R^p} - \frac{\underline{I}_L^p + \underline{I}_R^p}{\underline{I}_R^p}R_F \quad (12)$$

To determine R_F, (11) and (12) can be represented in the compact form as follow:

$$\underline{z}l = a_1 + ja_2 + (b_1 + jb_2)R_F \quad (13)$$

$$\underline{z}(D-l) = c_1 + jc_2 + (d_1 + jd_2)R_F \quad (14)$$

where

$$a_1 = \mathrm{Re}\left[\frac{\underline{V}_L^p}{\underline{I}_L^p}\right] \qquad a_2 = \mathrm{Im}\left[\frac{\underline{V}_L^p}{\underline{I}_L^p}\right] \qquad b_1 = \mathrm{Re}\left[-\frac{\underline{I}_L^p + \underline{I}_R^p}{\underline{I}_L^p}\right]$$

$$b_2 = \mathrm{Im}\left[-\frac{\underline{I}_L^p + \underline{I}_R^p}{\underline{I}_L^p}\right] \qquad c_1 = \mathrm{Re}\left[\frac{\underline{V}_R^p}{\underline{I}_R^p}\right] \qquad c_2 = \mathrm{Im}\left[\frac{\underline{V}_R^p}{\underline{I}_R^p}\right]$$

$$d_1 = \mathrm{Re}\left[-\frac{\underline{I}_L^p + \underline{I}_R^p}{\underline{I}_R^p}\right] \qquad d_2 = \mathrm{Im}\left[-\frac{\underline{I}_L^p + \underline{I}_R^p}{\underline{I}_R^p}\right]$$

Equations (13) and (14) can be grouped their real and imaginary parts separately, so the following expressions hold

$$\underline{z}l = (a_1 + b_1 R_F) + j(a_2 + b_2 R_F) \tag{15}$$

$$\underline{z}(D-l) = (c_1 + d_1 R_F) + j(c_2 + d_2 R_F) \tag{16}$$

Vectors $\underline{z}l$ and $\underline{z}(D-l)$ can be transformed in a polar form as they are determined by a vector magnitude and its angle θ. From (15) and (16) the angle θ, which must be located in the range 0 - 90°, can be determined as expressed in the following formulae

$$\tan\theta = \frac{a_2 + b_2 R_F}{a_1 + b_1 R_F} \tag{17}$$

$$\tan\theta = \frac{c_2 + d_2 R_F}{c_1 + d_1 R_F} \tag{18}$$

So far, R_F will be determined by (17) and (18), and used to solve the unknown collinear vectors

$$\frac{a_2 + b_2 R_F}{a_1 + b_1 R_F} = \frac{c_2 + d_2 R_F}{c_1 + d_1 R_F} \tag{19}$$

It is obvious that from (19) the quadratic equation which solves R_F can be formulated

$$R_F^2 + mR_F + n = 0 \tag{20}$$

where

$$m = \frac{a_2 d_1 + b_2 c_1 - a_1 d_2 - b_1 c_2}{b_2 d_1 - b_1 d_2}$$

$$n = \frac{a_2 c_1 - a_1 c_2}{b_2 d_1 - b_1 d_2}$$

Then the quadratic (20) provides two results

$$(R_F)_1 = \frac{-m + \sqrt{m^2 - 4n}}{2} \tag{21}$$

$$(R_F)_2 = \frac{-m - \sqrt{m^2 - 4n}}{2} \tag{22}$$

It is unable to identify the correct value of R_F. Substituting $(R_F)_1$ and $(R_F)_2$ into (17) gives the following expressions for phase angle θ

$$\theta_1 = \arctan\frac{a_2 + b_2 (R_F)_1}{a_1 + b_1 (R_F)_1} \tag{23}$$

$$\theta_2 = \arctan\frac{a_2 + b_2 (R_F)_2}{a_1 + b_1 (R_F)_2} \tag{24}$$

To get the true value for angle θ, the value which lies in the first quadrant of the complex plane and the one which is closer to the typical value of the line characteristic should be selected. Thus, the fault resistance R_F corresponding to the selected angle should be selected as well.

The selected fault resistance would be included in (15) and (16). Then substitute them into (6) where Unbalanced Fault Approach section already stated. The unknown distance to the fault can be calculated through the following formula

$$l\% = 100 \cdot \frac{(a_1 + b_1 R_F) + j(a_2 + b_2 R_F)}{(a_1 + b_1 R_F) + j(a_2 + b_2 R_F) + (c_1 + d_1 R_F) + j(c_2 + d_2 R_F)} \tag{25}$$

III. ATP-EMTP Simulation Results

The presented fault location algorithm has been evaluated using fault data obtained from ATP-EMTP software versatile simulations of faults in the overhead transmission line of a 400 kV, 100 km long. The parameters of the two networks and transmission line are listed in Table I and II, respectively.

TABLE I
PARAMETERS OF THE LOCAL TERMINAL AND REMOTE TERMINAL

Parameters	p- and n- sequence	0- sequence
Resistance [Ω/km]	0.065	0.195
Inductance [mH/km]	0.95493	2.86479
Capacitance [nF/km]	10.5	5.0

TABLE II
LINE PARAMETERS

Parameters	Local Terminal	Remote Terminal
LL RMS Voltage [kV]	416	400
Phase angle [°]	30	10
p- seq. Resistance [Ω]	1.0185892	0.6366183
p- seq. Inductance [mH]	50.9395	31.8309
0- seq. Resistance [Ω]	2.0371785	1.2732366
0- seq. Inductance [mH]	101.8589	60.6618

A. All Fault Types Evaluation

Single line to ground (SLG), double line (DL), double line to ground (DLG), and balanced three-phase to ground (3LG) faults were simulated at different locations with a variety of fault resistance along the line. In each case the fault inception time was set at $t = 23ms$. The sampling frequency was $f_s = 6.4kHz$. The data window size used for the Fast Fourier Transform (FFT) process to obtain the phasors quantities was $T_{dw} = 20ms$ (N=128 samples per data window). It was assumed that the line was loaded before the fault inception and all phasors were in a natural way perfectly synchronized.

Figs. 5 and 6 depict the voltages and current waveforms of a single line to ground fault simulated at 40 km over 100 km total length with a fault resistance $R_F = 10\Omega$ as observed from the local terminal of the line. Similar waveforms would be observed at the other terminal as well.

Sampled measurements of these voltages and currents were used as the input to the algorithm which developed in Matlab.

Consequently, the unknown fault location was calculated as depicted in Fig. 7.

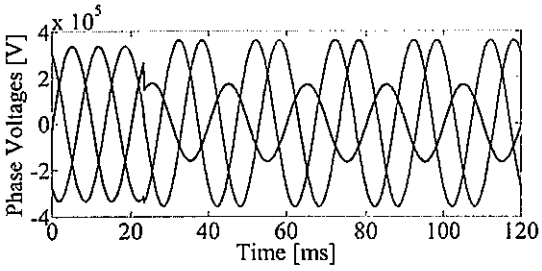

Fig. 5 Fault voltage waveforms at local terminal

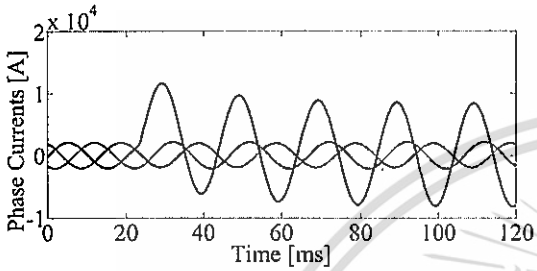

Fig. 6 Fault current waveforms at local terminal

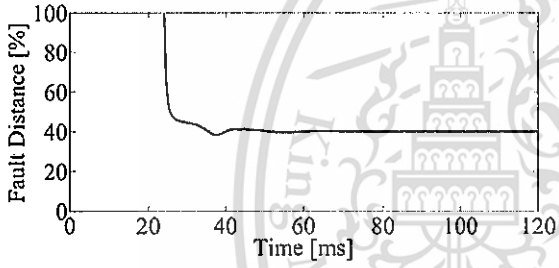

Fig. 7 SLG with R_F =10Ω estimated fault location (40km fault was simulated in ATP-EMTP)

From Fig. 7, it can be seen that the algorithm accurately determines the fault distance and converges to the solution shortly after the fault inception. The estimated distance to fault averaged over the interval 40-120 ms was 40.01684 km. Obviously, the errors occurred during the convergence process are due to the presence of the DC components in the fault current. Commonly, since FFT was used in this extraction process, it is known to be sensitive to the decaying of DC components.

In order to further demonstrate the algorithm's efficiency, unbalanced faults and balanced three-phase faults were assumed to be occurred at different points along the line were simulated. The results in percentage for the various fault location are presented in Figs. 8 and 9. Based on the results, it can be verified that accurate results were obtained over the range of transmission line.

In the derivation of the algorithm, the shunt capacitance was assumed to be neglected, but a realistic Pi-model in ATP-EMTP including line capacitance was used to simulate all fault types. Table III shows the results for a variety of the unbalanced faults and balanced three-phase faults with different locations and fault resistances by including line capacitance in the modeling. Results for 60 simulation tests have been presented. The errors presented in the results have been calculated as a percentage of the entire line length, in accordance with [9], and averaged over the interval 40-120 ms.

$$Error\,(\%) = \frac{\left|l_{calculate} - l_{exact}\right|}{D} 100\% \qquad (26)$$

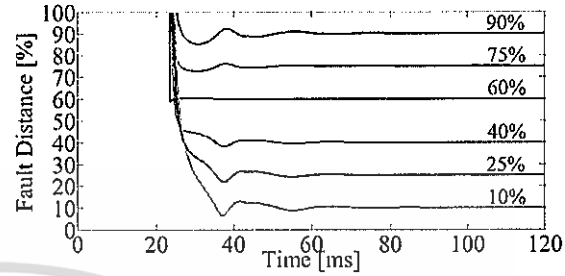

Fig. 8 Various SLG with R_F = 10 Ω estimated fault location over the range of line

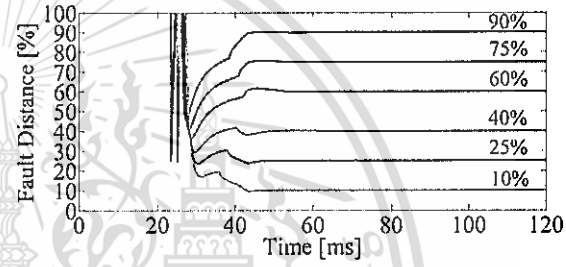

Fig. 9 Various 3LG with R_F = 10 Ω estimated fault location over the range of line

TABLE III
FAULT LOCATION ERROR [%] FOR ALL FAULTS TYPES INCLUDING LINE CAPACITANCE

Fault Types	Fault distance [%]					
	10	25	40	60	75	90
SLG, R_F = 0Ω	0.1210	0.0717	0.0337	0.0151	0.0543	0.0983
SLG, R_F = 10Ω	0.1201	0.0710	0.0333	0.0152	0.0539	0.0978
SLG, R_F =100Ω	0.1092	0.0635	0.0289	0.0155	0.0507	0.0902
DL, R_F = 0Ω	0.0703	0.0392	0.0157	0.0163	0.0408	0.0772
DL, R_F=100Ω	0.0665	0.0366	0.0141	0.0165	0.0425	0.0735
DLG, R_F = 0Ω	0.1371	0.0665	0.0249	0.0162	0.0408	0.0565
DLG, R_F=100Ω	0.1064	0.0505	0.0228	0.0162	0.0425	0.0663
3LG, R_F =0Ω	0.0366	0.0559	0.0424	0.0450	0.0145	0.0206
3LG, R_F =10Ω	0.0914	0.0946	0.0807	0.0177	0.0350	0.0573
3LG, R_F =100Ω	0.0393	0.0576	0.0429	0.0178	0.0147	0.0207

From Table III it can be concluded that the algorithm maintained a high level of accuracy in locating all fault types. The error of the estimation for faults occurred in the middle of line are relatively smaller than those occurred close to line terminal. There is smaller difference in the fault currents from both terminals, so the error caused by shunt capacitance also smaller.

B. Adding AWGN Ratio 40dB

Since this algorithm is based on the synchronized measured voltages and currents, it needs to use fast communication channels between two synchronized measurement units installed at the line terminal which can be introduced by some irritate noise. Noise ratio 40dB is considered as the severe noise introduced in the network. AWGN ratio 40dB was added to all simulation tests by Matlab. Results obtained for this condition were calculated by (26) with the averaged value of 10 time simulations in each case as given in Table IV.

From Table IV it can be seen that the accuracy of the algorithm is still applicable even considering with severe noise in the network.

TABLE IV
FAULT LOCATION ERROR [%] FOR ALL FAULT TYPES CONSIDERING SEVERE NOISE RATIO 40DB

Fault Types	Fault distance [%]					
	10	25	40	60	75	90
SLG, $R_F = 0\Omega$	0.2804	0.1681	0.0831	0.0144	0.0838	0.1455
SLG, $R_F = 10\Omega$	0.2841	0.1666	0.0837	0.0116	0.0808	0.1495
SLG, $R_F = 100\Omega$	0.2986	0.1768	0.0948	0.0082	0.0889	0.1627
DL, $R_F = 0\Omega$	0.1916	0.1170	0.0605	0.0134	0.0637	0.1276
DL, $R_F = 100\Omega$	0.1920	0.1148	0.0571	0.0122	0.0696	0.1287
DLG, $R_F = 0\Omega$	0.3419	0.1666	0.0773	0.0134	0.0711	0.1001
DLG, $R_F = 100\Omega$	0.3073	0.1521	0.0779	0.0132	0.0592	0.0840
3LG, $R_F = 0\Omega$	0.0991	0.0267	0.0041	0.0526	0.0964	0.1250
3LG, $R_F = 10\Omega$	0.0119	0.1028	0.1538	0.0069	0.1349	0.1045
3LG, $R_F = 100\Omega$	0.0900	0.0072	0.0180	0.1506	0.1323	0.1159

C. Synchronization Error Investigation

As mentioned, this algorithm implements with the perfectly synchronized measurements. SLG with fault resistance 10Ω was tested over the range of the entire line by considering the time delay (t_d) of the synchronized data sampling from both terminals. The errors presented in the results have been calculated by (26) and averaged over the interval 40-120 ms.

TABLE V
FAULT LOCATION ERROR [%] CONSIDERING SYNCHRONIZATION ERROR

Time Delay,[μs]	Fault distance [%]					
	10	25	40	60	75	90
10	0.3684	0.2647	0.1878	0.0263	0.0967	0.224
20	0.7333	0.5259	0.345	0.0459	0.1802	0.4107
50	1.7634	1.263	0.789	0.1021	0.4146	0.9357
70	2.4006	1.7191	1.064	0.1378	0.5583	1.2589
100	3.2905	2.3562	1.4487	0.189	0.7569	1.7077
200	5.7885	4.1481	2.5367	0.3477	1.2953	2.9455
500	10.6372	7.6716	4.7421	0.809	2.153	5.1424

From Table V it can be conclude that the fault location error was appeared to be higher by the fault occurred closed to the end of the terminals, and it was lower by the fault approached to the middle of the line. For $t_d \leq 20$ μs, the fault location error would be acceptable while $t_d > 20$ μs would not be considered as acceptable.

IV. CONCLUSIONS

In this work, a parameters-free algorithm using two-end synchronized measurement for fault location on transmission line has been presented. It does not require the line parameters to determine the distance to fault; making it robust, accurate, and reliable. The algorithm is based on the synchronously measured voltages and currents and used the FFTs which implemented in Matlab to obtain the phasor quantities.

The performed testing and evaluation with the fault data obtained from ATP-EMTP simulations have been proved satisfactory performance and high accuracy of the presented fault algorithm. Through algorithms testing on unbalanced faults and balanced three-phase faults with varying fault location and fault resistances, it was proved that the algorithm efficiently and accurately determines fault locations and it is unaffected by fault resistance.

The algorithm was also noticed to maintain a high accuracy even severe noise ratio 40dB was implemented. Non-ideal synchronization with time delay greater than 20μs would produce the adverse errors in fault location estimation. The authors are working on the distributed parameter line model utilizing two-end unsynchronized measurements.

ACKNOWLEDGMENT

The authors would like to give special acknowledgment to AUN/SEED-Net for providing the scholarship for master degree and High Voltage Engineering Laboratory, King Mongkut's Institute of Technology Ladkrabang for providing the facility to support this research work.

REFERENCES

[1] A.T. Johns, S. Jamali, "Accurate fault location technique for power transmission lines," *IEE Proceedings C Generation, Transmission and Distribution*, vol.137, no.6, pp.395-402, Nov 1990.

[2] D. Novosel, D.G.Hart, E. Udren, J. Garitty, "Unsynchronized two terminal fault location estimation", , *IEEE Trans. Power Deliv.*, vol.11, no.1, pp.130-138, Jan 1996.

[3] J-A Jiang; Y-H Lin; J-Z Yang; T-M Too; C-W Liu; , "An adaptive PMU based fault detection/location technique for transmission lines. II. PMU implementation and performance evaluation," , *IEEE Trans. Power Deliv.*, vol.15, no.4, pp.1136-1146, Oct 2000.

[4] M. Abe, N. Otsuzuki, T. Emura, M. Takeuchi, "Development of a new fault location system for multi-terminal single transmission lines", *IEEE Trans. Power Deliv.*, vol.10, no.1, pp.159-168, Jan 1995.

[5] Liao, Y., Elangovan, S.: 'Unsynchronized two-terminal transmission line fault-location without using line parameters', *IEE Proc. Gen. Transm. Distrib.*, 2006, 153, (6), pp. 639–643.

[6] Liao, Y., Kang, N.: 'Fault-location algorithms without utilizing line parameters based on the distributed parameter line model', *IEEE Trans. Power Deliv.*, 2009, 24, (2), pp. 579–584.

[7] Glover JD, Sarma M (1994) Power System Analysis and Design. PWS Publishing Company, Boston.

[8] G.Preston, Z.M. Radojević, C.H. Kim, V. Terzija, "New settings free fault location algorithm based on synchronised sampling," *IET ,Generation, Transmission & Distribution*, vol.5, no.3, pp.376-383, March 2011.

[9] IEEE Std C37.114-2004: 'IEEE Guide for Determining Fault Location on AC Transmission and Distribution Lines'. 2005, pp. 0–36.

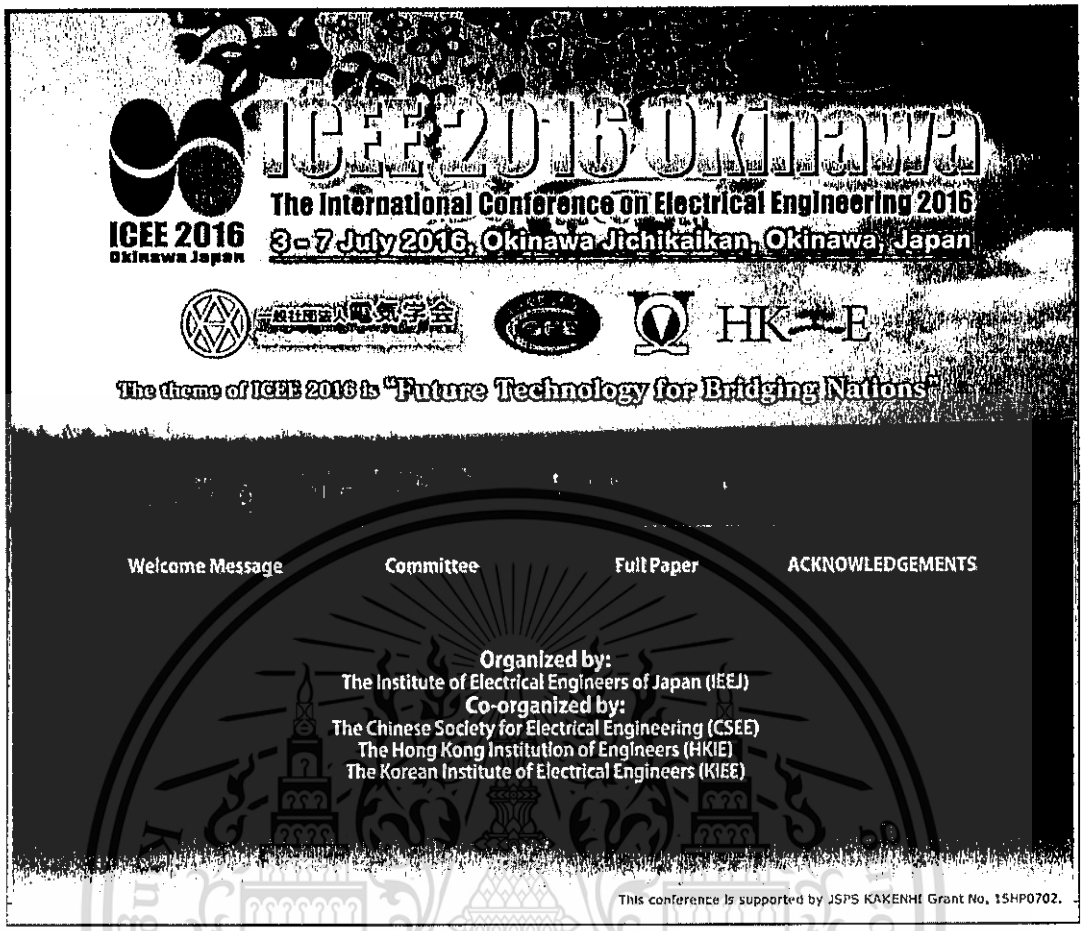

Oral Session

Session A-1 : 4-06 Inverter and Converter Technology (I)

Day 1 (July 4) 14:20-15:35 Room A

90014
Azmeer bin Ab Malek Muhammad Hazarul , Hiroaki Kakigano
Control Strategy of Dual Active Bridge DC-DC Converter for Enhancing Zero Voltage Switching Operation

90025
Shinya Sekizaki, Naoto Yorino, Yuki Nakamura, Yutaka Sasaki, Yoshifumi Zoka, Ichiro Nishizaki
A Theoretical and Experimental Study on Pseudo-synchronizing Power Inverter

90139
A.M. rashwan, Tomonobu Senjyu, Mahmoud A.Sayed, Y. A. Mobarak, Gaber Shabib
Predictive controller for a modular multilevel converter for offshore wind power transmission

90222
Atsushi Nakata, Akihiro Torii, Suguru Mototani
A Calculation Method of an Effective Value of a Function with Periodically Changing Amplitude in Power Electronics Equipment

90373
Hyeongjin Lee, Seungjoon Lee, Byoungwook Kang, Jaesun Huh, Jaechul Kim
Output Control of the Wind Farm Side Converter from DC Link for DC Voltage Stabilization with HVDC

Session B-1 : 2-01 Power System Planning and Scheduling (I)

Day 1 (July 4) 14:20-15:35 Room B

90272
Dongxin Sun, Masakazu Kato
Electric power generation scheduling with huge penetration of solar power

90342
Wataru Ukita, Akihiko Yokoyama
Optimal Weekly Operation Scheduling of Energy Storage Systems and Supply and Demand Simulation in a Power System with a Large Penetration of Renewable Energy

90371
Keita Sugimoto, Akihiko Yokoyama, Nobuyuki Kitagishi, Takeshi Nishimura, Koichiro ishikawa
Demand and Supply Planning Considering Ramp Rate of Power Plant in Small Balancing Group with a Large Penetration of Renewable Energy

90380
Yoshiaki Hatanaka, Yasuo Suzuoki, Toshihisa Funabashi, Takeyoshi Kato, Muneaki Kurimoto, Yusuke Manabe
A study on evaluation of PVS forecast update accuracy from the viewpoint of unit commitment rescheduling

90444
Mitsuru Shimamura, Daisuke Iioka, Hiroumi Saitoh

A Study of Effective Length of Vertical Grounding Wires Connected to Foundation of Wind Turbine

90353
Takahiro Imai, Hiromitsu Hirai, Steven Boggs, Kotaro Mura, Tetsuo Yoshimitsu
Influence of Nano-filled Matrix on Electrical Tree Propagation in Stator Winding Insulation

90495
Norrawit Tonmitr, Yuki Goto, Kazuki Ganaha, Eiji Kaneko, Takehiro Hayashida
Study on Various Influences of Polymer Materials to an Air Arc

Session B-6 : 2-07 Power System Modeling, Simulation and Analysis (II)

Day 2 (July 5) 15:45-17:00 Room B

90045
Masayuki Takeda, Isao Iyoda, Yoshimichi Ito
Suppression of Subsynchronous Torsional Interaction by Insertion of an Inverter in series

90210
Xuyang Pan, Ye Wang, Nicolas Chamollet, Guofei Chen
Applicability evaluation of aggregated wind power plant models based on IEC-standard generic wind turbine models

90147
Masanari Kumada, Mutsumi Aoki, Hiroyuki Ukai
Study of LFC Simulation in consideration of the Output Response Characteristic of the Thermal Power Plant

Session C1-6 : 2-02 Power System Protection, Operation and Control (III)

Day 2 (July 5) 15:45-17:00 Room C1

90145
Yu Fujita, Hiroshi Kobayashi, Mutsumi Aoki
Validation of Harmonic Voltage Suppression Method in Distribution System at 6.6kV using Loop Power Controller

90158
Daro Din, Peerawut Yutthagowith
Two-End Unsynchronized Data Sampling for Fault Location Algorithm on Long Transmission Line

90286
Kyung-Min LEE, Soon-Choul Choi, Chul-Won Park
Advanced Fault Location Technique for Distribution Line System of Two End Source

90539
WooSeok Seo, Sanghee Kang
A Novel Frequency Estimation Algorithm Based on DFT and Second Derivative

90329
Satoshi Hirayama, Yoshitaka Inui
Numerical Simulation of Rotary Arc Plasma in a Laval Nozzle

Session C2-6 : 4-01 Electrical Machines

Day 2 (July 5) 15:45-17:00 Room C2

90142
Shrinathan Esakimuthu Pandarakone, Chika Araki, Yukio Mizuno, Hisahide Nakamura
Diagnosis Method of Mechanical Failure in Low Voltage Induction Motor with the Aid of Support Vector Machine

90181
Christopher H. T. Lee, W. K. Lee, K. T. Chau
Development of Partitioned Stator Flux-Switching Machines for Electric Vehicles

90233
Baek Ju Sung, Do Sik Kim
The Failure Analysis and Deduction of Reliability Parameters for Clutch & Brake for Washing Machine

Two-End Unsynchronized Data Sampling for Fault Location Algorithm on Long Transmission Line

Daro DIN
International College
King Mongkut's Institute of Technology Ladkrabang, Bangkok 10520, Thailand

Peerawut YUTTHAGOWITH
Department of Electrical Engineering, Faculty of Engineering
King Mongkut's Institute of Technology Ladkrabang, Bangkok 10520, Thailand

Abstract

This paper delivers an impedance-based algorithm for fault location on long transmission line by processing two-end unsynchronized measurement. The distributed parameter line model with use of correction factors for representing series and shunt parameter is strictly taken into account. Unsynchronized measurement of voltages and currents from both terminals is considered as the input to process the symmetrical components. First, the synchronization operator of the unsynchronized data is determined by combining only positive- and negative-sequence components for all fault types. Thus, analytical synchronization of the inputs can be accomplished non-iteratively. Consequently, the unknown fault location can be performed. This presented algorithm has been simulated thoroughly with credible fault data modeling obtained from ATP-EMTP software. Through algorithm testing on various fault types with varying fault distance, fault resistance, and phase shift angle, it can be proved that the algorithm efficiently and accurately determines the distance to fault over the entire transmission line.

Keywords: ATP-EMTP, distributed parameter, fault location algorithm, transmission line, unsynchronized measurement.

1 INTRODUCTION

Failure on transmitting the electricity in power system can occur unexpectedly due to fault on overhead transmission line. Effective and accurate fault location algorithm is a beneficial task for speeding system restoration, reducing outage time, and integrating into modern substation control system.

Availability of fault location methods have been elaborated for decades. Numerous algorithms are derived by using techniques based on fundamental frequency of voltages and currents in term of impedance-based [1, 2]. References [3] and [4] were proposed to calculate the fault location by synchronized and unsynchronized data sampling, respectively. Performing synchronized measurement results highly accurate, but it costs much on the need of global positioning system (GPS). In turn, unsynchronized measurement appears more attractive. In order to overcome this method, a common time reference has to be identified by accomplishing the analytical synchronization. Conventional analysis on synchronization operator, which is really needed in this study, is calculated iteratively [4, 5]. In [6] were developed to avoid such iteration, but the stage of improving the precision of the presented algorithm with considering distributed parameter line model still needed iterative calculation. New algorithm in [7] was integrated to completely avoid iteration, but the determination of the unknown synchronization operator has to be separated between balanced and unbalanced fault. Moreover, the procedure of selecting the valid solution is not reached for all studied cases and continued to another step by comparing the determined synchronization angles with the unique solution obtained under using the lump line model.

The aim of the presented paper is to refine and validate the method for analytical synchronization corresponded to all fault types by considering the distributed parameter line model to assure the high accuracy of the fault location estimation from two terminals on fully long transposed transmission line. Only positive- and negative-sequence were combined together to get the specific value of synchronization operator and angle in all fault types. Then fault distance can be determined non-iteratively after the accomplishment of the synchronization from both terminals.

2 DERIVATION OF PROPOSED ALGORITHM

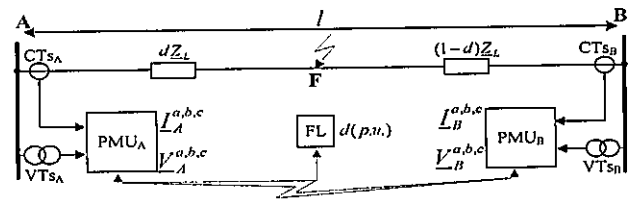

Figure 1. Representative diagram of two-end unsynchronized measurement for fault location

Considered two-end unsynchronized measurement diagram for faulted point on transmission line is depicted in Figure 1. Current transformers (CTs_A, CTs_B) and voltage transformers (VTs_A, VTs_B) are put at both terminals (A, B) to transform the signal to phasor measurement units (PMUs) in order to get currents ($\underline{I}_A^{a,b,c}, \underline{I}_B^{a,b,c}$) and voltages ($\underline{V}_A^{a,b,c}, \underline{V}_B^{a,b,c}$) in phasor quantities which are the input for fault locator device (FL). These PMUs are not associated with GPS, so this kind of measurement was considered as unsynchronized due to no common time reference.

The proposed algorithm is implemented for fault distance on fully transposed, so symmetrical components appears to be sufficient to fulfill the aim of this presented algorithm. Zero-sequence is not beneficial to consider due to the uncertain impedance data. Theoretically, according to the sequence component mathematical manipulation, negative-sequence does not contain in the three-phase fault. However, in practice a perfectly balanced system does not exist. Even if the system is 100% balanced, it does not mean that negative- and zero-sequence do not exist.

In [7] proposed the use of incremental positive-sequence, which is obtained by subtracting the pre-fault quantities from fault quantities, instead of negative-sequence in case of the determination of synchronization operator in balanced three-phase fault. It is worth to notice that the pre-fault signal is not always in the form of pure sinusoids since the indication of the appearing fault can be observed just before fault occurrence [6]. Thus, the consideration on using the incremental positive-sequence in such cases is unnecessary.

Due to these reasons, positive- and negative-sequence were assumed to be presented in all fault types in order to reduce the manipulation of the determination of the synchronization operator. Therefore, distance to faulted point can be obtained without performing fault type selection. The distributed parameter line model utilized with correction factors for symbolizing series and shunt parameters is considered in the equivalent circuit of faulted line for positive- (subscript 1) and negative-sequence (subscript 2) as presented in Figure 2.

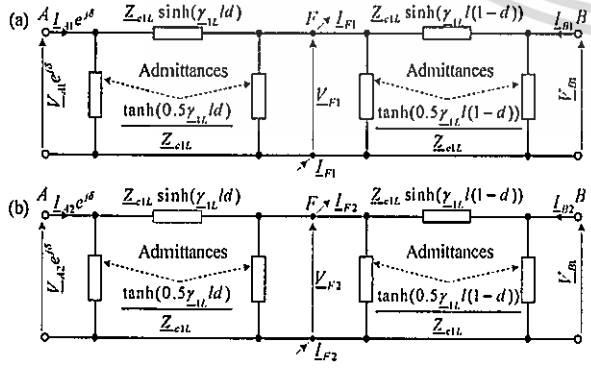

Figure 2. Distributed parameter line model of faulted line for (a) positive-sequence and (b) negative-sequence

Since fully transposed overhead line contains the identical impedance and admittance parameters for the positive- and negative-sequence, the surge impedance ($\underline{Z}_{c1L}$) and the propagation constant ($\underline{\gamma}_{1L}$) are also uniform, and positive-sequence is significantly used as shown in Figure 2. The voltage and current phasors from terminal B are supposed as the base, whereas those from terminal A are multiplied with the determined synchronization operator ($e^{j\delta}$) where δ is the synchronization angle.

After performing the analytical synchronization with the determined synchronization operator, it would be clearly stated that such measurements become synchronized and then fault distance can be located precisely as the cases of using synchronized measurement by applying the prominent formula [2] in term of positive-sequence as expressed in (1). However, this formula can also perform with negative-sequence.

$$d = \frac{1}{\underline{\gamma}_{1L}} \tanh^{-1}\left(\frac{\underline{V}_{B1}\cosh(\underline{\gamma}_{1L}l) - \underline{Z}_{c1L}\underline{I}_{B1}\sinh(\underline{\gamma}_{1L}l) - \underline{V}_{A1}^{syn.}}{\underline{V}_{B1}\sinh(\underline{\gamma}_{1L}l) - \underline{Z}_{c1L}\underline{I}_{B1}\cosh(\underline{\gamma}_{1L}l) - \underline{Z}_{c1L}\underline{I}_{A1}^{syn.}}\right) \quad (1)$$

where

$\underline{V}_{A1}^{syn.} = \underline{V}_{A1}e^{j\delta}$ synchronized positive-sequence voltage phasor at terminal A

$\underline{I}_{A1}^{syn.} = \underline{I}_{A1}e^{j\delta}$ synchronized positive-sequence current phasor at terminal A

$e^{j\delta} = \cos(\delta) + jsin(\delta)$ synchronization operator

$\underline{Z}_{c1L} = \sqrt{\underline{Z}'_{1L}/\underline{Y}'_{1L}}$ positive-sequence surge impedance

$\underline{\gamma}_{1L} = \sqrt{\underline{Z}'_{1L}\underline{Y}'_{1L}}$ positive-sequence propagation constant

$\underline{Z}'_{1L}$ positive-sequence line impedance(Ω/km)

$\underline{Y}'_{1L}$ positive-sequence line admittance (S/km)

$\underline{V}_{B1}, \underline{I}_{B1}$ positive-sequence voltage and current phasors at terminal B

d distance from A to faulted point F in p.u.

l total transmission line length (km)

2.1 Determination of Synchronization Operator

Through the consideration of the distributed parameter line model of faulted line in Figure 2, the positive-sequence voltage corresponded to faulted point F seen from both terminals with superscript A and B can be written as [7]:

$$\underline{V}_{F1}^{A} = \underline{V}_{A1}e^{j\delta}\cosh(\underline{\gamma}_{1L}ld) - \underline{Z}_{c1L}\underline{I}_{A1}e^{j\delta}\sinh(\underline{\gamma}_{1L}ld) \quad (2)$$

$$\underline{V}_{F1}^{B} = \underline{V}_{B1}\cosh(\underline{\gamma}_{1L}l(1-d)) - \underline{Z}_{c1L}\underline{I}_{B1}\sinh(\underline{\gamma}_{1L}l(1-d)) \quad (3)$$

The following trigonometric identities from (3) can be expressed as:

$$\cosh(\underline{\gamma}_{1L}l(1-d)) = \cosh(\underline{\gamma}_{1L}l)\cosh(\underline{\gamma}_{1L}ld) - \sinh(\underline{\gamma}_{1L}l)\sinh(\underline{\gamma}_{1L}ld) \quad (4)$$

$$\sinh(\underline{\gamma}_{1L}l(1-d)) = \sinh(\underline{\gamma}_{1L}l)\cosh(\underline{\gamma}_{1L}ld) - \cosh(\underline{\gamma}_{1L}l)\sinh(\underline{\gamma}_{1L}ld) \quad (5)$$

After the rearrangement by providing (4) and (5) into (3):

$$\underline{V}_{F1}^{B} = \underline{A}_1 \cosh(\underline{\gamma}_{1L}ld) + \underline{B}_1 \sinh(\underline{\gamma}_{1L}ld) \quad (6)$$

where

$$\underline{A}_1 = \underline{V}_{B1}\cosh(\underline{\gamma}_{1L}l) - \underline{Z}_{c1L}\underline{I}_{B1}\sinh(\underline{\gamma}_{1L}l)$$
$$\underline{B}_1 = -\underline{V}_{B1}\sinh(\underline{\gamma}_{1L}l) + \underline{Z}_{c1L}\underline{I}_{B1}\cosh(\underline{\gamma}_{1L}l)$$

By comparing $\underline{V}_{F1}^{A} = \underline{V}_{F1}^{B}$ which corresponded to (2) = (6) the following equation is represented as:

$$(\underline{C}_1 e^{j\delta} - \underline{A}_1)\cosh(\underline{\gamma}_{1L}ld) + (\underline{D}_1 e^{j\delta} - \underline{B}_1)\sinh(\underline{\gamma}_{1L}ld) = 0 \quad (7)$$

where

$\underline{A}_1, \underline{B}_1$ are specified in (6)
$\underline{C}_1 = \underline{V}_{A1}$
$\underline{D}_1 = -\underline{Z}_{c1L}\underline{I}_{A1}$

Once the positive-sequence was derived in (7), the analogous equation for negative-sequence was obtained by:

$$(\underline{C}_2 e^{j\delta} - \underline{A}_2)\cosh(\underline{\gamma}_{1L}ld) + (\underline{D}_2 e^{j\delta} - \underline{B}_2)\sinh(\underline{\gamma}_{1L}ld) = 0 \quad (8)$$

where

$$\underline{A}_2 = \underline{V}_{B2}\cosh(\underline{\gamma}_{1L}l) - \underline{Z}_{c1L}\underline{I}_{B2}\sinh(\underline{\gamma}_{1L}l)$$
$$\underline{B}_2 = -\underline{V}_{B2}\sinh(\underline{\gamma}_{1L}l) + \underline{Z}_{c1L}\underline{I}_{B2}\cosh(\underline{\gamma}_{1L}l)$$
$$\underline{C}_2 = \underline{V}_{A2}$$
$$\underline{D}_2 = -\underline{Z}_{c1L}\underline{I}_{A2}$$

As stated, only positive- and negative-sequence are sufficient to get the synchronization operator. Thus, (7) and (8) are combined to form the equation as follows:

$$(\underline{C}_1 e^{j\delta} - \underline{A}_1)(\underline{D}_2 e^{j\delta} - \underline{B}_2) - (\underline{D}_1 e^{j\delta} - \underline{B}_1)(\underline{C}_2 e^{j\delta} - \underline{A}_2) = 0 \quad (9)$$

where

$\underline{A}_1, \underline{B}_1, \underline{C}_1, \underline{D}_1$ are specified in (6) and (7)
$\underline{A}_2, \underline{B}_2, \underline{C}_2, \underline{D}_2$ are specified in (8)

From (9), synchronization operator is obviously determined by solving the quadratic equation below:

$$\underline{E}(e^{j\delta})^2 + \underline{F}e^{j\delta} + \underline{G} = 0 \quad (10)$$

where

$$\underline{E} = \underline{C}_1\underline{D}_2 - \underline{D}_1\underline{C}_2$$
$$\underline{F} = \underline{D}_1\underline{A}_2 + \underline{B}_1\underline{C}_2 - \underline{C}_1\underline{B}_2 - \underline{A}_1\underline{D}_2$$
$$\underline{G} = \underline{A}_1\underline{B}_2 - \underline{B}_1\underline{A}_2$$

in which

$\underline{A}_1, \underline{B}_1, \underline{C}_1, \underline{D}_1$ are specified in (6) and (7)
$\underline{A}_2, \underline{B}_2, \underline{C}_2, \underline{D}_2$ are specified in (8)

Basically, two solutions are acquired by the quadratic equation. To distinguish the real value of synchronization operator, crucial selection was provided in order to perform the analytical synchronization in the next section.

2.2 Selection of Valid Solution for the Determined Synchronization Operator

To select the valid solution is to clearly discriminate the magnitude of the determined synchronization operators. One is rejected if its magnitude is not close to unity.

$$(1-\varepsilon) > \left|e^{j\delta_i}\right| > (1+\varepsilon) \quad (11)$$

where

ε error margin, which is considered as the tolerance of the possible error in synchronization operator determination
i index representing both solutions of the synchronization operator in which contains the synchronization angle

The possibility in error margin $\varepsilon = 0.01$ was applied in the evaluation section to declare the effectiveness of the proposed method. It is fact that Euler equation provides:

$$e^{j\delta} = \cos(\delta) + jsin(\delta) = 1 \quad (12)$$

It is obvious that once the valid solution of the determined synchronization operator is selected, the synchronization angle is followed by the selected valid solution since it is in the phasor quantity. The condition (11) appears definitely sufficient to perform the synchronization of the initially measured signals in all fault types.

3 ATP-EMTP EVALUATION AND DISCUSSION

The presented algorithm has been simulated and validated thoroughly with credible fault data modeling obtained from ATP-EMTP software versatile simulations of fault implemented on the test transmission line containing 400kV, 300km long. The parameters of both networks and transmission line are listed in the Table 1.

Table 1. Parameters of the test networks

Components	Parameters	
Terminal A	RMS Voltage	416 kV
	Phase Shift	$\alpha_A = 30°$
	$\underline{Z}_{1SA}$	(1.312+j15.0) Ω
	$\underline{Z}_{0SA}$	(2.334+j26.6) Ω
Terminal B	RMS Voltage	400 kV
	Phase Shift	$\alpha_B = 10°$
	$\underline{Z}_{1SB}$	(2.624+j30.0) Ω
	$\underline{Z}_{0SB}$	(4.668+j53.2) Ω
Transmission line from A to B	$\underline{Z}'_{1L}$	(0.0276+j0.3151) Ω/km
	$\underline{Z}'_{0L}$	(0.2750+j1.0265) Ω/km
	$\underline{C}'_{1L}$	13.0 nF/km
	$\underline{C}'_{0L}$	8.5 nF/km
	l	300 km

3.1 All Considered Fault Types Evaluation

Single line to ground (SLG), double line to ground (DLG), and three-phase to ground fault (3LG) faults were simulated

at different locations with a variety of fault resistance as well as ground resistance along the line. The represented models were depicted in Figure 3. The sampling frequency was set f_s = 10kHz. The data window size used for Fast Fourier Transform (FFT) process to obtain the phasors quantities was T_{dw} = 20ms (N = 200 samples per data window). It was assumed that the line was loaded and the fault inception time was set at t = 40ms in all considered cases. The CTs and VTs were deliberately modeled as errorless instrument transformers. Second order Butterworth analog anti-aliasing filters designed for 500Hz of the cutoff frequency which agrees to 10th harmonic were applied by built-in function in Matlab to filter the secondary signals of the CTs and VTs.

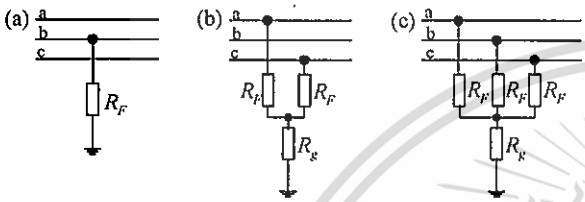

Figure 3. Represented models of considered fault: (a) SLG, (b) DLG, and (c) 3LG

Basically, the signals of considered faults obtained from ATP-EMTP simulations are perfectly synchronized. To demonstrate the effectiveness of the presented algorithm, all measured signals from terminal A were artificially delayed by 18° which firmly tallies to 10 samples in 50Hz digitalized at 10kHz. Through the performed evaluation, 54 simulations with different scenarios and results have been proposed and gathered in Tables 2-7, respectively. In these tables, a variety of different fault specifications i.e. fault types, fault resistances and ground resistances which are the certain factors affected to accuracy of the fault distance has been considered over the entire line length. The verifications of the distance to faulted point were used the averaged value over the interval (100-120) ms.

Based on the condition (11), synchronization operators and angles are successfully selected as valid solution which is close to actual value (18°) whereas another solution differs very much from it. The relative error of the synchronization angle does not exceed 0.02°. This shows the strength of the presented algorithm which starts with quite accurate identification of the synchronization angle. Once the synchronization operator is determined, the fault distance is calculated by using (1) and provided the high level of accuracy in locating all fault types as given from Tables 2-7.

It is obvious that errors occurred during the convergence are due to the presence of the DC components in the fault current. Commonly, since FFT was used in this extraction process, it is known to be sensitive to the decaying of DC components. The relative error of the distance to fault in all cases does not exceed 0.12%. Based on evaluative results, it can be concluded that the proposed algorithm is unaffected by fault resistance and ground resistance for all fault types.

Table 2. SLG evaluation verified by using positive-sequence with $R_F = 1\Omega, \delta_{actual} = 18°$

Fault Distance	Determined Synchronization Operators and Synchronization Angles				Verified Fault Distance	
d [p.u.]	$\lvert e^{j\delta_1}\rvert$	$\lvert e^{j\delta_2}\rvert$	δ_1 [°]	δ_2 [°]	d [p.u.]	error [%]
0.1	1.0002	1.2363	17.9864	162.116	0.1012	0.12
0.2	1.0002	1.2333	17.9864	162.122	0.2006	0.06
0.3	1.0001	1.2311	17.9865	162.126	0.3004	0.04
0.4	1.0001	1.2298	17.9866	162.128	0.4003	0.03
0.5	1.0001	1.2293	17.9867	162.129	0.5003	0.03
0.6	1.0001	1.2297	17.9868	162.128	0.6002	0.02
0.7	1.0001	1.2309	17.987	162.125	0.7001	0.01
0.8	1.0001	1.233	17.9872	162.122	0.7999	0.01
0.9	1.0002	1.2361	17.9873	162.12	0.8996	0.04

Table 3. SLG evaluation verified by using positive-sequence with $R_F = 50\Omega, \delta_{actual} = 18°$

Fault Distance	Determined Synchronization Operators and Synchronization Angles				Verified Fault Distance	
d [p.u.]	$\lvert e^{j\delta_1}\rvert$	$\lvert e^{j\delta_2}\rvert$	δ_1 [°]	δ_2 [°]	d [p.u.]	error [%]
0.1	1.0002	1.2363	17.9864	162.116	0.1004	0.04
0.2	1.0002	1.2333	17.9864	162.122	0.2	0
0.3	1.0001	1.2311	17.9865	162.126	0.3	0
0.4	1.0001	1.2298	17.9866	162.128	0.4001	0.01
0.5	1.0001	1.2293	17.9867	162.129	0.5002	0.02
0.6	1.0001	1.2297	17.9868	162.128	0.6003	0.03
0.7	1.0001	1.2309	17.9869	162.125	0.7004	0.04
0.8	1.0001	1.2331	17.9871	162.122	0.8005	0.05
0.9	1.0002	1.2361	17.9872	162.119	0.9005	0.05

Table 4. DLG evaluation verified by using positive-sequence with $R_F = 1\Omega, R_g = 1\Omega, \delta_{actual} = 18°$

Fault Distance	Determined Synchronization Operators and Synchronization Angles				Verified Fault Distance	
d [p.u.]	$\lvert e^{j\delta_1}\rvert$	$\lvert e^{j\delta_2}\rvert$	δ_1 [°]	δ_2 [°]	d [p.u.]	error [%]
0.1	1.0002	1.2363	17.9864	162.116	0.1004	0.04
0.2	1.0002	1.2333	17.9864	162.122	0.2002	0.02
0.3	1.0001	1.2311	17.9864	162.13	0.3002	0.02
0.4	1.0001	1.2297	17.9861	162.144	0.4002	0.02
0.5	1.0001	1.2291	17.9854	162.167	0.5002	0.02
0.6	1.0001	1.2293	17.984	162.196	0.6002	0.02
0.7	1	1.2305	17.9817	162.225	0.7002	0.02
0.8	1	1.233	17.9784	162.231	0.8002	0.02
0.9	1	1.2367	17.9749	162.214	0.9002	0.02

Table 5. DLG evaluation verified by using positive-sequence with $R_F = 1\Omega, R_g = 50\Omega, \delta_{actual} = 18°$

Fault Distance	Determined Synchronization Operators and Synchronization Angles				Verified Fault Distance	
d [p.u.]	$\lvert e^{j\delta_1}\rvert$	$\lvert e^{j\delta_2}\rvert$	δ_1 [°]	δ_2 [°]	d [p.u.]	error [%]
0.1	1.0002	1.2363	17.9864	162.116	0.1007	0.07
0.2	1.0002	1.2333	17.9864	162.122	0.2002	0.02
0.3	1.0001	1.2311	17.9864	162.13	0.3002	0.02
0.4	1.0001	1.2297	17.9861	162.144	0.4002	0.02
0.5	1.0001	1.2291	17.9854	162.167	0.5003	0.03
0.6	1.0001	1.2293	17.984	162.196	0.6003	0.03
0.7	1	1.2305	17.9817	162.225	0.7004	0.04
0.8	1	1.233	17.9784	162.231	0.8004	0.04
0.9	1	1.2367	17.9748	162.213	0.9005	0.05

Table 6. 3LG evaluation verified by using positive-sequence with $R_F = 1\Omega, R_g = 1\Omega,\ \delta_{actual} = 18°$

Fault Distance	Determined Synchronization Operators and Synchronization Angles				Verified Fault Distance	
d [p.u.]	$\lvert e^{j\delta_1}\rvert$	$\lvert e^{j\delta_2}\rvert$	δ_1 [°]	δ_2 [°]	d [p.u.]	error [%]
0.1	1.0002	1.2363	17.9864	162.116	0.1001	0.01
0.2	1.0002	1.2333	17.9864	162.122	0.2001	0.01
0.3	1.0001	1.2311	17.9864	162.13	0.3001	0.01
0.4	1.0001	1.2297	17.9862	162.143	0.4	0
0.5	1.0001	1.229	17.9855	162.165	0.4999	0.01
0.6	1.0001	1.2292	17.9843	162.194	0.5998	0.02
0.7	1	1.2303	17.9823	162.222	0.6997	0.03
0.8	1	1.2328	17.9794	162.231	0.7997	0.03
0.9	1	1.2365	17.9762	162.218	0.8996	0.04

Table 7. 3LG evaluation verified by using positive-sequence with $R_F = 1\Omega, R_g = 50\Omega,\ \delta_{actual} = 18°$

Fault Distance	Determined Synchronization Operators and Synchronization Angles				Verified Fault Distance	
d [p.u.]	$\lvert e^{j\delta_1}\rvert$	$\lvert e^{j\delta_2}\rvert$	δ_1 [°]	δ_2 [°]	d [p.u.]	error [%]
0.1	1.0002	1.2363	17.9864	162.116	0.1001	0.01
0.2	1.0002	1.2333	17.9864	162.122	0.2001	0.01
0.3	1.0001	1.2311	17.9864	162.13	0.3001	0.01
0.4	1.0001	1.2297	17.9862	162.143	0.4	0
0.5	1.0001	1.229	17.9855	162.165	0.4999	0.01
0.6	1.0001	1.2292	17.9843	162.194	0.5998	0.02
0.7	1	1.2303	17.9823	162.222	0.6997	0.03
0.8	1	1.2328	17.9794	162.231	0.7997	0.03
0.9	1	1.2365	17.9762	162.218	0.8996	0.04

3.2 Investigation on Additive White Gaussian Noise

The use of PMUs in the reality can be disturbed by noise. This includes electronic noise even some external events that affect the measured phenomenon. Noise ratio 40dB is considered as the severe noise introduced in the network. Additive White Gaussian Noise (AWGN) whose signal-to-noise ratio (SNR) is 40dB has been added to voltages and currents from both terminals by Matlab. The error presented in the results obtained for this condition have been used the averaged value of 10 time simulations within terminal (100-120) ms in each case as given in Table 8.

From Table 8, it can be concluded that the algorithm still maintained a high level of accuracy in locating all fault types even the effect of severe noise in the network has been considered and maximum error does not more than 0.123%.

Table 8. All fault types evaluation considering AWGN

Fault Distance	Verified Fault Distance Error [%]					
	SLG	DLG	3LG	SLG	DLG	3LG
[p.u.]	$R_F = 1\Omega$	$R_F = 1\Omega, R_g = 1\Omega$		$R_F = 50\Omega$	$R_F = 1\Omega, R_g = 50\Omega$	
0.1	0.123	0.044	0.013	0.054	0.066	0.013
0.2	0.057	0.02	0.011	0.007	0.021	0.012
0.3	0.041	0.018	0.01	0.002	0.018	0.01
0.4	0.037	0.02	0	0.004	0.021	0.001
0.5	0.035	0.022	0.006	0.025	0.031	0.006
0.6	0.017	0.023	0.015	0.028	0.032	0.018
0.7	0.004	0.024	0.024	0.048	0.039	0.027
0.8	0.014	0.022	0.032	0.049	0.041	0.031
0.9	0.037	0.02	0.04	0.052	0.05	0.04

3.3 Investigation on Phase Shift Angle

Phase shift angle from both terminals which considered as one of the affected factors was further investigated in order to ensure the efficiency of the presented algorithm. Phase shift angle was changed by setting the terminal B as delayed ($\alpha_B = -10°, -20°, -30°$), leading ($\alpha_B = 10°, 20°, 30°$), and no phase shift angle ($\alpha_A = \alpha_B = 0°$) to the terminal A. Tables 9-11 show the results of all fault types considering different phase shift angles. The errors presented in the results have been averaged over the interval (100-120) ms.

From Tables 9-11, it can be confirmed that the high accuracy of the presented algorithm is still applicable even different phase shift angles are considered. The maximum error of fault distance and determined synchronization angle in all cases do not exceed 0.08% and 0.138°, respectively.

4 CONCLUSIONS

In this study, an impedance-based algorithm for fault location on fully transposed transmission line by processing two-end unsynchronized measurement has been presented. The distributed parameter line model is strictly taken into account to ensure the high accuracy of the presented algorithm.

Table 9. SLG evaluation considering different phase shift angles with $R_F = 10\Omega, \alpha_A = 0°, \delta_{actual} = 18°$

Fault Distance	Determined Synchronization Angle and Verified Fault Distance Error													
	$\alpha_B = -30°$		$\alpha_B = -20°$		$\alpha_B = -10°$		$\alpha_B = 0°$		$\alpha_B = 10°$		$\alpha_B = 20°$		$\alpha_B = 30°$	
[p.u.]	δ_2 [°]	error [%]	δ_1 [°]	error [%]	δ_1 [°]	error [%]	δ_1 [°]	error [%]	δ_1 [°]	error [%]	δ_1 [°]	error [%]	δ_2 [°]	error [%]
0.1	17.9859	0.06	17.9864	0.08	17.9863	0.08	17.9859	0.07	17.9845	0.06	17.9753	0.04	17.9213	0.05
0.2	17.9864	0.02	17.9864	0.04	17.9864	0.03	17.9861	0.02	17.985	0	17.9784	0.02	17.9402	0.01
0.3	17.9865	0.03	17.9865	0.03	17.9865	0.02	17.9863	0.01	17.9856	0.01	17.9809	0.04	17.9534	0.03
0.4	17.9865	0.03	17.9866	0.03	17.9866	0.02	17.9865	0	17.9861	0.01	17.9828	0.04	17.9608	0.04
0.5	17.9862	0.04	17.9867	0.04	17.9868	0.02	17.9868	0.01	17.9865	0.01	17.9839	0.04	17.9622	0.04
0.6	17.9857	0.04	17.9868	0.04	17.9869	0.02	17.987	0.01	17.9869	0.01	17.9841	0.04	17.9578	0.04
0.7	17.9853	0.04	17.987	0.04	17.9871	0.03	17.9872	0.01	17.987	0.01	17.9831	0.04	17.9479	0.03
0.8	17.9848	0.03	17.9871	0.04	17.9872	0.03	17.9874	0.02	17.9869	0	17.981	0.03	17.9334	0.01
0.9	17.9845	0.02	17.9871	0.04	17.9873	0.03	17.9873	0.03	17.9863	0.01	17.9773	0.02	17.9152	0.01

Table 10. DLG evaluation considering different phase shift angles with $R_F = 1\Omega, R_g = 10\Omega, \alpha_A = 0°, \delta_{actual} = 18°$

Fault Distance	Determined Synchronization Angle and Verified Fault Distance Error													
	$\alpha_B = -30°$		$\alpha_B = -20°$		$\alpha_B = -10°$		$\alpha_B = 0°$		$\alpha_B = 10°$		$\alpha_B = 20°$		$\alpha_B = 30°$	
[p.u.]	δ_2 [°]	error [%]	δ_1 [°]	error [%]	δ_1 [°]	error [%]	δ_1 [°]	error [%]	δ_1 [°]	error [%]	δ_1 [°]	error [%]	δ_2 [°]	error [%]
0.1	17.9859	0.04	17.9864	0.04	17.9863	0.04	17.9859	0.07	17.9845	0.03	17.9753	0.03	17.9213	0.03
0.2	17.9864	0	17.9864	0	17.9864	0.01	17.9861	0.02	17.985	0.01	17.9783	0.01	17.9402	0.01
0.3	17.9866	0.01	17.9864	0.01	17.9863	0.01	17.9863	0.01	17.9853	0.02	17.9804	0.02	17.9531	0.01
0.4	17.9866	0.02	17.9861	0.02	17.986	0.02	17.9865	0	17.9849	0.02	17.9805	0.02	17.9592	0.01
0.5	17.9864	0.02	17.9854	0.02	17.9851	0.02	17.9868	0.01	17.9832	0.01	17.9775	0.02	17.9575	0
0.6	17.986	0.03	17.9839	0.02	17.9832	0.02	17.987	0.01	17.9793	0.01	17.9702	0.01	17.9469	0.01
0.7	17.9852	0.04	17.9816	0.02	17.9802	0.02	17.9872	0.01	17.9729	0	17.958	0	17.9271	0.03
0.8	17.9837	0.04	17.9784	0.03	17.976	0.01	17.9874	0.02	17.964	0.01	17.9418	0.01	17.8997	0.05
0.9	17.982	0.05	17.9751	0.03	17.9715	0.01	17.9873	0.03	17.9545	0.02	17.9245	0.02	17.8686	0.06

Table 11. 3LG evaluation considering different phase shift angles with $R_F = 1\Omega, R_g = 10\Omega, \alpha_A = 0°, \delta_{actual} = 18°$

Fault Distance	Determined Synchronization Angle and Verified Fault Distance Error													
	$\alpha_B = -30°$		$\alpha_B = -20°$		$\alpha_B = -10°$		$\alpha_B = 0°$		$\alpha_B = 10°$		$\alpha_B = 20°$		$\alpha_B = 30°$	
[p.u.]	δ_2 [°]	error [%]	δ_1 [°]	error [%]	δ_1 [°]	error [%]	δ_1 [°]	error [%]	δ_1 [°]	error [%]	δ_1 [°]	error [%]	δ_2 [°]	error [%]
0.1	17.9859	0.01	17.9864	0.01	17.9863	0.01	17.9859	0.01	17.9845	0.01	17.9753	0.01	17.9213	0.01
0.2	17.9864	0.01	17.9864	0.01	17.9864	0.01	17.9861	0.01	17.985	0.01	17.9783	0.01	17.9402	0.01
0.3	17.9866	0.01	17.9864	0.01	17.9864	0.01	17.9861	0.01	17.9853	0	17.9804	0	17.9528	0
0.4	17.9865	0.01	17.9862	0	17.9861	0	17.9859	0	17.9851	0	17.9807	0.01	17.9582	0.01
0.5	17.9862	0	17.9855	0.01	17.9853	0.01	17.9848	0.01	17.9835	0.01	17.9778	0.02	17.9549	0.02
0.6	17.9857	0.01	17.9843	0.02	17.9837	0.02	17.9826	0.02	17.9801	0.02	17.9708	0.03	17.9421	0.03
0.7	17.9847	0.02	17.9823	0.03	17.981	0.03	17.9788	0.03	17.9742	0.03	17.9591	0.03	17.9202	0.04
0.8	17.9833	0.03	17.9794	0.03	17.9772	0.03	17.9735	0.04	17.9659	0.04	17.9431	0.04	17.8919	0.04
0.9	17.9816	0.04	17.9762	0.04	17.973	0.04	17.9677	0.04	17.9568	0.04	17.9257	0.04	17.862	0.05

The presented algorithm is formulated in term of phasors of the symmetrical components. Only positive- and negative-sequence components were used to determine the unknown synchronization operator and angle for all fault types. Thus, analytical determination of synchronization operator of the inputs can be accomplished non-iteratively by solving the quadratic equation in phasor quantity which contains absolute value of magnitude for synchronization operator and phase for synchronization angle. The procedure of selecting the valid solution has been provided to sufficiently discriminate the real synchronization operator among two solutions, and it is definitely reliable for all trial tests. Consequently, the unknown fault location is calculated precisely as the case of using synchronized measurement after making the analytical synchronization.

Through overall algorithm testing and evaluation with the credible fault data modeling obtained from ATP-EMTP simulations, the accuracy of the presented algorithm is very high and definitely acceptable. Based on all successful trial tests, it can be proved that the algorithm is unaffected by fault resistance, phase shift angle, and still maintained the high accuracy even adding severe noise AWGN ratio 40dB.

ACKNOWLEDGMENTS

The authors would like to give special acknowledgment to AUN-SEED/Net for providing the scholarship for master degree and High Voltage Engineering Laboratory, King Mongkut's Institute of Technology Ladkrabang for providing the facility to support this research work.

REFERENCES

[1] M.B. Djuric, Z.M. Radojevic, V.V.Terzija,"Time domain solution of fault distance estimation and arcing faults detection on overhead lines,", IEEE Trans. on Power Del., vol.14, no.1, pp.60-67, Jan 1999.

[2] A.T. Johns, S. Jamali, "Accurate fault location technique for power transmission lines," Proc. Inst. Elect. Eng. C, vol.137, no.6, pp. 395-402, Nov 1990.

[3] G.Preston, Z.M. Radojević, C.H. Kim, V. Terzija, "New settings free fault location algorithm based on synchronised sampling," IET ,Gen., Transm. Distrib., vol.5, no.3, pp.376-383, March 2011.

[4] Y. Liao, S. Elangovan, "Unsynchronized two-terminal transmission line fault-location without using line parameters," Proc. Inst. Elect. Eng., Gen. Transm. Distrib., vol. 153, no. 6, pp. 639–643, 2006.

[5] Y. Liao, "Unsynchronized fault location based on distributed parameter line model," Elect. Power Components Syst., vol. 35, no. 9, pp. 1061–1077, 2007.

[6] J. Izykowski, R. Molag, E. Rosolowski, and M. M. Saha, "Accurate location of faults on power transmission lines with use of two-end unsynchronized measurements," IEEE Trans. Power Del., vol. 21, no. 2, pp. 627–633, Apr. 2006.

[7] J. Izykowski, E. Rosolowski, P. Balcerek, M. Fulczyk, and M. M. Saha "Accurate noniterative fault-location algorithm utilizing two-end unsynchronized measurements," IEEE Trans. Power Del., vol. 26, no. 2, pp. 547–554, Apr. 2011.

Contact E-mail Address: daro_din@ymail.com